

**PREPARATION OF $\text{Ba}_x\text{Sr}_{1-x}\text{TiO}_3$ THIN FILMS BY CHEMICAL SOLUTION
DEPOSITION AND THEIR ELECTRICAL CHARACTERIZATION**

**A THESIS SUBMITTED TO
THE GRADUATE SCHOOL OF NATURAL AND APPLIED SCIENCES
OF
THE MIDDLE EAST TECHNICAL UNIVERSITY**

BY

UMUT ADEM

**IN PARTIAL FULFILLMENT OF THE REQUIREMENTS FOR THE DEGREE OF
MASTER OF SCIENCE**

**IN
THE DEPARTMENT OF METALLURGICAL & MATERIALS
ENGINEERING**

DECEMBER 2003

Approval of the Graduate School of Natural and Applied Sciences

Prof. Dr. Canan ÖZGEN
Director

I certify that this thesis satisfies all the requirements as a thesis for the degree of Master of Science.

Prof. Dr. Bilgehan ÖGEL
Head of Department

This is to certify that we have read this thesis and that in our opinion it is fully adequate, in scope and quality, as a thesis for the degree of Master of Science.

Prof. Dr. Macit ÖZENBAŞ
Supervisor

Examining Committee Members

Prof. Dr. Muharrem TİMUÇİN

Prof. Dr. Macit ÖZENBAŞ

Prof. Dr. Ali KALKANLI

Prof. Dr. Raşit TURAN

Asst. Prof. Dr. Mustafa GÖKTEPE

ABSTRACT

PREPARATION OF BST THIN FILMS BY CHEMICAL SOLUTION DEPOSITION AND THEIR ELECTRICAL CHARACTERIZATION

Adem, Umut

M.S., Department of Metallurgical & Materials Engineering

Supervisor: Prof. Dr. Macit Özenbaş

December 2003, 98 pages

In this study, barium strontium titanate (BST) thin films with different compositions ($\text{Ba}_{0.9}\text{Sr}_{0.1}\text{TiO}_3$, $\text{Ba}_{0.8}\text{Sr}_{0.2}\text{TiO}_3$, $\text{Ba}_{0.7}\text{Sr}_{0.3}\text{TiO}_3$, $\text{Ba}_{0.5}\text{Sr}_{0.5}\text{TiO}_3$) were produced by chemical solution deposition technique. BST solutions were prepared by dissolving barium acetate, strontium acetate and titanium isopropoxide in acetic acid and adding ethylene glycol as a chelating agent and stabilizer to this solution, at molar ratio of acetic acid/ethylene glycol, 3:1. The solution was then coated on Si and Pt//Ti/SiO₂/Si substrates at 4000 rpm for 30 seconds. Crack-free films were obtained up to 600 nm thickness after 3 coating – pyrolysis cycles by using 0.4M solutions.

Crystal structure of the films was determined by x-ray diffraction while morphological properties of the surface and the film-substrate interface was examined by scanning electron microscope (SEM).

Dielectric constant, dielectric loss and ferroelectric parameters of the films were measured. Sintering temperature, film composition and the thickness of the films

were changed in order to observe the effect of these parameters on the measured electrical properties.

The dielectric constant of the films was decreased slightly in 1kHz-1 MHz range. It was seen that dielectric constant and loss of the films was comparable to chemical solution deposition derived films on literature. Maximum dielectric constant was obtained for the $\text{Ba}_{0.7}\text{Sr}_{0.3}\text{TiO}_3$ composition at a sintering temperature of 800°C for duration of 3 hours. Dielectric constant increased whereas dielectric loss decreased with increasing film thickness.

BST films have composition dependent Curie temperature. For Ba content greater than 70 %, the material is in ferroelectric state. However, fine grain size of the films associated with chemical solution deposition and Sr doping causes the suppression of ferroelectric behaviour in BST films. Therefore, only for $\text{Ba}_{0.9}\text{Sr}_{0.1}\text{TiO}_3$ composition, slim hysteresis loops with very low remanent polarization values were obtained.

Keywords: BST, Pt/Ti/SiO₂/Si substrate, DRAM, Chemical Solution Deposition.

ÖZ

BST İNCE FİLMLEİN KİMYASAL ÇÖZELTİDEN BİRİKTİRME YÖNTEMİYLE HAZIRLANMASI VE ELEKTRİKSEL KARAKTERİZASYONU

Adem, Umut
M.S., Metalurji ve Malzeme Mühendisliği Bölümü
Tez Yöneticisi: Prof. Dr. Macit Özenbaş

Aralık 2003, 98 sayfa

Bu çalışmada, değişik bileşimlerde ($Ba_{0.9}Sr_{0.1}TiO_3$, $Ba_{0.8}Sr_{0.2}TiO_3$, $Ba_{0.7}Sr_{0.3}TiO_3$, $Ba_{0.5}Sr_{0.5}TiO_3$) baryum stronsiyum titanat (BST) ince filmler kimyasal çözeltiden biriktirme yöntemiyle üretildi. BST çözeltileri, baryum asetat, stronsiyum asetat ve titanyum izopropoksiti asetik asit içinde çözdürerek ve kararlılaştırıcı olarak 3:1 asetik asit/etilen glikol mol oranında etilen glikol eklenmesiyle hazırlandı. 0.4M çözelti kullanılarak, 3 kaplama-piroliz döngüsü sonunda, 600 nm kalınlığa kadar çatlaksız filmler elde edildi.

Filmlerin kristal yapıları x-ışını kırınımı ile belirlenirken, yüzeyin ve film-altlık arayüzeyinin morfolojik özellikleri taramalı elektron mikroskobu ile incelendi.

Filmlerin dielektrik sabiti, dielektrik kaybı ve ferroelektrik parametreleri ölçüldü. Sinterleme sıcaklığı, filmlerin bileşimi ve film kalınlığı bu parametrelerin ölçülen elektriksel özelliklere etkisini gözlemlemek amacıyla değiştirildi.

Filmlerin dielektrik sabiti 1kHz-1MHz aralığında yavaşça azaldı. Filmlerin dielektrik sabitleri ve kayıplarının, literatürdeki diğer kimyasal solüsyondan biriktirme ile hazırlanan filmlerle karşılaştırılabilir olduğu görüldü. En yüksek dielektrik sabiti $Ba_{0.7}Sr_{0.3}TiO_3$ kompozisyonu için 800°C'de 3 saat sinterlenerek elde edildi. Dielektrik sabiti, film kalınlığıyla artarken dielektrik kaybı azaldı.

BST filmler bileşime bağlı Curie sıcaklığına sahiptirler. Ba miktarı % 70'ten fazla olduğunda, malzeme ferroelektrik yapıdadır. Fakat, kimyasal solüsyondan biriktirmeye bağlı ince tane boyu ve Sr katkılanması ferroelektrik davranışı bastırmaktadır. Bu yüzden, sadece $Ba_{0.9}Sr_{0.1}TiO_3$ bileşimi için, düşük artık polarizasyonlu dar polarizasyon döngüleri elde edildi.

Anahtar Sözcükler: BST, Pt/Ti/SiO₂/Si altlık, DRAM, Kimyasal Çözeltiden Biriktirme.

To my parents

ACKNOWLEDGEMENTS

I am grateful to my supervisor Prof. Dr. Macit Özenbaş for his guidance, impatience and understanding throughout my thesis.

I would like to thank to Dr. İbrahim Çam for his continuous help during the dielectric and ferroelectric measurements and for his comments. I also would like to thank to technical staff of Metallurgical Engineering Department, especially, Mr. Necmi Avcı for x-ray diffraction studies and Mr. Cengiz Tan for SEM studies.

I cannot pay my debt to my lab friends: Tuna, whose friendship and knowledge, I admire and acknowledge and Altan who inspired me to add more fun and sports to research and life.

Finally, I would like to thank to all my friends who were with me: Galip, Ertuğ, Aytaç, Gül and all.

TABLE OF CONTENTS

ABSTRACT	iii
ÖZ.....	v
DEDICATION.....	vii
ACKNOWLEDGEMENTS.....	viii
TABLE OF CONTENTS.....	ix
LIST OF TABLES.....	xi
LIST OF FIGURES.....	xiii

CHAPTER

1. INTRODUCTION.....	1
2. LITERATURE SURVEY	4
2.1. Dielectric and Ferroelectric Properties of Materials	4
2.1.1. Dielectric Properties	4
2.1.2. Polarization	8
2.1.3. Ferroelectric Phenomena	8
2.2. Ferroelectric Materials	12
2.2.1. Ferroelectric Materials.....	12
2.2.2. Hysteresis Loops	12
2.2.3 Barium Strontium Titanate System	14
2.2.4. Applications of BST Thin Films	20
2.2.4.1 BST Films in DRAMs	21
2.3. BST films on Si and Pt/Ti/SiO ₂ /Si substrates.....	24
2.4. Chemical Solution Deposition Technique.....	26
2.4.1. Process Chemistry	26

2.4.2. Spin Coating Process	29
2.4.3. BST Solution Preparation	31
2.4.3.1. Solvents and Precursors	31
2.4.3.2. Drying, Firing, Annealing of BST films	31
3. EXPERIMENTAL PROCEDURE.....	34
3.1. Solution Preparation.....	34
3.1.1. Starting Materials	34
3.1.2. Solution Preparation	35
3.2. Coating of Films on Substrates.....	40
3.2.1. Preparation of substrates.....	40
3.2.2. Spin Coating.....	41
3.2.3. Heat Treatment of the Films	42
3.3. Characterization of Films	43
3.3.1. Structural and Morphological Analysis.....	43
3.3.2. Dielectric and Ferroelectric Measurements.....	44
4. RESULTS AND DISCUSSION	48
4.1. Improvement of Film Quality	49
4.2. Dilution of the Solution.....	52
4.3. Crystalline Film Formation	53
4.4. Morphology of the BST Films.....	60
4.5. Dielectric Properties of BST Films.....	68
4.6. Ferroelectric Properties of BST Films	83
5. CONCLUSIONS AND FURTHER SUGGESTIONS.....	87
REFERENCES	90
APPENDIX.....	97

LIST OF TABLES

TABLE

2.1. Advantages and limitations of processes for producing BST thin films [10, 11].	17
2.2. Major applications of BST films with relevant properties.	21
2.3. Relative permittivity values and charge storage densities for medium dielectric constant materials [6].....	23
2.4. Different precursors and solvents for some sol-gel derived BST films.	32
3.1. BST solutions with different compositions and their corresponding polarization states.	34
3.2. Specifications of Pt/Ti/SiO ₂ /Si substrate (INOSTEK Korea).	41
3.3. X-ray energies of elements of BST film and Pt/Ti/SiO ₂ /Si substrate.	44
4.1. Compositions of Ba _x Sr _{1-x} TiO ₃ films that were produced in this study listed according to the substrates they were coated on.	49
4.2. Thermal expansion coefficients of Pt, BaTiO ₃ and SrTiO ₃ [35, JCPDS].....	51
4.3 Grain sizes of 1 μm thick BST films sintered at different temperatures.	63
4.4. Dielectric properties of some sol-gel derived films with different processing parameters. Properties of films that were deposited using other common BST deposition techniques are also provided to give an idea.....	74
4.5. Change in dielectric properties with increasing film thickness, for	

different compositions.	77
4.6. Dielectric Constant and Loss of $Ba_xSr_{1-x}TiO_3$ films.....	80
4.7. Ferroelectric properties of $Ba_{0.9}Sr_{0.1}TiO_3$ films on Pt/Ti/SiO₂/Si substrates.	86

LIST OF FIGURES

FIGURE

2.1. Charging current I_C and loss current I_l in a dielectric [4].....	6
2.2. Schematic of (a) the polarization behaviour of a ferroelectric material below its Curie point, (b) the change in permittivity at a ferroelectric-paraelectric phase transition and (c) the polarization behaviour of a ferroelectric material above its Curie point [6].....	10
2.3. The displacement of Ti^{+4} ion, for $PbTiO_3$, from the body center of the cubic perovskite structure, resulting in distortion of cubic structure and formation of tetragonal perovskite structure [7].	11
2.4. Creation of net polarization by poling [7].	11
2.5. Classification of crystals according to the symmetry and polarization they possess [8].....	13
2.6. Hysteresis loop for a $PbTiO_3$ thin film [7].	14
2.7. Effect of several isovalent substitutions on the ferroelectric-paraelectric transition temperature of ferroelectric $BaTiO_3$ [11].	15
2.8. Lattice parameter change and stability regions of ferroelectric and paraelectric phases of BST with composition [10].....	18

2.9. Variation of dielectric constant with temperature for bulk and thin film BST [17].....	19
2.10. Four stages of spin-coating shown schematically [25].	29
3.1. Flow chart for solution preparation (first route) and coating of films.	36
3.2. Flow chart for solution preparation (second route) and coating.....	37
3.3. SEM micrographs showing the surface of electroded BST films, (a)×400 (b) ×16.	45
3.4. Schematic of the modified Sawyer-Tower circuit.	47
4.1. SEM micrographs, (top) showing surface cracks of 3 layers Ba _{0.5} Sr _{0.5} TiO ₃ film (500 nm) coated by using first solution: solution containing 2 propanol, (bottom) showing crack-free surface of 3 layers Ba _{0.5} Sr _{0.5} TiO ₃ film (600nm) coated by using second solution: solution containing ethylene glycol, both films were sintered at 800°C for 3 hours.....	50
4.2. XRD spectra of Ba _{0.5} Sr _{0.5} TiO ₃ films on Si substrate sintered at 600°C, 700°C and 800°C for 3 hours.....	54
4.3. XRD spectra of (a) 5 layers, 1 μm thick Ba _{0.5} Sr _{0.5} TiO ₃ film on Si, sintered at 800°C (b) 5 layers, 1 μm thick Ba _{0.8} Sr _{0.2} TiO ₃ film on Si, sintered at 800°C.....	55
4.4. X-ray diffractograms for Ba _{0.5} Sr _{0.5} TiO ₃ thin films coated on Pt/Ti/SiO ₂ /Si substrates and sintered at 600°C, 700°C and 800°C using first solution route.....	58
4.5. X-ray diffractograms for Ba _{0.5} Sr _{0.5} TiO ₃ thin films coated on different Pt/Ti/SiO ₂ /Si substrates and sintered at 700°C, 750°C and 800°C using second	

solution route (using ethylene glycol).....	59
4.6. X-ray diffractograms of $Ba_{0.5}Sr_{0.5}TiO_3$, $Ba_{0.7}Sr_{0.3}TiO_3$ and $Ba_{0.9}Sr_{0.1}TiO_3$ films (from bottom to top) sintered at 800°C for 3 hours.	60
4.7. X-ray diffractograms of (110) peaks of $Ba_{0.5}Sr_{0.5}TiO_3$, $Ba_{0.7}Sr_{0.3}TiO_3$ and $Ba_{0.9}Sr_{0.1}TiO_3$ films (from bottom to top) sintered at 800°C for 3 hours.....	61
4.8. Cross-section SEM micrograph of 2 layers $Ba_{0.5}Sr_{0.5}TiO_3$ film on Pt/Ti/SiO ₂ /Si substrate, (top ×5000, middle ×10000, bottom ×20000).	64
4.9. Cross-section SEM micrograph of 3 layers $Ba_{0.5}Sr_{0.5}TiO_3$ film on Pt/Ti/SiO ₂ /Si substrate, sintered at 800°C for 3 hours.	65
4.10. SEM micrograph of $Ba_{0.5}Sr_{0.5}TiO_3$ film on Si substrate.	65
4.11. EDS spectra of $Ba_{0.5}Sr_{0.5}TiO_3$ film on Si substrate, sintered at 800°C for 3 hours.....	66
4.12. EDS spectra of Si substrate.	66
4.13. EDS spectra of 6 layers $Ba_{0.5}Sr_{0.5}TiO_3$ film on Pt/Ti/SiO ₂ /Si substrate	67
4.14. EDS spectra of Pt/Ti/SiO ₂ /Si substrate.	67
4.15. The change of dielectric constant with frequency for 3 layers $Ba_{0.7}Sr_{0.3}TiO_3$ film (t = 600 nm).	68
4.16. The change of dielectric constant with frequency for 3 layers $Ba_{0.7}Sr_{0.3}TiO_3$ film (t = 600 nm).	69

4.17. Change in dielectric constant (at 1 kHz) with different sintering temperatures, for 3 layers $\text{Ba}_{0.5}\text{Sr}_{0.5}\text{TiO}_3$ films.	70
4.18. Dielectric constant of BST films with different compositions as a function of frequency for 600 nm films.....	71
4.19. The decrease in the Curie temperature of BaTiO_3 with Sr addition [11]	72
4.20. Dielectric constant of BST films with different compositions as a function of frequency for 400 nm films.	72
4.21. Dielectric loss as a function of frequency for 600 nm (3 layers) $\text{Ba}_x\text{Sr}_{1-x}\text{TiO}_3$ films.....	75
4.22. Dielectric loss of $\text{Ba}_{0.5}\text{Sr}_{0.5}\text{TiO}_3$ films as a function of frequency sintered at different temperatures for 600 nm films.	76
4.23. SEM micrograph of the surfaces of Pt/Ti/SiO ₂ /Si substrate: (top) prior to any thermal treatment, (middle) after annealing at 800°C for 1 hour. White dots are hillocks of Pt, (bottom) after annealing at 800°C for 3 hours. White dots have grown in size.	81
4.24. C-V curve for a 3 layers $\text{Ba}_{0.7}\text{Sr}_{0.3}\text{TiO}_3$ film.	84
4.25. C-V curve for a 3 layers $\text{Ba}_{0.9}\text{Sr}_{0.1}\text{TiO}_3$ film.	84
4.26. Polarization vs electric field behaviour for 600 nm $\text{Ba}_{0.9}\text{Sr}_{0.1}\text{TiO}_3$ film	85
A.1. Polarization versus electric field behaviour for 600 nm $\text{Ba}_{0.9}\text{Sr}_{0.1}\text{TiO}_3$ film at $V_x = 3.5$ V.....	97
A.2. Polarization versus electric field behaviour for 600 nm $\text{Ba}_{0.9}\text{Sr}_{0.1}\text{TiO}_3$ film at $V_x = 3$ V.....	98

A.3. Polarization versus electric field behaviour for 600 nm Ba_{0.9}Sr_{0.1}TiO₃ film at V_x = 2.5 V.....98

CHAPTER 1

INTRODUCTION

In the late 1980s, conventional processing methods for producing electroceramic materials (powder compacting, tape casting or screen printing techniques followed by sintering processes) were increasingly supplemented by thin film deposition techniques such as sputtering, pulsed laser deposition (PLD), chemical solution deposition (CSD), and chemical vapor deposition (CVD). During these deposition processes the electroceramic materials are synthesized on a microscopic scale without powder processing as an intermediate step, usually at temperatures much below the typical sintering temperatures for bulk ceramics [1].

This trend of thin film production was motivated by two events. Firstly, the newly discovered HTSC (high temperature superconductors) promised to show considerably larger current densities if deposited as thin films. Secondly, the idea originating in the late 1960s of ferroelectric-semiconductor memories was taken up again by utilizing the experience gained with the highly advanced Si semiconductor technology. These pioneering lines led to a broad research and development effort worldwide in order to combine the large variety of functions offered by the electroceramic thin films with the standard integrated circuit chips [1].

Ferroelectric thin films have been receiving renewed attention for electronic applications since 1989. The initial interest was for ferroelectric non-volatile memories (i.e. FeRAMs [ferroelectric random access memories]), and this was

followed by the development of ferroelectric thin films in the paraelectric phase, for use as high permittivity dielectrics for DRAMs (dynamic random access memories).

Most recently, there has been a substantial interest in the use of high permittivity oxides as a replacement of SiO₂ as the gate dielectric in mainstream Si CMOS (complimentary metal-oxide-semiconductor) devices [2].

For DRAMs, improvements in density, cost, speed, and immunity with scaling are critical. Up to recent years, SiO₂ has been used as the capacitor dielectric material for information storage in dynamic random access memories (DRAMs). To compensate for the charge storage density loss resulting from scaling (reducing the dimensions thus the area of the capacitor), thickness of SiO₂ layer has to be decreased continuously. However, it was seen that SiO₂ thickness couldn't be reduced below a critical value that is set by the start of quantum mechanical tunneling of electrons through the dielectric. This tunneling creates a high leakage current that makes charge storage impossible. So, to further increase the storage density, materials with high dielectric constant are expected to be employed to increase the capacitance per unit area of the storage cell while keeping the thickness thick enough to prevent leakage current. Ta₂O₅ was the first such material introduced into production of DRAMs, using metal-insulator-semiconductor (MIS) structures. Later, higher dielectric constant (K) materials will be introduced, to increase the capacitance per unit area. Finally, materials with $K > 100$ will need to be exploited. Barium Strontium Titanate (BST) is such a material, but it has serious problems that make it doubtful whether BST can effectively be utilized as the storage capacitor dielectric. The most difficult problem is that it is very difficult to scale BST's thickness into the desired range without preventing high leakage [3]. The high dielectric constant, low dielectric loss and lack of fatigue or aging problems are the major advantages of BST thin films for DRAM applications.

BST thin films are synthesized by generic thin film deposition techniques: RF-magnetron sputtering, pulsed laser deposition (PLD), metalorganic chemical vapor deposition (MOCVD) and chemical solution deposition (CSD). CSD method offers

advantages like stoichiometry control, homogeneity, low sintering temperatures and most importantly low capital cost, making it process of choice for scientific research and development.

In this study, BST films were deposited by coating the BST solutions prepared by chemical solution technique on Si and Pt/Ti/SiO₂/Si substrates using spin-coating technique, in order to measure dielectric properties and to check whether the dielectric properties are promising for DRAM applications and possibly for uncooled infrared detector and microwave monolithic integrated circuit applications. This thesis is composed of five chapters. Chapter 1 presents an introduction to DRAMs and the materials for this memory technology, underlining the need for a high dielectric constant material like BST. Chapter 2 consists of information on theory of dielectrics, material properties and application fields of BST, common deposition methods for BST thin films and chemical solution deposition in particular. Chapter 3 describes the experimental procedure, mainly solution preparation, coating and heat treatment of the BST films. Chapter 4 consists of the results on solution characterization, crystallization studies, microstructural characterization and dielectric measurements and discusses the results by correlating the properties to microstructure and processing parameters. Conclusions and further suggestions are presented in Chapter 5.

CHAPTER 2

LITERATURE SURVEY

2.1. Dielectric and Ferroelectric Properties of Materials

2.1.1. Dielectric Properties

Dielectric materials are insulators, as they do not conduct electricity. The dielectric constant (relative dielectric constant or relative permittivity) is a measure of the ability of a material to store charge relative to vacuum and is a characteristic property of a material. Capacitance of a material is defined as charge stored in the material per unit voltage applied:

$$C \text{ (Farad)} = Q \text{ (Coulomb)} / V \text{ (Volt)} \quad \text{Eq. [2.1]}$$

For a parallel plate capacitor having no dielectric between the plates, capacitance is equal to

$$C = \frac{\epsilon_0 \times A}{d} \quad \text{Eq. [2.2]}$$

where ϵ_0 is the permittivity of vacuum, A is the area of each plate, and d is the distance between the plates. When a dielectric material is placed between the plates, the capacitance changes to

$$C = \frac{\epsilon \times A}{d} \quad \text{Eq. [2.3]}$$

Relative dielectric constant K (ϵ_r), is the ratio of permittivity of the medium to the permittivity of free space, ϵ/ϵ_0 .

In addition to dielectric constant, three other properties are important in determining the insulating characteristics of a material: Electrical resistivity (ρ), the dissipation factor ($\tan\delta$) and the dielectric strength.

ρ is simply a measure of the resistance that a unit cube of the material offers to current flow in a given (dc) field. In an ac field, the electrical resistivity and dielectric constant are related by the dissipation factor which measures the energy loss per cycle (usually in the form of heat) from the material.

If a sinusoidal potential $V = V_0 \exp(i\omega t)$ is applied to the dielectric, the charge must vary with time, which constitutes a charging current, I_c :

$$Q = CV; \text{ so } I_c = \frac{dQ}{dt} = C \frac{dV}{dt} = i\omega CV = \omega CV_0 \exp[i(\omega t + \pi/2)] \quad \text{Eq. [2.4]}$$

The charging current in an ideal dielectric thus leads the applied voltage by $\pi/2$ radians (90°) [4].

In addition to the charging current associated with the storage of electric charge by the dipoles, a loss current must also be considered for real dielectrics. The loss current arises from two sources: (1) The long-range migration of charges, e.g., dc Ohmic conduction and (2) the dissipation of energy associated with rotation or oscillation of dipoles. The latter contribution to the dielectric losses is a consequence of the charged particles having a specific mass and, therefore, an inertial resistance to being moved. Electrical energy from the field is lost in the overcoming of this inertia

during polarization. The ac conduction from the inertial resistance and the dc conduction are both in phase with the applied voltage

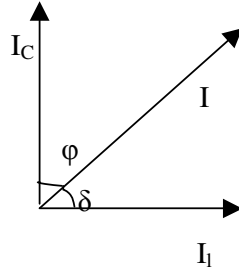


Figure 2.1. Charging current I_C and loss current I_l in a dielectric [4].

Consequently a loss current in the dielectric can be written as

$$I_l = (G_{dc} + G_{ac})V \quad \text{Eq. [2.5]}$$

where G is the conductance in units of Siemens, mho, or ohm^{-1} . The total current I_T for a real dielectric material is thus the sum of equations [2.4] and [2.5]:

$$I_T = I_C + I_l = (i\omega C + G_{dc} + G_{ac})V \quad \text{Eq. [2.6]}$$

As shown in Figure 2.1, the total current in a real dielectric is a complex quantity which leads the voltage by an angle $(90 - \delta)$ where δ is called the loss angle [4].

An alternative way of expressing the concept of a real dielectric possessing both charging and loss processes is to use a complex permittivity to describe the material:

$$\epsilon^* = \epsilon' - j\epsilon'' \quad \text{and} \quad k^* = \epsilon^* / \epsilon_0 = k' - ik'' \quad \text{Eq. [2.7]}$$

where ϵ' and ϵ'' are the real and imaginary parts of complex permittivity, respectively whereas k^* , k' and k'' are complex relative dielectric constant, real part of complex relative dielectric constant and imaginary part of complex relative dielectric constant, respectively [4]. Thus, the total current in the dielectric can now be expressed in terms of the single material parameter k^* , since

$$C = k^* \times C_0 \text{ where } C_0 \text{ is the capacitance of vacuum, so } Q = CV = k^* C_0 V \text{ Eq. [2.8]}$$

$$\text{and } i = \frac{dQ}{dt} = C \frac{dV}{dt} = k^* C_0 i\omega V = (k' - ik'') C_0 i\omega V_0 \exp(i\omega t) \text{ Eq. [2.9]}$$

$$\text{and thus } I_T = i\omega k' C_0 V + \omega k'' C_0 V \text{ Eq. [2.10]}$$

The first term on the right-hand side of the equation [2.10] describes the charge storage in the dielectric and k' is thus called the charging constant or often just the dielectric constant and ϵ'' and k'' are referred to as dielectric loss factor and relative loss factor, respectively. The loss tangent, loss angle, or dissipation factor, $\tan \delta$, is defined as

$$\tan \delta = \epsilon'' / \epsilon' = k'' / k' \text{ Eq. [2.11]}$$

The dissipation factor represents the relative expenditure of energy to obtain a given amount of charge storage. Commonly, $\tan \delta \times 100$, called as “percent dissipation” is used [5]. The product, k'' or $k' \tan \delta$ is sometimes termed as the total loss factor, and provides the primary criterion for evaluating the usefulness of a dielectric as an insulator. The inverse of the loss tangent, $Q = 1 / \tan \delta$, is used as a Figure of merit in high frequency insulation applications.

2.1.2. Polarization

When a material is placed in an electric field, the atoms and the molecules of the materials become polarized so that we have a distribution of the dipole moments in the material. An electrical dipole moment, p , is simply a separation between a negative and a positive charge Q of equal magnitude: $p = Q \times a$, where Q is the electrical charge and a is the vector from the negative to the positive charge. This separation of positive and negative charges and the resulting induced dipole moment are termed as polarization, P , which is equal to the total dipole moment induced in the material by the electric field: $P = N \times p_{av}$, where N is the number of molecules per unit volume and p_{av} is the average dipole moment per molecule. The polarization, P , induced in a dielectric medium when it is placed in an electric field depends on the field itself. To express the dependence of P on the field, E , we define a quantity called the electric susceptibility, χ , so that

$$P = \chi \epsilon_0 E. \quad \text{Eq. [2.12]}$$

There are four primary mechanisms of polarization in ceramics and glasses. Each mechanism involves a short-range motion of the charge and contributes to the total polarization of the material. These are: electronic polarization, ionic (atomic) polarization, dipolar (orientational) polarization and interfacial polarization. Of these mechanisms, dipolar polarization is important for ferroelectrics. It is responsible for dielectric constant values of 10^4 or more in such materials. Rather than rotating, the dipoles align and reverse align by cooperative ion displacements in ferroelectrics [5].

2.1.3. Ferroelectric Phenomena

Crystals are divided into 32 classes of point groups according to the symmetry they possess. Of these 32 groups 20 of 21 are non-centrosymmetric (lacking center of symmetry) and develop potential difference when a stress is applied on them. These are piezoelectric materials. 10 of 20 non-centrosymmetric groups have spontaneous polar axis and this spontaneous polarization depends on temperature. These 10

groups are pyroelectric. Ferroelectrics are subset of pyroelectrics; their spontaneous polarization is reversible by the application of electric field (Figure 2.2).

As an example, for PbTiO_3 , (Figure 2.3 shows the paraelectric and ferroelectric phases and the displacement of Ti^{+4} ion from the equilibrium position in the tetragonal phase below Curie temperature) the Ti^{+4} ion is displaced up or down from the body center position in the unit cell, this distorted structure is stable up to a temperature, 490°C (120°C for BaTiO_3), which is so called Curie temperature of the material, the temperature at which a paraelectric material goes into a phase transition from a non-polar phase to polar ferroelectric phase. This displacement is the origin of spontaneous polarization. The centers of negative and positive charges do not coincide. Since the Ti ion is displaced from the equilibrium body center position with respect to barium and oxygen ions there is a net polarization or dipole moment (positive and negative charges separated by a distance) exists in the unit cell. The alignment of dipole moments in the same direction along neighboring unit cells creates the domains. The domains oriented in different directions are separated by boundaries, called domain walls.

Above the Curie point, the temperature of phase transition, the dielectric permittivity falls off with temperature according to the Curie-Weiss law (Figure 2.2)

$$\varepsilon = \varepsilon_0 + \frac{C}{T - T_0} \sim \frac{C}{T - T_0} \quad \text{Eq. [2.13]}$$

where C is the Curie constant, T_0 ($T_0 \leq T_c$) is the Curie-Weiss temperature. In the paraelectric regime, the spontaneous polarization is zero but the permittivity remains high.

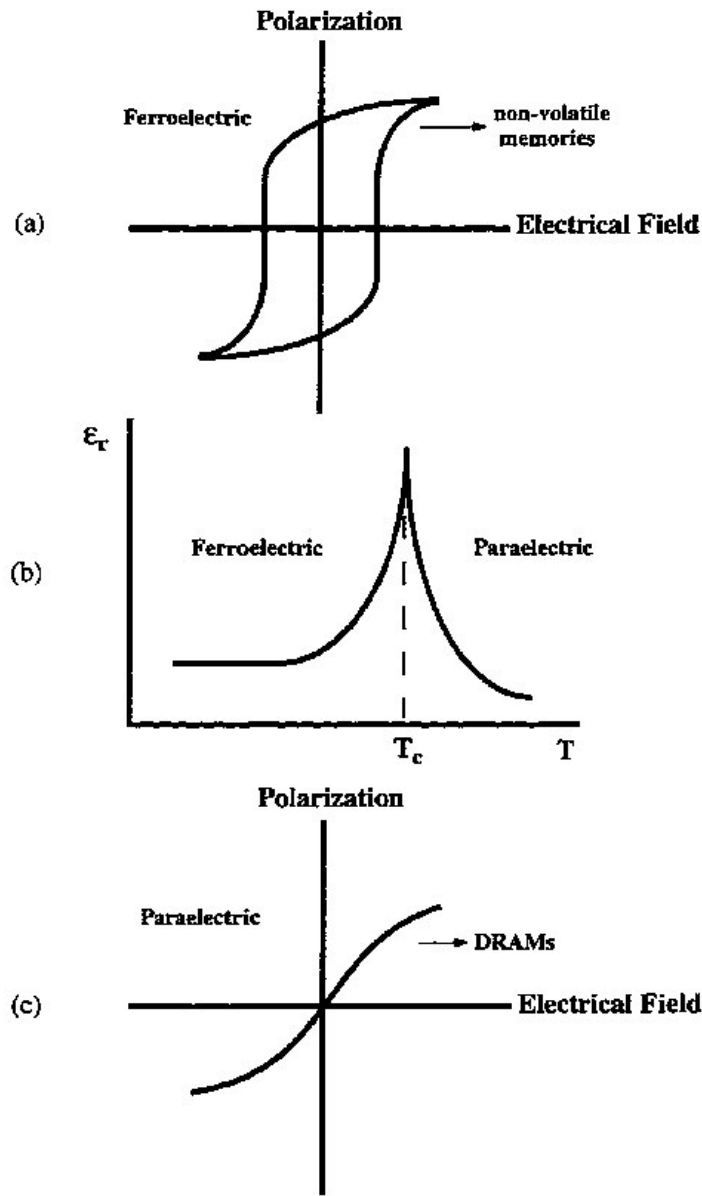


Figure 2.2. Schematic of (a) the polarization behaviour of a ferroelectric material below its Curie point, (b) the change in permittivity at a ferroelectric-paraelectric phase transition and (c) the polarization behaviour of a ferroelectric material above its Curie point [6].

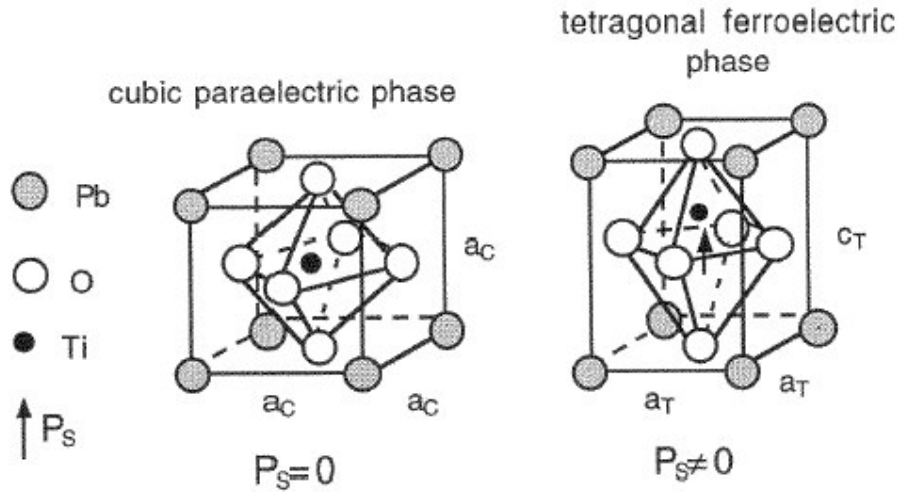


Figure 2.3. The displacement of Ti^{+4} ion, for PbTiO_3 , from the body center of the cubic perovskite structure, resulting in distortion of cubic structure and formation of tetragonal perovskite structure [7].

With no electric field, the net spontaneous polarization is 0 due to random orientation of dipoles in the domains. But when you apply an electric field, or “pole” the material, the domains are oriented in the same direction by domain wall movement and the material will have a net spontaneous polarization as shown in Figure 2.4.

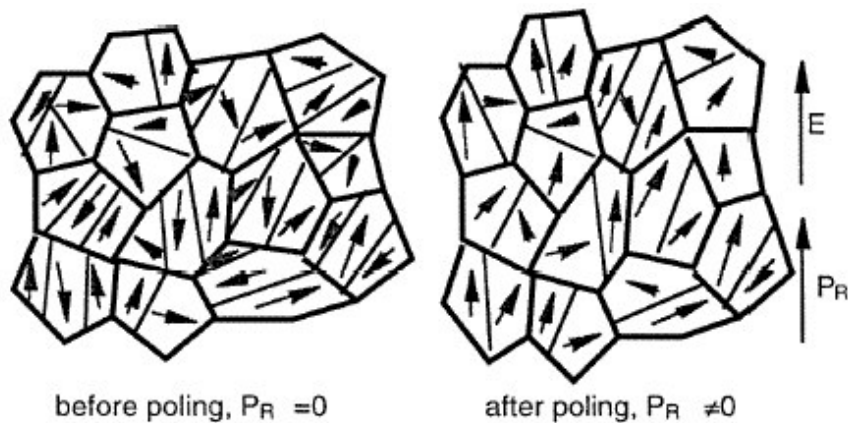


Figure 2.4. Creation of net polarization by poling [7].

2.2. Ferroelectric Materials

2.2.1. Ferroelectric Materials

Ferroelectric ceramics were born in the early 1940s with the discovery of the phenomenon of ferroelectricity as the source of the unusually high dielectric constant in the ceramic barium titanate capacitors. Since that time, they have been the heart and soul of several multibillion dollar industries, ranging from high-dielectric constant capacitors to later developments in piezoelectric transducers, positive temperature coefficient devices, and electrooptic light valves. Materials based on two compositional systems, barium titanate and lead zirconate titanate, have dominated the field throughout their history. The more recent developments in the field of ferroelectric ceramics, such as medical ultrasonic composites, high-displacement piezoelectric actuators (Moonies, RAINBOWS), photostrictors, and thin and thick films for piezoelectric and integrated-circuit applications have served to keep the industry young amidst its growing maturity [8].

Figure 2.5 shows the classes of crystals according to the symmetry they possess. Ferroelectric materials that are technologically important are ceramic perovskites that constitute BaTiO₃ (Barium Titanate), PZT (Lead Zirconate Titanate), PLZT (Lead Lanthanum Zirconate Titanate), PT (Lead titanate), PMN (Lead Magnesium Niobate) and solid solutions of elements that form the perovskite structure.

2.2.2. Hysteresis Loops

The ferroelectric materials give non-linear polarization response to the applied electric field. Figure 2.6 shows the hysteresis behaviour of a ferroelectric film [7]. With the application of the electric field domains start to align with the applied E-field, and polarization goes linear with the applied field. Then, further increase in the electric field helps domain walls to move easily and polarization starts to increase faster. When all the domains are oriented in the same direction the polarization saturates, further application of the electric field will not make any difference. This

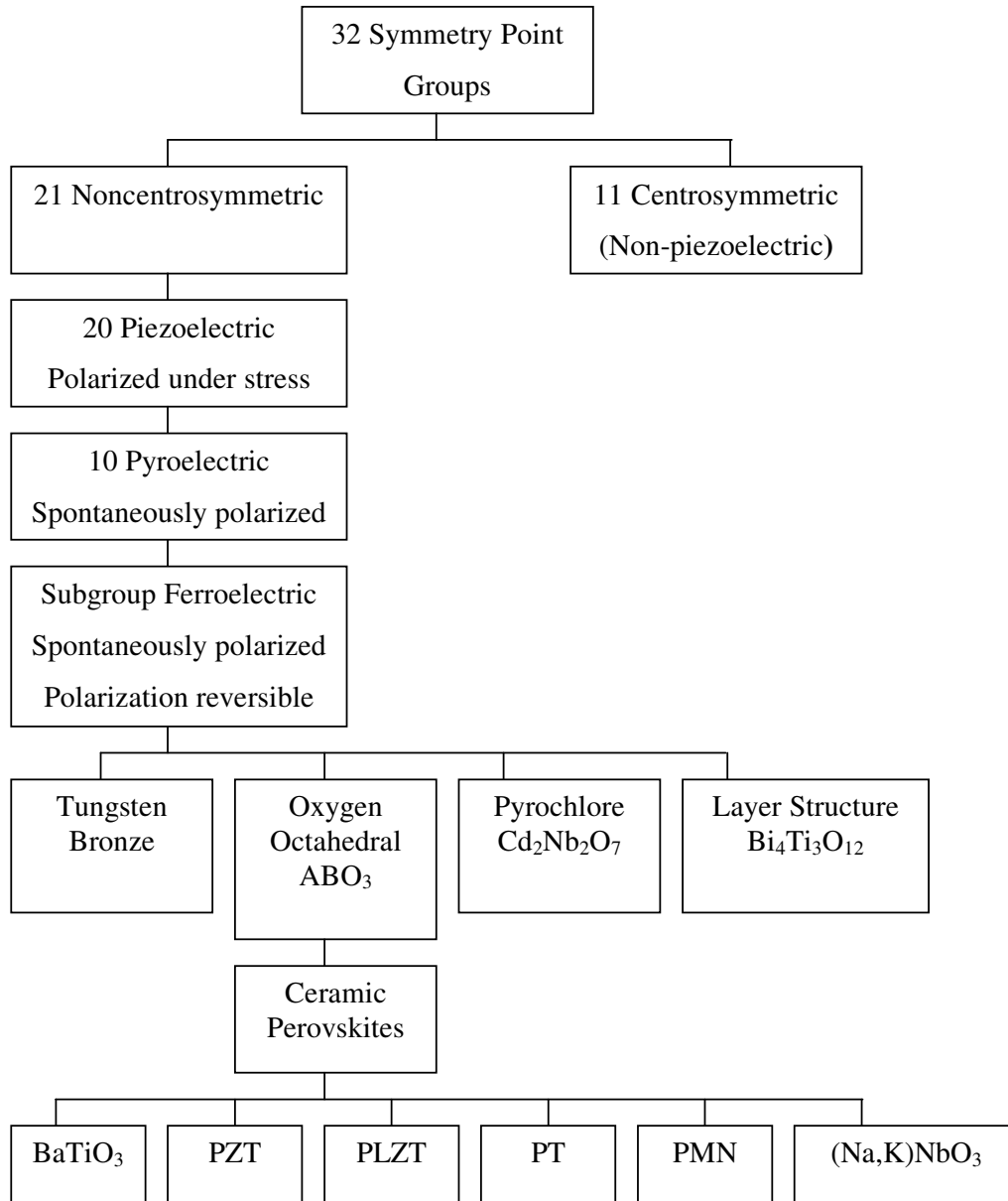


Figure 2.5. Classification of crystals according to the symmetry and polarization they possess [8].

maximum polarization value is called saturation polarization, P_s . When E-field is removed, polarization drops to a certain value, P_r called remnant polarization; polarization remained in the material when the applied field is 0. The application of electric field in the opposite direction causes alignment of domains in the opposite

direction and at a certain value of electric field called coercive field, ($-E_c$) the net polarization in the material becomes zero. When the electric field is increased in the reverse direction, polarization saturates again, this time in the reverse direction. Then to complete the cycle, electric field is removed, material will have $-P_r$. Application of electric field in the initial direction, brings the material to zero polarization state at coercive field, E_c .

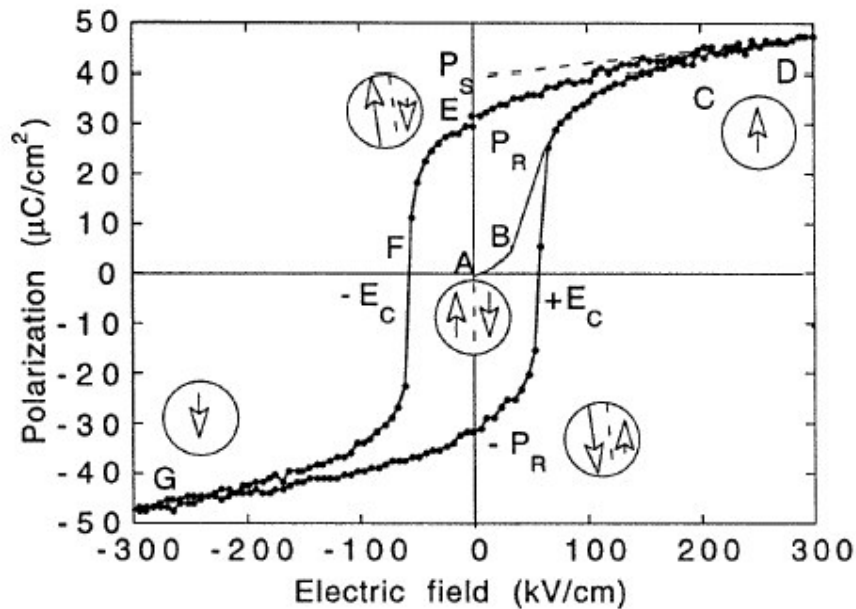


Figure 2.6. Hysteresis loop for a PbTiO_3 thin film [7].

2.2.3 Barium Strontium Titanate System

BaTiO_3 is a ferroelectric perovskite and has been well studied in bulk ceramic form where the measured permittivities are well into thousands. BaTiO_3 in bulk form is still used as multilayer or discrete capacitors. It derives its high dielectric constant from an ionic displacement and therefore differs from lower dielectric constant materials such as SiO_2 , which experience an electronic displacement only with changing applied voltage [9].

Various elements have been doped to ceramic BaTiO_3 and the effect of alloying elements on the ferroelectric-paraelectric transition temperature has been reported. Figure 2.7 gives the effect of isovalent alloying elements on the Curie temperature (ferroelectric-paraelectric transition temperature, T_c) of bulk BaTiO_3 . The utilization of BaTiO_3 - SrTiO_3 solid solution allows the Curie temperature of BaTiO_3 be shifted from 120°C to around room temperature for $\text{Ba}_x\text{Sr}_{1-x}\text{TiO}_3$ films. For Sr addition into BaTiO_3 , the linear drop of T_c is 3.4°C per mol%. Therefore, 30 mol% Sr ($x = 0.7$) would bring the T_c down to room temperature [10].

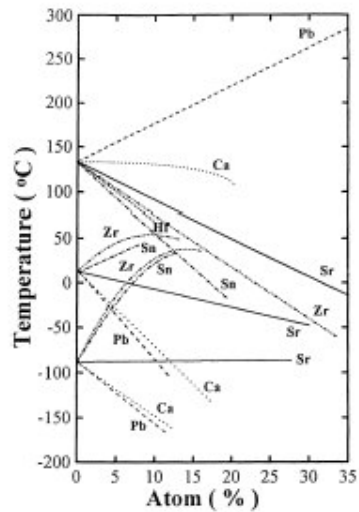


Figure 2.7. Effect of several isovalent substitutions on the ferroelectric-paraelectric transition temperature of ferroelectric BaTiO_3 [11].

BST as thin films have been under investigation for about 15 years starting from 90's. The initial interest in BST thin films was due to its high dielectric constant, low dielectric loss, high dielectric breakdown and composition dependent Curie temperature enabling it to be in paraelectric state as well as ferroelectric state, all of which makes it a candidate for replacing SiO_2 as charge storage dielectric for DRAMs (dynamic random access memories) [12, 13]. Recently, research on BST thin films concentrates also on uncooled infrared detector applications [14, 15] and

on microwave monolithic integrated circuit applications [16], exploiting its pyroelectric and electric field dependent (tunable) dielectric constant, respectively.

BST films are polycrystalline. Their properties heavily depend on composition, stoichiometry, microstructure (grain size and grain size distribution), film thickness, characteristics of the electrode material, and homogeneity of the film. The BST thin film growth method significantly affects the composition, stoichiometry, crystallinity and grain size of the film and, consequently, its dielectric properties. A variety of techniques (Table 2.1) such as rf-sputtering, laser ablation, metalorganic chemical vapor deposition (MOCVD), metalorganic deposition (MOD) and sol-gel processing have been used to deposit BST thin films. Above methods are highly competitive, each having advantages and disadvantages in terms of homogeneity, processing temperature and processing cost. Because of the multicomponent nature of BST films, precise microscopic control of stoichiometry is essential for obtaining uniform single-phase films.

$Ba_xSr_{1-x}TiO_3$ films are not only paraelectric at the DRAM operating temperature range (0-70°C ambient and 0-100°C on chips) but also achieve maximum permittivity around the operating temperature. On the other hand, the volatilities of the BST components are lower than the Pb-based ferroelectric materials, thereby making it relatively easier to introduce into fabrication facilities [10]. Similar to $SrTiO_3$, it does not exhibit much frequency dependence of dielectric constant.

Barium-rich compositions of BST should be ferroelectric in theory, since BST is below its Curie temperature at room temperature for Ba-rich compositions. For mol % $Sr \leq 0.25$, the structure is ferroelectric tetragonal perovskite, for other compositions, for % $Sr \geq 0.25$, the structure changes to paraelectric cubic perovskite. Figure 2.8 shows the changes in the lattice parameter of $Ba_xSr_{1-x}TiO_3$ with composition. For thin films, only a few researchers reported hysteresis loops as an evidence of ferroelectricity. Cheng et al. explain the possible reasons for the disappearance of ferroelectricity in sol-gel derived BST thin films as follows: [14]

Table 2.1. Advantages and limitations of processes for producing BST thin films [10, 11].

METHOD	ADVANTAGES	LIMITATIONS
Chemical Solution Deposition	<ul style="list-style-type: none"> • Inexpensive, low capital investment • Rapid sampling of materials • Homogeneity • Low processing temperatures 	<ul style="list-style-type: none"> • Phase control • Morphology • Reproducibility
Pulsed Laser Deposition	<ul style="list-style-type: none"> • Rapid sampling of materials • Quickly produce new materials 	<ul style="list-style-type: none"> • Morphology • Point defect concentration • Scalability (small areas only) • Uniformity • High residual stress
Sputtering	<ul style="list-style-type: none"> • Cost • Uniformity • Scalability • Standard IC processing • Low growth temperatures 	<ul style="list-style-type: none"> • Point defect concentration • Residual stresses • Stoichiometry control • Slow deposition rate for oxides
MOCVD	<ul style="list-style-type: none"> • Uniformity • Morphology • Small • Scalability 	<ul style="list-style-type: none"> • Immature technology • Precursor stability • Precursor availability • Expensive

- It was observed that below a certain grain size called as critical grain size, although the material is in ferroelectric state (it is below its ferroelectric-paraelectric transition temperature), there was no anomaly observed for dielectric constant at the transition temperature. The reasons for the disappearance of the anomaly is not known precisely [7]. This critical size for the existence of ferroelectricity of BaTiO_3 (around 120 nm) is much larger than that of PbTiO_3 (around 7 nm). As an example, Cheng et al. gives the research of Tahan et al. [13] whose films having grain sizes ranging from 20 to 50 nm, and no ferroelectricity was present.

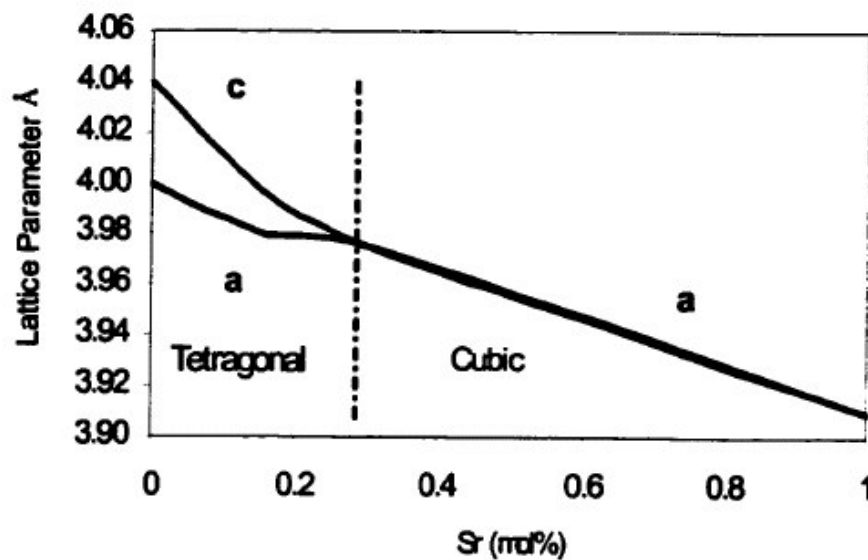


Figure 2.8. Lattice parameter change and stability regions of ferroelectric and paraelectric phases of BST with composition [10].

- The sol-gel deposition of BaTiO_3 films commonly results in polycrystalline, granular films with grain diameters of lower than 70 nm due to random nucleation in the pyrolyzed gel films. This is in contrast to $\text{Pb}(\text{Zr}, \text{Ti})\text{O}_3$ films, which can easily be grown by the sol-gel method into a columnar or epitaxial structure, because of heterogeneous nucleation from nanocrystalline pyrochlore phase into the perovskite phase at the substrate.

- The tetragonality (c/a) of BST films decreases with the increasing strontium content and a small value of c/a value may not be sufficient to create charge separation and spontaneous polarization in the films, so the fabrication of BST ferroelectric film is even more difficult than that of BaTiO_3 .

Figure 2.9 shows the variation of dielectric constant with temperature for bulk and thin film $\text{Ba}_{0.7}\text{Sr}_{0.3}\text{TiO}_3$. As can be seen from the graph, bulk BST undergoes a maximum in dielectric permittivity around 310K (slightly above room temperature) as addition of 30 % Sr to barium titanate shifts the Curie temperature of barium titanate to room temperature from 120°C . In contrast, thin film BST does not show a peak or anomaly in dielectric permittivity due to the absence of ferroelectricity in relation to the reasons above.

However, some researchers including Cheng, have been successful at fabricating ferroelectric BST thin films. The main point in their succession was achieving to fabricate BST films with columnar grains, having grain diameters greater than 100 nm, by coating very thin individual layers (< 10 nm [14]) using highly diluted solutions.

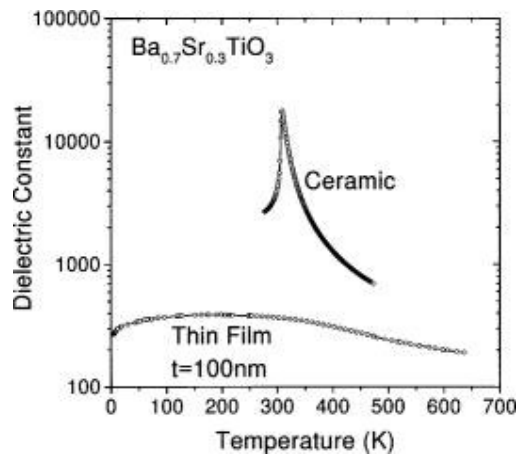


Figure 2.9. Variation of dielectric constant with temperature for bulk and thin film BST [17].

2.2.4. Applications of BST Thin Films

The primary electronic devices for which BST films investigated are (Table 2.2): DRAM capacitor dielectrics, uncooled infrared detectors and monolithic microwave integrated circuits.

Numerous reports are available in the literature involving the study of BST films for DRAM applications as well as on the study of BST thin films for microwave dielectric applications (such as phase shifters, varactors, delay lines etc). However, more studies on BST for DRAM applications have been reported because for these applications, synthesis of polycrystalline thin films is sufficient, whereas for microwave dielectric applications oriented grain or epitaxially grown films are required. The presence of grain boundaries increases the dielectric loss and may consequently limit the performance [16].

In sol-gel processing the precursor solution is either spin or dip-coated on the substrate at room temperature, in contrast, in almost all the other techniques (rf sputtering, electron beam evaporation, chemical vapor deposition and laser ablation) substrates are heated during film deposition. The hot substrates provide the adatom mobility of the deposited species and also act as an effective nucleation site to control the growth orientations of the films. When lattice matched substrates having identical crystal structures and similar thermal expansion coefficients are used, substrates promote epitaxial growth.

All the sol-gel deposited films are amorphous after deposition and needed to be post annealed at relatively high temperatures for crystallization. Films become stressed due to removal of organics during annealing. The other possible contributions of stress are due to lattice parameter mismatch between film and substrate and also due to change from amorphous to crystalline state. This intrinsic and extrinsic stress often destroys the ordered growth influenced by single crystalline substrate. Therefore, most of the sol-gel derived films are reported to be polycrystalline in nature [18].

Table 2.2. Major applications of BST films with relevant properties.

Application	Composition	Property	Reference
DRAM (Dynamic Random Access Memory)	$Ba_{0.5}Sr_{0.5}TiO_3$ (Paraelectric)	High dielectric constant, low leakage current	[19]
Uncooled infrared Detector	$Ba_{0.85}Sr_{0.15}TiO_3$ (Ferroelectric)	High dielectric constant and high pyroelectric coefficient	[15]
Phase Shifter	$Ba_{0.6}Sr_{0.4}TiO_3$ (Paraelectric)	Low dielectric loss, high tunability	[16]

2.2.4.1 BST Films in DRAMs

The main interest in producing high dielectric constant BST thin films is due to the efforts of semiconductor industry about finding an alternative high dielectric constant material for usage in DRAM's (dynamic random access memories).

The DRAM is the primary working medium for information storage in the ubiquitous microelectronic devices that comprise the entire litany of electronic systems. DRAM works very simply by using a submicron-sized capacitor, representing one bit of memory, to store a given amount of electrical charge: if the charge is present, it represents a digital "1"; if not then the bit is a "0". Each bit is addressed using a CMOS-FET (Complimentary Metal Oxide Semiconductor Field Effect Transistor), which acts as a valve for adding or removing the charge from the capacitor upon the application of a voltage. It is accepted that DRAM is volatile, and the information

held by a DRAM is accessed at speeds approaching those at which the microprocessor operates, while archival storage is handled by other means, such as magnetic media or flash memory, that operate much more slowly. Information in a DRAM must be refreshed by rewriting each bit on regular basis, as the charge in the capacitor “leaks” away, causing volatility. This refresh time is typically 256 ms [12].

In order to increase the stored charge density, DRAM’s should scale down, meaning that their size will be reduced. Scaling of DRAM’s results in shrinkage of SiO₂/Si capacitor area. Since, capacitance of the cell is directly proportional to the area, to maintain the same charge storage density, the thickness of the dielectric SiO₂ layer should be decreased according to parallel plate capacitor equation: $C = \frac{K \times \epsilon_0 \times A}{d}$, where K is the relative dielectric constant, A is the area of the top electrode, ϵ_0 is the permittivity of free space (8.85×10^{-12} Farad/m), and d is the thickness of the film.

But as SiO₂ thickness is decreased below critical 10 nanometers, the leakage current increases abruptly due to direct tunneling in the oxide layer. So scientists and engineers realized that to maintain the same capacitance density (capacitance per area), something other than reducing the thickness of oxide layer should be done.

These research efforts found two paths for solution to this scaling limit problem. First path is the production of complex shaped capacitors that have larger area than so called “planar capacitors”. But this solution increases the processing costs and it is not easily applicable to Si technology. Second path is the replacement of SiO₂ gate dielectric with a higher dielectric constant material so that thicker oxides can be placed on Si while maintaining the capacitance density and low leakage current during scaling. For example SiO₂ has a dielectric constant 3.9, replacement of SiO₂ with Si₃N₄ (has a dielectric constant between 7 and 9) can maintain the same capacitance density while having small enough leakage current due to prevention of tunnelling current by increasing the physical thickness of the oxide [12].

In the recent years thin film perovskite materials with high dielectric constant such as PZT, SrTiO₃ and (Ba,Sr)TiO₃ (BST) have been investigated as dielectric materials for future DRAM's. The best suited dielectric material would have a low leakage current and a high dielectric constant and would also be in paraelectric phase to avoid from fatigue from ferroelectric domain switching. SrTiO₃ has a smaller dielectric constant than BST and PZT is in ferroelectric phase at room temperature. Thus, BST is very appealing for DRAM capacitors [10].

So, the research is mainly focused on high and medium dielectric materials. The medium dielectric constant materials include Ta₂O₅, TiO₂, ZrO₂ and Y₂O₃ as main candidates. The candidates other than BST have dielectric constants smaller than 40 (Table 2.3), but BST has a dielectric constant ≥ 200 (for a 20 nm film). This means that BST can be exploited for more generations than Ta₂O₅ (tantalum pentoxide) which is now in the production line.

Table 2.3. Relative permittivity values and charge storage densities for medium dielectric constant materials [6].

Material	Relative Permittivity	C/A (fF/ μm^2)
Ta ₂ O ₅	25	13.8 (20.4)
TiO ₂	30-40	9.3
ZrO ₂	14-28	9.9
Y ₂ O ₃	17	4.7
Si ₃ N ₄ (comparison)	7	7-8.6

But, BST has some disadvantages:

- The additional set of new materials required to isolate and integrate BST in Si based chips.

- The thickness dependence of its dielectric constant.
- Like in most high-permittivity dielectrics, a significant time dependence exists for the polarization response which can limit the fraction of stored charge that can be read from a cell at the nanosecond timescales being approached by commercial microelectronic devices. This places particularly stringent tolerances on film quality, most conveniently measured in terms of dielectric loss tangent, which must be less than 0.005 for the DRAM dielectric.

- BST failure mechanisms are poorly understood and entirely different from those of SiO₂.

Despite its disadvantages, BST is still the only candidate material nominated for future use in DRAM cells starting from 2005 as declared in 2001 ITRS (International Technology Roadmap for Semiconductors) report [3]. This fact is the motivation for research and development in the field.

2.3. BST films on Si and Pt/Ti/SiO₂/Si substrates

The interaction between a thin film and its substrate can be a very important factor in determining the electrical properties of the film. When such a film is integrated into a device, there is an interface between the film and the substrate, and between the film and one or more electrodes deposited over the film. The device is usually subjected to further processing, involving heating the system to several hundred degrees, so the interactions between the film and the electrodes become more pronounced [20].

There are a number of criteria which affect the choice of the electrodes for thin dielectric films [21]:

- The electrode must have sufficiently low resistance,
- It must be chemically compatible with the semiconductor, and not react with the film,
- It must display adequate adhesion to both the film and underlying structure,
- It must be morphologically stable under the processing conditions,
- It may need to act as a diffusion barrier for oxygen and other species,

- It must provide suitable interfacial electronic properties,
- It may be necessary to utilize the electrode to control the film structure and orientation (As an example, recently MgO substrate is used for epitaxial growth of BST thin films instead of Pt/Ti/SiO₂/Si substrates [16]).

The traditional SiO₂ or Si-O-N dielectrics are grown directly onto silicon (which itself used as one capacitor electrode or plate), in a configuration known as a metal-insulator-semiconductor (MIS) capacitor. But, because of reaction with silicon, this cannot be adopted for the BST dielectric. Therefore a configuration was required in which the BST was in contact with a different bottom electrode, in a metal-insulator-metal (MIM) configuration. In addition, BST must be processed at relatively high temperatures and oxygen partial pressures (to form the oxide structure), with the implication that the electrodes must be stable against oxidation, and with the additional requirement for an oxygen barrier under the electrode to ensure that the contact (termed the plug) down to the underlying access transistor is not oxidized. Thus, the electrode material below BST should be a noble metal or a conductive oxide [12].

Gold and silver react with the perovskites during processing, having solid solubility in the perovskite lattice. Therefore, platinum has remained as the only viable metal for use as the bottom electrode for the ferroelectric-dielectric film devices, having the properties of high thermal conductivity, good stability in a high temperature oxygen environment, and its high Schottky barrier height which gives rise to a low leakage current.

Thus, the most commonly used metal electrode has been platinum. Since the adhesion of Pt to SiO₂ is poor, an adhesion layer has been typically used [21]. The material for this adhesion layer is usually Ti. So the bottom electrode combination for most ferroelectric materials is Pt/Ti/SiO₂/Si.

A serious problem associated with the utilization of Pt/Ti/SiO₂/Si electrode stack is the formation of hillocks at the surface of the substrate at elevated annealing temperatures. Hillocks are thin elevated features which protrude from the metal surface (Pt in this case) during thermal cycling [21]. The formation of hillocks has

been an obstacle in the development of ferroelectric devices, because they may cause the electrical short in the ferroelectric capacitor. The formation of hillocks in the Pt/Ti electrodes has been reported by many researchers. The hillock is believed to be related to compressive stress relief in Pt films which is mainly caused by the oxidation of Ti diffused along the grain boundaries during annealing [22].

2.4. Chemical Solution Deposition Technique

2.4.1. Process Chemistry

Chemical solution deposition techniques namely sol-gel processing and metalorganic deposition are extensively used for production of perovskite ceramic thin films and also specifically for barium strontium titanate thin films.

The wet chemical methods such as sol-gel and metalorganic deposition (MOD) have advantages over other thin film deposition techniques in that better composition control and better homogeneity can more easily be achieved. In addition, the process may be more economical for production, because no high vacuum systems are needed [23]. This lower capital investment cost also made this technique attractive not only for making usable devices but also for scientific research.

Materials that are used in modern ceramic and device technology require high purity and close control over composition and microstructure. Since the chemical reactants for CSD can be purified conveniently by distillation and crystallization, films of high purity can be fabricated by CSD [24]

A very important advantage of CSD is that as the elements that will form the final compound mix at the molecular level, this means that the diffusion distances in the inorganic film after pyrolysis required to achieve thermodynamically stable phases are very short. This ultimate mixing and high reactivity also results in homogeneous and dense films [24].

The basic principle of chemical solution deposition is to prepare a solution of elements of the desired compound in a solvent and then coating this solution to a substrate and let the solution polymerize to form a gel and then fire this gel to obtain an inorganic oxide [24]

There are essentially two kinds of sol-gel technology. The first or colloidal method involves the dispersion of colloidal particles in a liquid to form a sol and then the destabilization of the sol to form a gel. The second method involves the polymerization of organometallic compounds such as alkoxides to produce a gel with a continuous network. The preparation of BST films in this thesis is based on forming a solution of alkoxides of Ba, Sr and Ti.

Various precursors-solvents and stabilizers are employed in the production of films. Since, the precursors (and solvents) used in the production determines the final product, different precursors yield different solutions and films.

Important and typical precursors for making solid solutions are alkoxides of the general composition $M(O-R)_n$, where R is an alkyl radical (CH_3 , C_2H_5 , etc.). Their properties and reactions affect the preparation process and determine the product features.

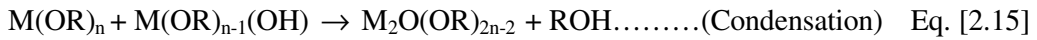
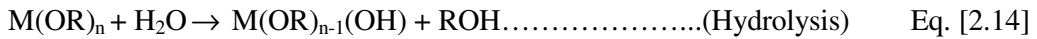
The ideal compound to be used as precursors should satisfy following criteria:

- It should have high metal content: To minimize the volume change during the change from metalorganic solution to inorganic film.
- High solubility in a common solvent with other starting compounds.
- It should be chemically compatible with other compounds in the formulation.
- Cost effective to produce: As the capital equipment requirements are small (e.g. no high vacuum systems are needed), the cost of sol-gel is low, and the precursors should not change this advantage.
- Thermally decompose without evaporating, melting or leaving a carbon deposit.

Criteria for solvents:

- Solvents should have high vaporization rates: they should evaporate as quickly as possible. Vaporization depends on vapor pressure and also interaction between solvent and solute.
- Solvent must be carefully selected in order to get a solution with high concentration of necessary components, proper viscosity, and surface tension [24].

After coating the solution on the substrate, gelation; the transition from a solution into a solid starts by hydrolysis and condensation. The reactions are as follows:



By hydrolysis and condensation of alkoxides, a polymeric product is formed, organometallics and solvents reacts to form M-O-M (Metal-Oxide-Metal) bonds leading to gelation of the solution. To some extent, it may be possible to control the degree of gelation by using proper amount of water. Following parameters control degree of gelation: Water amount, solvent, temperature, complex ligands, and pH value.

In film coating, the homogeneity of the gels is very important. The major advantage of sol-gel processing for the preparation of ceramic materials is the fact that in a dried homogeneous gel, the atoms are arranged in a manner closer to that in the desired final crystalline phase than would be the case in a mixture of crystallites of the same composition. Sintering behaviour is therefore improved [24].

2.4.2. Spin Coating Process

There are mainly two methods for the coating of solutions in CSD process: Dip coating and spin coating. Spin coating is used more extensively than dip coating and it is the process used in this study so only it will be described.

Bornside et al. [25] divide spin coating process into four stages: deposition, spin-up, spin-off, and evaporation, although evaporation may accompany the other stages. Figure 2.10 shows the stages of spin coating schematically.

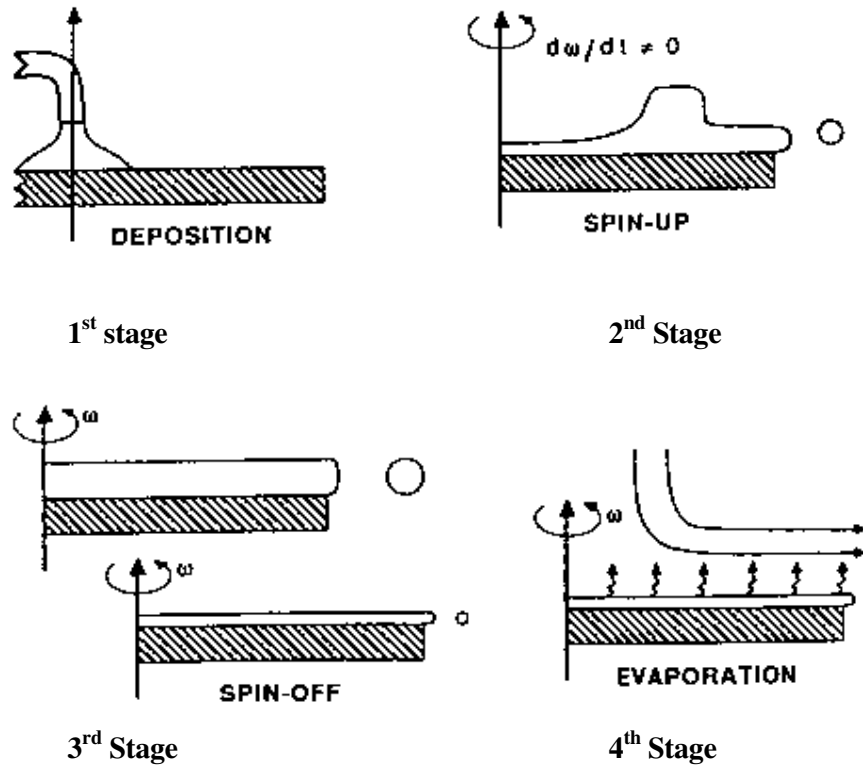


Figure 2.10. Four stages of spin-coating shown schematically [25].

An excess of liquid is dispensed on the surface during the deposition stage. For many solutions it is beneficial to dispense through a sub-micron sized filter to eliminate particles that could lead to flaws. It is important that the solution wets the surface of the substrate completely. In the spin-up stage, at which the substrate is accelerated to the desired rotation speed, the liquid flows radially outward, driven by the centrifugal force. In the spin-off stage, excess liquid flows to the perimeter and leaves as droplets. This stage is characterized by gradual fluid thinning. Fluid viscous forces dominate the thinning behaviour. As the film thins, the rate of removal of excess liquid by spin-off slows down, because the thinner the film, the greater the resistance to flow, and because the concentration of the non-volatile components increases raising the viscosity. In the fourth stage, evaporation takes over as the primary mechanism of thinning. A spun film arrives its final thickness by evaporation after the film becomes so thin and viscous that its flow stops [26].

Advantage of spin coating is that a film of liquid tends to become uniform in thickness during spin-off and, once uniform, tends to remain so provided that the viscosity is no shear dependent and does not vary over the substrate. This tendency arises due to the balance between two main forces: centrifugal force, which drives flow radially outward, and the viscous force (friction), which acts radially inward.

The thickness $h(t)$ of an initially uniform film during spin-off is described by [27],

$$h(t) = h_0 / (1 + 4\rho w^2 h_0^2 t / 3\mu)^{1/2} \quad \text{Eq. [2.17]}$$

where h_0 is the initial thickness, t is time, and w is the angular velocity: solution density ρ and solution viscosity μ assumed constant. Even films that are not uniform initially tend monotonically toward uniformity, sooner or later following the above equation.

Spinning is initially done at a slow rate to assure complete coverage of the substrate, followed by fast spinning for a longer duration.

2.4.3. BST Solution Preparation

2.4.3.1. Solvents and Precursors

For BST solutions, mainly alkoxides are used as precursors. In Table 2.4, some precursors and solvents used for BST solution preparation are listed.

For Ba and Sr precursors usually Ba and Sr acetates are preferred, whereas for titanium, either titanium (IV) isopropoxide or titanium (IV) butoxide is preferred. The molecular modification caused by chelation (modification of a chemical species by reacting with a solvent) reduces the susceptibility of the starting reagents to hydrolysis and condensation. This is important because the different hydrolysis and condensation rates of different alkoxides cause formation of inhomogeneous gels [24]. Titanium alkoxide is usually stabilized using chelating agents such as acetic acid and acetylacetone. The type of the precursors, thus the precursor structure influences the microstructure and dielectric properties. Usually, acetates are dissolved in acetic acid, then Ti precursor which can be stabilized before is added to this solution, and finally acetic acid or alcohol is added to dilute the solution.

2.4.3.2. Drying, Firing, Annealing of BST films

Thermal decomposition and crystallization behavior of the films is strongly dependent on precursors. The solvents evaporate at 150°-250°C. The Ba and Sr precursors decompose into carbonates at temperatures depending on the chain length of the alkoxide precursors. For short alkyl chain length alkoxides, including acetates and propionates, carbonates of Ba and Sr are formed at approximately 350°C. For acetate-based precursors, BaCO₃ and SrCO₃ are stable up to 550°C, with TiO₂ phase. Generally for alkoxides with short-chain alkyl groups, independent of the titanium alkoxide used, the crystallization of BST phase is delayed due to a formation of intermediate phase at temperatures around 650°C. This phase is said to be a complex carbonate phase, (Ba,Sr)₂Ti₂O₅CO₃. Then above this temperature, carbonates react to form crystalline (Ba,Sr)TiO₃. The crystallization is complete at 700-800°C [31].

Table 2.4. Different precursors and solvents for some sol-gel derived BST films.

Precursors	Solvents	Investigators
Barium acetate Strontium Acetate Titanium butoxide	Glacial acetic acid Acetylacetone	[14]
Barium acetate Strontium Acetate Titanium (IV) isopropoxide	Glacial acetic acid Ethylene Glycol	[13]
Barium acetate Strontium Acetate Titanium (IV) isopropoxide	n-propanol Glacial acetic acid	[28]
Barium carbonate Strontium carbonate Titanium (IV) isopropoxide	Ethylene glycol Citric acid	[29]
Barium acetate Strontium Acetate Tetrabutyl titanate	Methanol Glacial acetic acid Ethylene glycol dimethyl ether Acetylacetone (stabilizer)	[30]

For sol-gel derived barium titanate films, the decomposition pathway from the amorphous pyrolyzed material into the desired microstructure is believed to take place via intermediate carbonate (BaCO_3 and TiO_2) phases which first form at temperatures between 300° and 400°C . Other transitory phases, namely, $\text{BaTi}_2\text{O}_2\text{CO}_5$, have also been reported. Although BaTiO_3 perovskite phase is thermodynamically stable at temperatures as low as 410°C , typically, it is not observed in solution-deposited films until temperatures of 550°C or 650°C . Evidently, the rate of decomposition of species such as $\text{BaTi}_2\text{O}_2\text{CO}_5$ or the reaction rate of titania and BaCO_3 to yield BaTiO_3 as shown below is not rapid at temperatures between 400°C and 600°C :



These results for the retarded formation of BaTiO_3 are apparently in agreement with a study of the crystallization rate of $\text{Ba}_x\text{Sr}_{1-x}\text{TiO}_3$ thin films compared to PbTiO_3 and lead zirconate titanate (PZT). It was found that the crystallization rate in solution derived $\text{Ba}_x\text{Sr}_{1-x}\text{TiO}_3$ thin films was 300 times slower than in PbTiO_3 [18].

CHAPTER 3

EXPERIMENTAL PROCEDURE

3.1. Solution Preparation

The $Ba_xSr_{1-x}TiO_3$ solutions with compositions in the ferroelectric ($x \geq 0.75$) and paraelectric ($x < 0.75$) range were produced. The ferroelectric compositions were $Ba_{0.8}Sr_{0.2}TiO_3$ and $Ba_{0.9}Sr_{0.1}TiO_3$ whereas the paraelectric compositions were $Ba_{0.5}Sr_{0.5}TiO_3$ and $Ba_{0.7}Sr_{0.3}TiO_3$. The following table (Table 3.1) shows the compositions produced in this study.

Table 3.1. BST solutions with different compositions and their corresponding polarization states.

Composition Produced	Polarization State
$Ba_{0.9}Sr_{0.1}TiO_3$	Ferroelectric
$Ba_{0.8}Sr_{0.2}TiO_3$	Ferroelectric
$Ba_{0.7}Sr_{0.3}TiO_3$	Paraelectric
$Ba_{0.5}Sr_{0.5}TiO_3$	Paraelectric

3.1.1. Starting Materials

For solution preparation two different routes were tried. So, both routes will be explained. First solution was stable only for a week and the films produced by using the first route cracked even for the highly diluted films, for film thickness greater

than 400 nm. That's why a second solution system was tried. The precursors for the first solution were Ba acetate, $\text{Ba}(\text{CH}_3\text{CO}_2)_2$ [Aldrich-USA], Sr acetate, $\text{Sr}(\text{CH}_3\text{CO}_2)_2$ [Aldrich-USA], Ti(IV) isopropoxide, $\text{Ti}(\text{OCH}(\text{CH}_3)_2)_4$ [Aldrich-USA], and the solvents were glacial acetic acid, CH_3COOH [Merck-Germany] and 2-propanol $(\text{CH}_3)_2\text{CHOH}$ [Merck-Germany]. In the second solution, 2-propanol was substituted by ethylene glycol, $\text{HOCH}_2\text{CH}_2\text{OH}$ [Merck-Germany].

3.1.2. Solution Preparation

The first solution preparation method was adapted from Dien et. al. [28]. First, Ba & Sr acetates (for $x = 0.5$, equimolar amounts) were simultaneously dissolved in acetic acid at room temperature, at acetic acid / acetates mole ratio 25:1 and stirred by magnetic stirrer. A clear solution was obtained after an hour. Heating acetic acid to 80°C accelerates the dissolution of acetates. Then Ti(IV) isopropoxide was dissolved relatively easily in 2-propanol in another beaker by stirring (molar ratio 2-propanol:Ti(IV) isopropoxide = 30:1). Then the two solutions were mixed to obtain the parent solution. To remove residual particles, ultrasonic stirrer was used. The solution was filtrated by a filter paper and then stored. A flow chart of film preparation is given in figure 3.1. Amount of acetic acid is important because acetic acid prevents the reaction of Ti(IV) isopropoxide with water, which was formed by the reaction of 2-propanol with acetic acid:



The parent solution was diluted by adding acetic acid to obtain crack free films. Dilution with acetic acid was done at molar ratio of acetic acid / Ti(IV) isopropoxide 80:1. The diluted solution was not stable as the concentrated one. It was stable for 2-3 days, whereas the concentrated solution was stable for a week.

The second solution preparation method (Figure 3.2) was adapted from Tahan et. al. [32]. 25 milliliters of solution is taken as a base. Acetic acid to ethylene glycol ratio

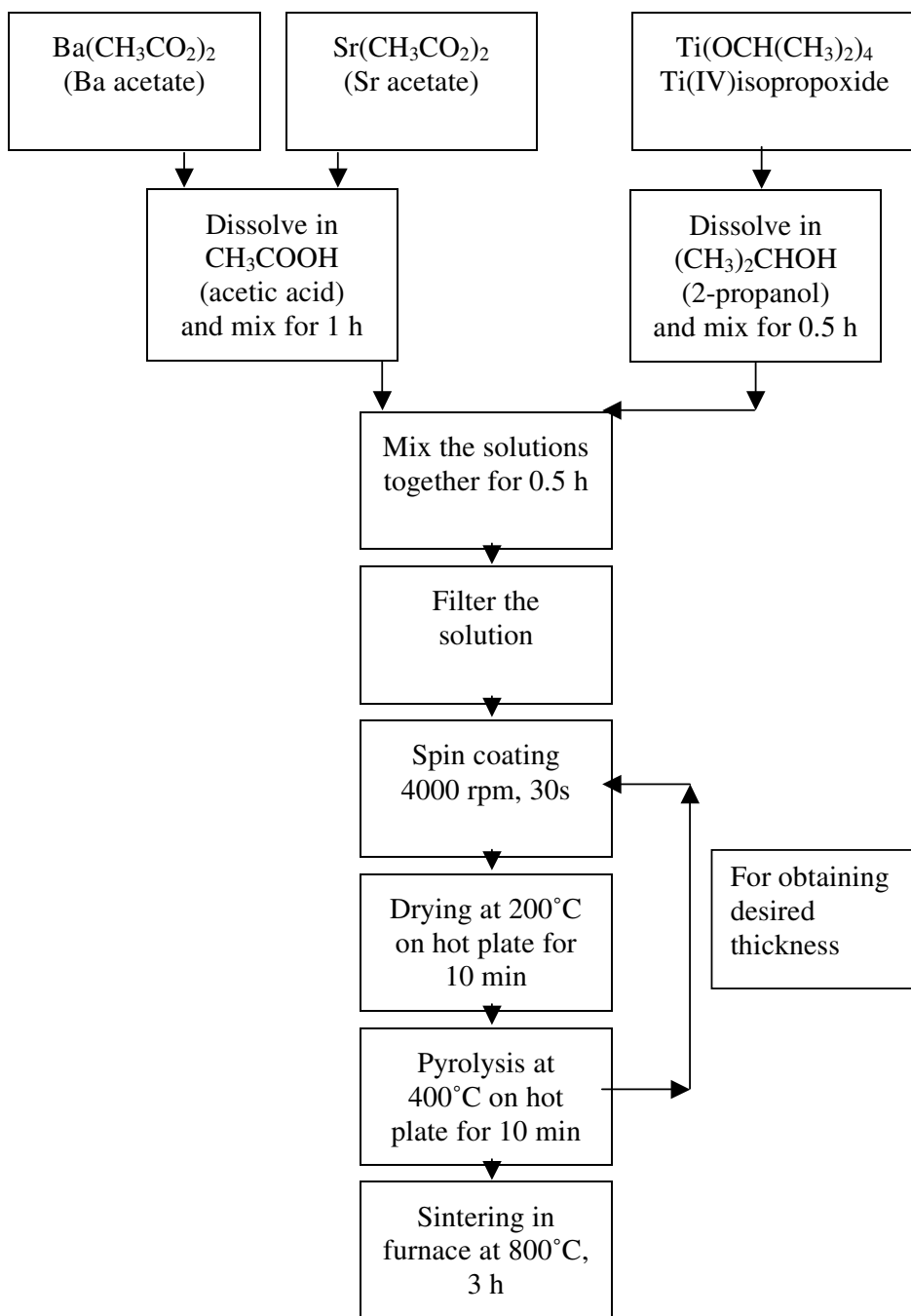


Figure 3.1. Flow chart for solution preparation (first route) and coating of films.

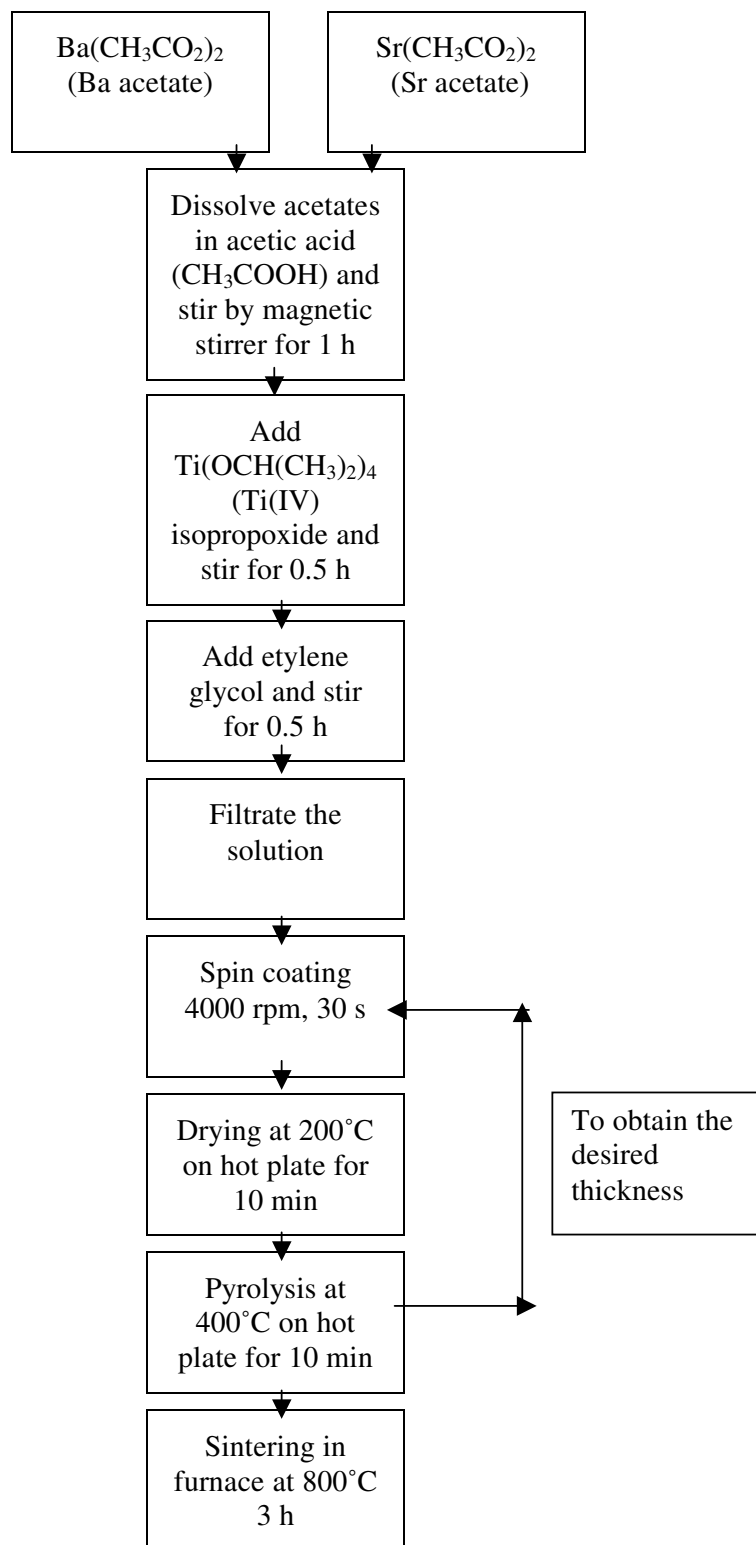


Figure 3.2. Flow chart for solution preparation (second route) and coating.

was taken as 3:1, as suggested. 0.4M and 0.75M solutions were prepared. In each case, calculations were repeated to determine the amounts of alkoxides.

Calculation for 0.4M $\text{Ba}_{0.5}\text{Sr}_{0.5}\text{TiO}_3$ solutions is provided as an example. Molarity is defined as number of moles of solute / number of liters of solution

$0.4\text{M} = x \text{ moles of BST} = x \text{ moles of Ti(IV) isopropoxide} / 0.025 \text{ liters of solution}$
Then, $x = 0.4 * 0.025 = 0.01 \text{ moles of Ti(IV) isopropoxide}$, then for $\text{Ba}_{0.5}\text{Sr}_{0.5}\text{TiO}_3$ composition, number of moles of Ba acetate = $x / 2 = 0.005 = \text{number of moles of Sr acetate}$.

Molecular weights of alkoxides are: Ba acetate: 255.43 gr/mol, Sr acetate: 205.71 gr/mol, Ti(IV)isopropoxide: 284.26gr/mol. So, molecular weights of precursors that will be added to the 25 ml solution are: Ba acetate: 2.84 gr, Sr acetate: 1.03 gr and Ti(IV)isopropoxide: 1.27gr.

The amounts of ethylene glycol and acetic acid were calculated for 25 ml. solution, using the molar ratio acetic acid to ethylene glycol 3:1. The amount of acetic acid was 19.82 gr. whereas ethylene glycol added was 6.83 gr. Molecular weights of these solvents were: Acetic acid: 60.05 gr/mol, Ethylene glycol: 62.07 gr / mol; 1 liters of ethylene glycol is 1.11 kg, whereas 1 liters of acetic acid is 1.05 kg.

First, Ba & Sr acetates (for $x = 0.5$, equimolar amounts) were simultaneously dissolved in acetic acid at room temperature, and mixed by magnetic stirrer. All acetic acid was added at once in order to prevent the formation of small aggregates of acetates. A clear solution was obtained around an hour, exact dissolution time depending on the concentration of the solution; the more acetic acid in the solution the easier the dissolution of acetates. Then Ti(IV) isopropoxide was added to the solution and stirred for 30 minutes. Finally, ethylene glycol was introduced to the solution, and solution mixture was stirred for additional 30 minutes. It was observed that ethylene glycol helps the dissolution of acetates. The solution was heated at 90°C for 1 hour to promote the reaction between the components of the solution.

Then, the solution was cooled to room temperature, filtrated by a filter paper and stored. The stock solution was stable for months.

Different alkoxides of different elements show a wide range of reactivity towards water which makes the preparation of multicomponent homogeneous systems difficult and also presents difficulties with premature gelation during film processing. This can be overcome by adding a chelating organic ligand into the solution to control the hydrolysis rates of the highly reactive alkoxide. Chelated solutions are more stable in air and are easy to handle in processing [27].

When trying to incorporate titanium into a sol-gel solution, it is common to use one of several commercially available alkoxides and to reduce its reactivity by modifying it with some appropriate chemical modifier, due to the different activities of alkoxides mentioned above. Acetic acid, as a modifier to the titanium alkoxide used in our study, titanium isopropoxide (TIP), was studied by Birnie [33]. Acetic acid (HOAc) is a popular modifier partly because it can easily dissolve a wide variety of different precursor molecules, helping the creation of a multitude of multi-cation solutions. However, the acetic acid can drive an esterification reaction with any alcohol that is present, thus liberating water into the solution. The esterification reaction can present some potential problems for sol-gel routes because, if the reaction is not controlled, the water liberated can cause precursor condensation reactions (and ultimately precipitation) in the solution. This is especially important when TIP – HOAc solutions are heated in order to dissolve other precursor components [33]. Thus, the gradual generation of water by the esterification reaction (during subsequent processing) can put restrictions on the time and temperature that might be used for carrying out these reactions. On the other hand, it has been pointed out that the esterification reaction is an efficient method for introducing water homogeneously into a solution and therefore avoiding the problems associated with mixing irregularities. Since the water generation (and therefore the solution hydrolysis) is a critical variable in sol-gel processing, it is important to understand how this varies with time and temperature [33].

The alcohol used in this study is ethylene glycol and ethylene glycol reacts with acetic acid to form an ester [34]:



The water generated by this reaction enhances hydrolysis and condensation. The addition of ethylene glycol as a cross-linking agent therefore leads to the polymerization of the precursor solution resulting in stable M-O-M (M: Metal, O: Oxide) linkages, with a decreased tendency to precipitation [32].

Coming back to the chelation, in the solution system used in this study, acetic acid reacts with titanium(IV) isopropoxide, according to the equation:



The modification of alkoxide compounds dictates the structure and properties of resulting species. The susceptibility of the starting reagents to hydrolysis and condensation is reduced by chelation, along with changes in other precursor properties such as pyrolysis behaviour [32].

Both solutions were diluted in order to prevent cracking and to decrease porosity.

3.2. Coating of Films on Substrates

3.2.1. Preparation of substrates

Prior to deposition, the surface of the substrates should be clean for good wetting and adhesion of the film to the substrate. Si and Pt/Ti/SiO₂/Si substrates were cleaned using standard procedure. They were ultrasonically rinsed in acetone, followed by rinsing in methanol and finally in deionized water and drying. Before cleaning, the substrates were cut into small pieces out of a wafer. The dimensions of the pieces

were 1cm to 1cm, in square shape, as spin coating demands symmetrical substrates for homogenous coating. The specifications of the Pt/Ti/SiO₂/Si substrates (INOSTEK - Korea) are given in Table 3.2.

Table 3.2. Specifications of Pt/Ti/SiO₂/Si substrate (INOSTEK Korea).

SUBSTRATE: SILICON WAFER	
Crystal Growth Method	CZ (PRIME)
Orientation	<100>
Thickness (µm)	525 ± 20
SiO ₂ LAYER	
Film Growth Method	Thermal Oxidation
Thickness (Å)	3000
Ti LAYER	
Film Growth Method	DC Magnetron Sputtering
Thickness (Å)	100
Pt LAYER	
Film Growth Method	DC Magnetron Sputtering
Thickness (Å)	1500
Orientation	(111)

3.2.2. Spin Coating

A double-sided tape was used to stick the substrate on the head of the spin coater then excess amount of solution was added on the substrate dropwise using Pasteur pipettes. The solution was coated on substrates by spinning with a spin coater (Chemat Technology Spin Coater) at 1000 rpm for 6 seconds for complete coverage of the substrate, and then at different speeds for different durations. Optimum spinning speed and time was determined as 4000 rpm for 30 seconds for 0.4M solution.

Individual layers coated are thin. So, multiple coating – pyrolysis cycles were needed to achieve the required thickness. The cracking of films due to shrinkage of films during drying is the reason for making use of multiple coating of layers because there is a limit for the thickness of the individual layer imposed by cracking considerations. This limit is up to 1 μm generally and is dependent on the nature of the precursors. For 0.4M solutions, each layer after coating and heat treatment was 200 nm thick, for spinning at 4000 rpm for 30 seconds.

3.2.3. Heat Treatment of the Films

Heat treatment step controls the microstructure of the films and microstructure controls the properties of the material. Specifically for this study, electrical properties like dielectric constant, dielectric loss and also ferroelectric properties depend on heat treatment parameters: time and temperature. Appropriate heat treatment can improve these properties by control of grain size and morphology; amount of crystallization and by prevention of cracking.

The as-deposited films were amorphous. The films were sintered in order to obtain crystalline perovskite films. The desired film thicknesses of 0.3 - 1 μm were obtained by multiple coating – heat treatment cycles. Coated films were instantaneously placed on a hot plate and dried at 200°C for 10 minutes. After cooling to room temperature, they were placed again on a hot plate preheated to 400°C and left to pyrolysis for 10 minutes.

Then, after obtaining the desired thickness by spin coating – pyrolysis cycles, annealing (sintering) was done at 600°, 700°, 750° and 800°C for 3 hours. Temperature parameter was changed while keeping time parameter constant at 3 hours. The sintering was done in low temperature furnace under air atmosphere by controlling the heating and cooling rates. The heating and cooling rate was 10°C / minutes in order to prevent cracking especially during cooling after the crystalline BST film develops due to slight thermal expansion coefficient difference between BST film and the substrate.

3.3. Characterization of Films

3.3.1. Structural and Morphological Analysis

The surface of the films was checked for cracks or inhomogeneities between the cycles of coating, pyrolysis and sintering with optical microscope.

The crystal structure of the films was determined by x-ray diffraction using Hanawalt's method. Philips Diffractometer with monochromatic Co- K_{α} radiation ($\lambda = 1.79021 \text{ \AA}$) was used as diffractometer. 2θ range between 20° - 80° was scanned. Crystallinity and possible orientation of the film was also checked by investigating the diffractograms and comparing with the powder diffractograms.

The surface and cross-section of the films were examined by scanning electron microscopy (SEM-Jeol JSM-6400). BST films were coated by 250 \AA nickel or gold as a conductive layer to prevent discharge. Baltec SCD 050 sputter coater was used for Ni coating. Thickness of the films was approximated from the cross-section SEM views. The composition of the films could not be controlled with EDS (energy dispersive spectroscopy) unit of the SEM. It can be seen from Table 3.3 that similar energy values of barium $L_{\alpha 1}$ and $L_{\beta 1}$ and the titanium $K_{\alpha 1}$ and $K_{\beta 1}$ peaks (4.465, 4.827, 4.510 and 4.931 keV) impose difficulties on peak deconvolution.

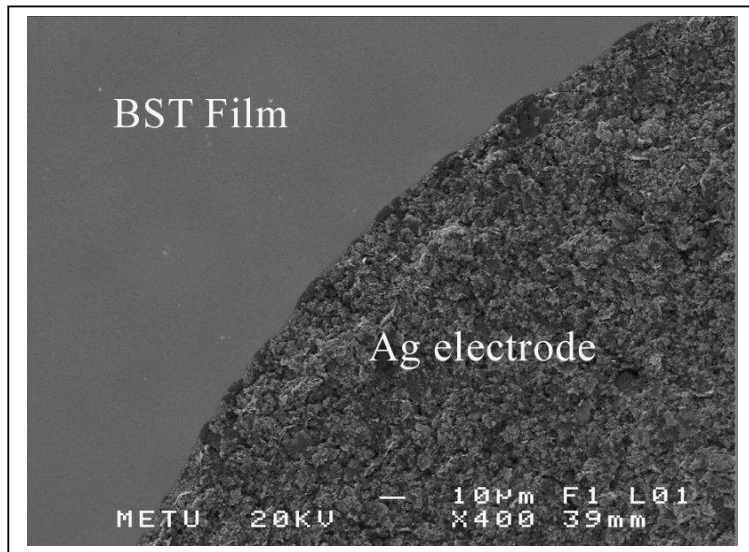
It is therefore not possible to get quantitative information using EDS. Also, another problem arises due to the submicron thickness of the films. Due to this small thickness electron beam easily penetrates through the film and accesses the underlying electrode material stack. The contribution of x-rays from Ti layer present on the substrate below Pt also deflects the total number of counts from Ti.

Table 3.3. X-ray energies of elements of BST film and Pt/Ti/SiO₂/Si substrate.

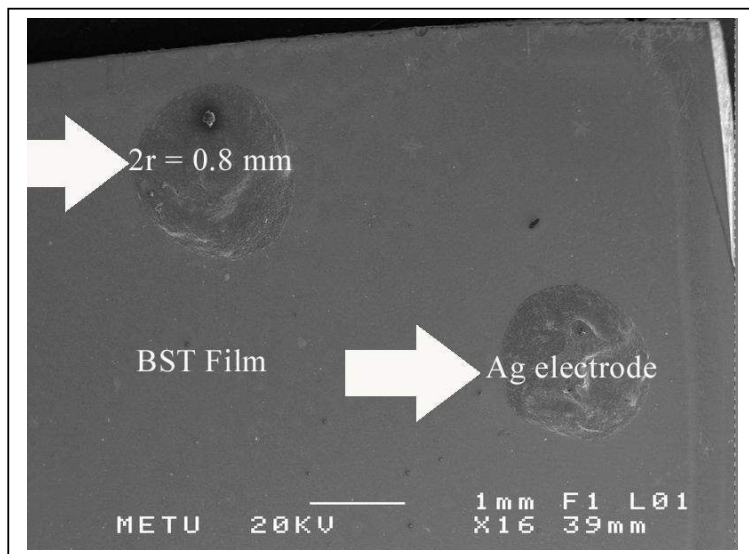
	Elements (Transitional energies in keV)					
	Ba	Sr	Ti	O	Pt	Si
K _{α1}	32.20	14.16	4,51	1,05	66,85	1,74
K _{β1}	36,38	15,84	4,93		75,77	1,83
L _{α1}	4,47	1,81	4,52		9,44	
L _{β1}	4,83	1,87	4,58		11,07	
L _{β2}	5,16				11,25	
L _{γ1}	5,53				12,94	
L _{γ3}	5,81	2,20			13,36	
L _λ	5,95	1,58	0,40		8,27	
M _α					2,05	
M _β					2,13	
M _γ	0,97				2,33	
M _ζ	0,60				1,60	

3.3.2. Dielectric and Ferroelectric Measurements

Dielectric measurements were made by using HP 4194A Impedance-Gain Phase Analyzer. MIM (Metal-Insulator-Metal) structure was formed in order to measure the dielectric properties. The bottom metal electrode in MIM structure was Pt layer of substrate (Pt/Ti/SiO₂/Si – Inostek-Korea), Ti as an adhesion layer between Pt and SiO₂. BST film was served as the insulator. To form the top metal electrode, silver paint (Agar Scientific) was used. The Ag solid compound was dissolved in IBMK (isobutylmethylketone) and deposited as small points on BST layer. 4 points were placed on each film, in order to see the possible change in measured properties. Figure 3.3 shows the Ag electrodes. Average radius of hemi-spherical like contacts vary between 0.8-1 mm.



(a)



(b)

Figure 3.3. SEM micrographs showing the surface of electroded BST films, (a) $\times 400$ (b) $\times 16$.

Capacitance and dielectric loss of the films was measured in the frequency range 100 Hz -10 MHz. Capacitance of the films was converted to dielectric constant by using the following formula assuming the parallel plate configuration:

$$C = \frac{K \times \epsilon_0 \times A}{d} \quad \text{Eq. [3.4]}$$

where K is the relative dielectric constant, A is the area of the top electrode (A_g), ϵ_0 is the permittivity of free space (8.85×10^{-12} Farad/m), and d is the thickness of the film.

The behavior of the films under voltage was tested by applying a dc voltage and monitoring the corresponding capacitance change, again by using HP 4194A Impedance-Gain Phase Analyzer.

Hysteresis loop was drawn by forming modified Sawyer-Tower circuit using a waveform generator, a HP 54645A oscilloscope and a large capacitance capacitor. The modified Sawyer-Tower circuit (Figure 3.4) was constructed by connecting a large capacitance capacitor in series to the BST film. Since, the charge on the two capacitors in series is the same, the voltage will drop mainly on the large capacitance capacitor (capacitance = 10 nF) according to $C = Q / V$. The voltage applied (V_x) is displayed on the x-axis on the oscilloscope, and voltage drop on the large capacitance capacitor (V_y) is displayed on y-axis. The measurements were made at 1 kHz. Since, charges on both the sample and the large capacitor are the same ($Q_s = Q_y$), the charge on the BST film (Q_s) can be found by finding the charge on the 10 nF capacitor which is equal to the multiplication of voltage drop on the large capacitor (V_y) and its capacitance. The charge is converted to polarization, $P = Q_s/A$, by simply dividing the charge of the capacitor to electrode area and voltage applied is converted to the electric field by dividing it to the film thickness, d. The equations followed in the construction of P-E curve are given below:

$$P = Q_s / A = (C_y * V_y) / A, \quad \text{Eq. [3.5]}$$

$$E = V_x / d$$

Eq. [3.6]

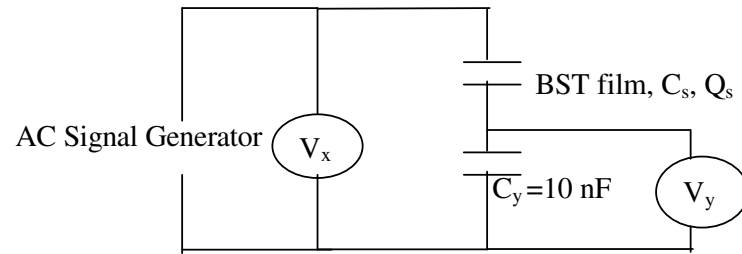


Figure 3.4. Schematic of the modified Sawyer-Tower circuit.

CHAPTER 4

RESULTS AND DISCUSSION

In this study, the aim was synthesizing BST solution by chemical deposition technique and obtaining homogeneous and crack-free BST films with satisfactory electrical properties. Two different systems of BST solution were tried in order to obtain a homogenous solution and reduce cracking in the coated films. Processing parameters like solution concentration, spinning speed, and sintering temperature were varied to obtain well-crystallized, homogeneous and dense films. X-ray diffraction and SEM were used for crystal structure determination and BST film-substrate interface control, respectively. Once the optimum parameters were set, effect of composition, sintering temperature and film thickness on electrical properties was studied by measuring dielectric constant and loss. The change of electrical properties with these parameters was correlated to microstructural changes. Dielectric properties of the films were measured with changing frequency. Capacitance – Voltage and ferroelectric measurements were also done.

Four different compositions of BST films were produced. $\text{Ba}_{0.5}\text{Sr}_{0.5}\text{TiO}_3$ and $\text{Ba}_{0.8}\text{Sr}_{0.2}\text{TiO}_3$ were coated on Si substrates and $\text{Ba}_{0.5}\text{Sr}_{0.5}\text{TiO}_3$, $\text{Ba}_{0.7}\text{Sr}_{0.3}\text{TiO}_3$ and $\text{Ba}_{0.9}\text{Sr}_{0.1}\text{TiO}_3$ were coated on Pt/Ti/SiO₂/Si substrates. Due to the reaction of BST film and the Si substrate and resulting silicide and SiO₂ formation, the electrical properties of BST films that were coated on bare Si substrates were not measured; they were utilized for crystallization studies only. Therefore, dielectric and ferroelectric properties of BST films coated on Pt/Ti/SiO₂/Si substrates of composition $\text{Ba}_{0.5}\text{Sr}_{0.5}\text{TiO}_3$, $\text{Ba}_{0.7}\text{Sr}_{0.3}\text{TiO}_3$ and $\text{Ba}_{0.9}\text{Sr}_{0.1}\text{TiO}_3$ were measured.

Table 4.1. Compositions of $Ba_xSr_{1-x}TiO_3$ films that were produced in this study listed according to the substrates they were coated on.

Composition of the films	Substrate	Electrical Measurements
$Ba_{0.5}Sr_{0.5}TiO_3$ (paraelectric)	Si	No
$Ba_{0.8}Sr_{0.2}TiO_3$ (ferroelectric)	Si	No
$Ba_{0.5}Sr_{0.5}TiO_3$ (paraelectric)	Pt/Ti/SiO ₂ /Si	Yes
$Ba_{0.7}Sr_{0.3}TiO_3$ (paraelectric)	Pt/Ti/SiO ₂ /Si	Yes
$Ba_{0.9}Sr_{0.1}TiO_3$ (ferroelectric)	Pt/Ti/SiO ₂ /Si	Yes

4.1. Improvement of Film Quality

In the first solution preparation route, second solvent was 2-propanol in addition to acetic acid. Films that were coated using that solution were cracked after 400 nm even for the 0.28M solution. The reason of cracking for sol-gel derived films is the large volume change during drying. During drying, wet solution changes into an amorphous mixture of carbonaceous metal ions. The cracks during deposition of the films are most likely to occur in the drying stage. In this stage, wet coating is transformed into harder amorphous solid, during this transformation, considerable shrinkage occurs, leading to cracks. When the solvent evaporates, a film containing the desired elements forms on the substrate. Since the network film is a plastic or viscoelastic solid, its tendency to crack during drying and firing is substantially reduced [27].

Ethylene glycol is known to possess high boiling point and high latent heat of vaporization, due to this property, ethylene glycol retains the atomic mobility and reduces the tendency to crack [27]. Instead of 2-propanol, ethylene glycol was added to the solution in order to prevent cracking of the films, following the same solution route with Tahan et. al. [32]. By this addition, crack-free films up to 600 nm thickness were obtained. In Figure 4.1, surface SEM micrographs of two films coated

by using first and second solutions are given. Surface cracks can be seen for the film coated using first solution.

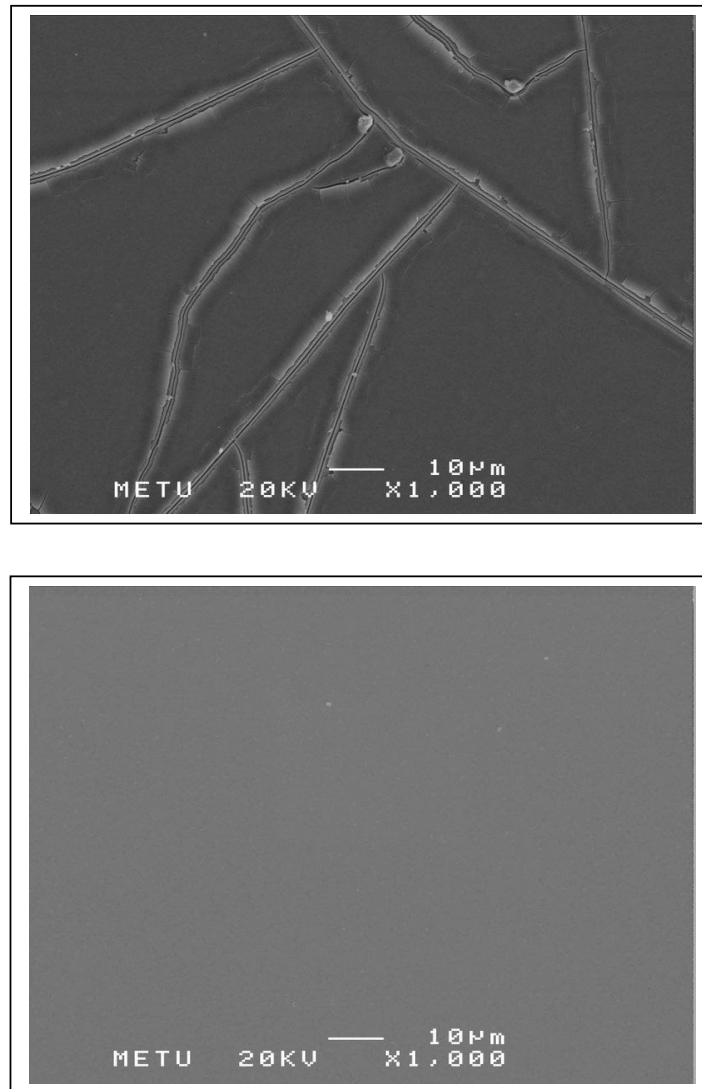


Figure 4.1. SEM micrographs, (top) showing surface cracks of 3 layers $\text{Ba}_{0.5}\text{Sr}_{0.5}\text{TiO}_3$ film (500 nm) coated by using first solution: solution containing 2-propanol, (bottom) showing crack-free surface of 3 layers $\text{Ba}_{0.5}\text{Sr}_{0.5}\text{TiO}_3$ film (600nm) coated by using second solution: solution containing ethylene glycol, both films were sintered at 800°C for 3 hours.

Films may also crack due to thermal expansion coefficient differences between the film (BST) and Pt layer of the substrate. Lopez et al. [34] relates the cracking to mismatch in thermal expansion coefficients of BST and underlying Pt substrate. Table 4.2 shows the thermal expansion coefficients and lattice parameters for bottom Pt layer, BaTiO₃ (BT) and SrTiO₃.

Table 4.2. Thermal expansion coefficients of Pt, BaTiO₃ and SrTiO₃ [35, 53].

Material	Thermal Expansion Coefficient (1/°C)	Lattice Parameter (Å)
Pt	9×10^{-6}	3.97
BaTiO ₃	9.8×10^{-6}	3.994
SrTiO ₃	11×10^{-6}	3,901

Although Lopez et al. had approximated thermal expansion coefficient of BST to that of BT (he had taken it as 4×10^{-6} 1/°C), instead of averaging the thermal expansion coefficients of BT and ST (which are 9.8×10^{-6} 1/°C and 11×10^{-6} 1/°C, respectively), so that they assumed a larger difference in thermal expansion coefficients than it really is, it is nevertheless probable that films might crack due to this difference. This thermal expansion coefficient difference might develop strains especially during cooling, after the formation of inorganic oxide [27]. That's why controlled heating and cooling was applied to the films, with heating and cooling rates as low as 10°C/min.

Solution viscosity is an important parameter in sol-gel processing, which depends on concentration, type of the solvent, and possible reactions between the components of the solution. It can also be adjusted by controlled hydrolysis and by adding cross-linking agents or by adding acid to destroy large molecules formed in the solution [27]. Since film thickness and uniformity are dependent on solution viscosity, the

proper spinning speed also depends on viscosity. The films were coated by spinning at different spinning rates in order to obtain homogeneous and uniform films. The films were spun at 3000, 4000 and 7500 rpm (revolutions per minute) for 30 seconds each. The surface of the films spun at 7500 rpm had a dull appearance, showing regions of inhomogeneity whereas the films spun at 4000 & 3000 rpm had bright and clear surfaces. Therefore, 7500 rpm was not an appropriate spinning speed. Coating thickness is inversely proportional to spinning speed [26], so the higher spinning speed results in lower thickness. So, in order to obtain a thinner layer, 4000 rpm was chosen as the spinning speed. The thickness of the individual layer coated from 0.4 M solution, spun at 4000 rpm for 30 seconds was already high, around 200 nm.

4.2. Dilution of the Solution

BST solutions were diluted for three main purposes:

1. Layers coated from diluted solutions are thinner than those coated by using concentrated solutions. So, during drying the sudden volume change occurring due to evaporation of solvents is less for layers coated from diluted solutions than those coated from concentrated ones. This prevents cracking due to sudden shrinkage. In this study, the films derived from the second route are crack-free. However, as explained before, that was the addition of ethylene glycol instead of 2-propanol not the concentration of the solution which made the difference. Among the films derived from the second route though, the ones derived from the 0.4 M solution are crack-free compared to the ones derived from the 0.75 M solution.

2. Results indicate that, the porosity in the film increases with increase in precursor solution concentration. The lower porosity in the film deposited using dilute solution is due to the fact that individual layers are thin and hence thermally cycled more times which results in effective pyrolysing of the organics compared to the film prepared from the concentrated solution. In sol-gel preparation, the individual layer on pyrolysis leaves behind pores in the film, which will be covered by subsequent layers. The more the number of layers, the less the density of pores. Also, the

individual layers of the films prepared from the concentrated solution are thicker than the film prepared from dilute solution, hence require less number of layers to attain required thickness and incorporates more carbonatious decomposition products in the film. On annealing to high crystallization temperature, these embedded impurities burn-off leaving behind pores in the film and in the process changes the microstructure [19].

3. By preparing thinner layers using the highly diluted solution, multiple nucleation sites within the film are avoided, and the nucleation on the underlying layer (either the substrate or the prior-crystallized $\text{Ba}_{0.8}\text{Sr}_{0.2}\text{TiO}_3$ layer) can be enforced, which results in layer-by-layer homoepitaxial growth within an individual grain [36]. However, that is the case when the solution concentration is very low (around 0.05M) and when rapid thermal annealing is applied to every layer produced. Due to precursors and solvents we used, it was not possible to get such dilute solutions.

4.3. Crystalline Film Formation

The crystal structure of $\text{Ba}_x\text{Sr}_{1-x}\text{TiO}_3$ thin films was determined by x-ray diffraction. The analysis of diffractograms was made by Hanawalt method. Initially, only films of composition $\text{Ba}_{0.8}\text{Sr}_{0.2}\text{TiO}_3$ and $\text{Ba}_{0.5}\text{Sr}_{0.5}\text{TiO}_3$ were coated on Si substrates to study film formation. The effect of sintering temperature on the degree of crystallization was also studied. The composition used for this comparative study was $\text{Ba}_{0.5}\text{Sr}_{0.5}\text{TiO}_3$. Three $\text{Ba}_{0.5}\text{Sr}_{0.5}\text{TiO}_3$ films were coated using the same number of layers and sintered at 600°C, 700°C and 800°C. All films crystallized into cubic BST phase, BST peaks completely fitting to the JCPDS file of $\text{Ba}_{0.5}\text{Sr}_{0.5}\text{TiO}_3$, 39-1395. The intensity of BST peaks sintered at 600°C was quite large, showing well crystallization of the films. The peaks were larger at 700°C indicating a better crystallinity was achieved. At 800°C, the peaks were even larger, and the major [110] peak was achieved to its maximum. The optimum crystallization temperature was chosen as 800°C, after comparing the diffraction peaks of films annealed at 600°C, 700°C and 800°C. The x-ray diffraction spectra can be seen in Figure 4.2.

The composition difference between $\text{Ba}_{0.5}\text{Sr}_{0.5}\text{TiO}_3$ and $\text{Ba}_{0.8}\text{Sr}_{0.2}\text{TiO}_3$ films in terms of diffraction angle, 2θ , can be seen comparatively in Figure 4.3. Both films were sintered at 800°C for 3 hours. The d-spacings between the planes increase while 2θ values decrease with the decrease in the Sr content according to Bragg's law ($\lambda = 2d\sin(\theta)$).

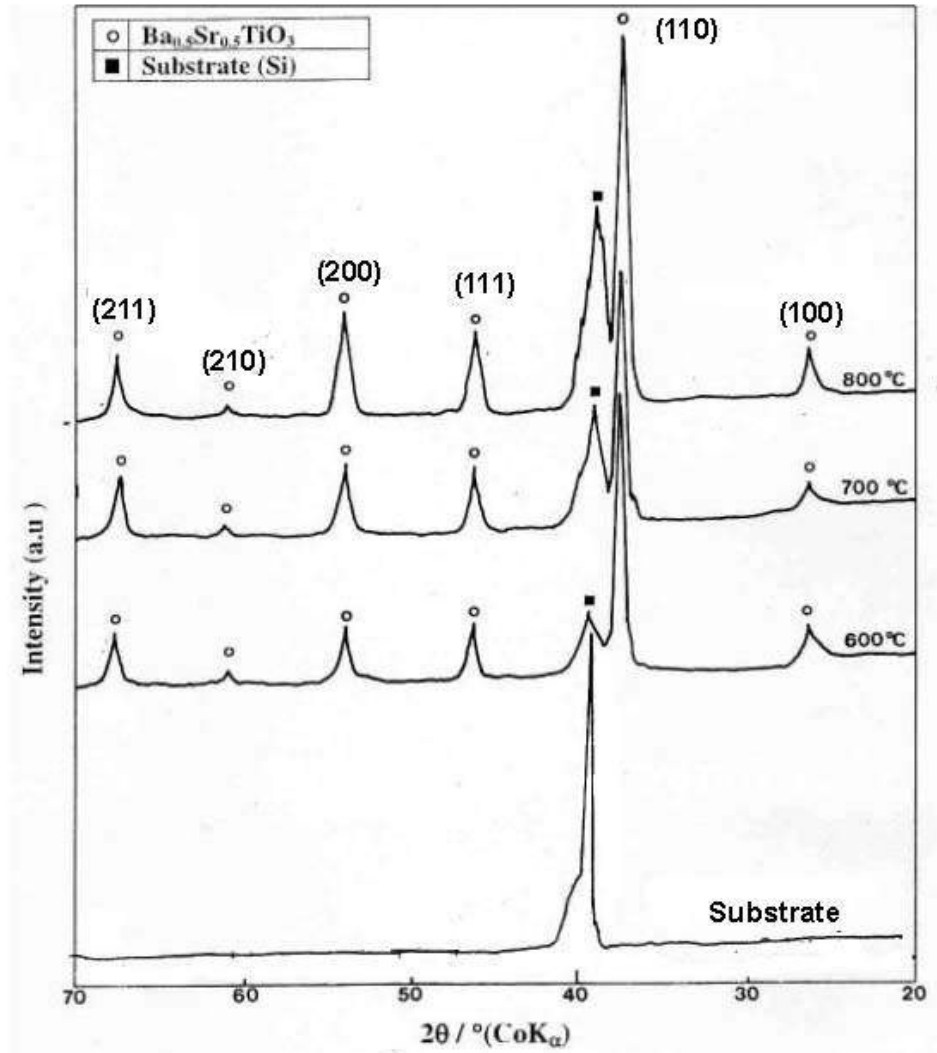


Figure 4.2. XRD spectra of $\text{Ba}_{0.5}\text{Sr}_{0.5}\text{TiO}_3$ films on Si substrate sintered at 600°C , 700°C and 800°C for 3 hours.

X-ray diffractograms can also be used as evidence for the differentiation and stoichiometry of the composition of BST films. The complete fit of intensity and position of diffraction peaks for $\text{Ba}_{0.5}\text{Sr}_{0.5}\text{TiO}_3$ films to JCPDS file shows that the stoichiometry holds, whereas the shift in the 2θ values to lower angles for $\text{Ba}_{0.8}\text{Sr}_{0.2}\text{TiO}_3$ films indicates that the films contain less Sr. For $\text{Ba}_{0.8}\text{Sr}_{0.2}\text{TiO}_3$ thin films, JCPDS file of $\text{Ba}_{0.77}\text{Sr}_{0.23}\text{TiO}_3$ was used (JCPDS: 44-0093).

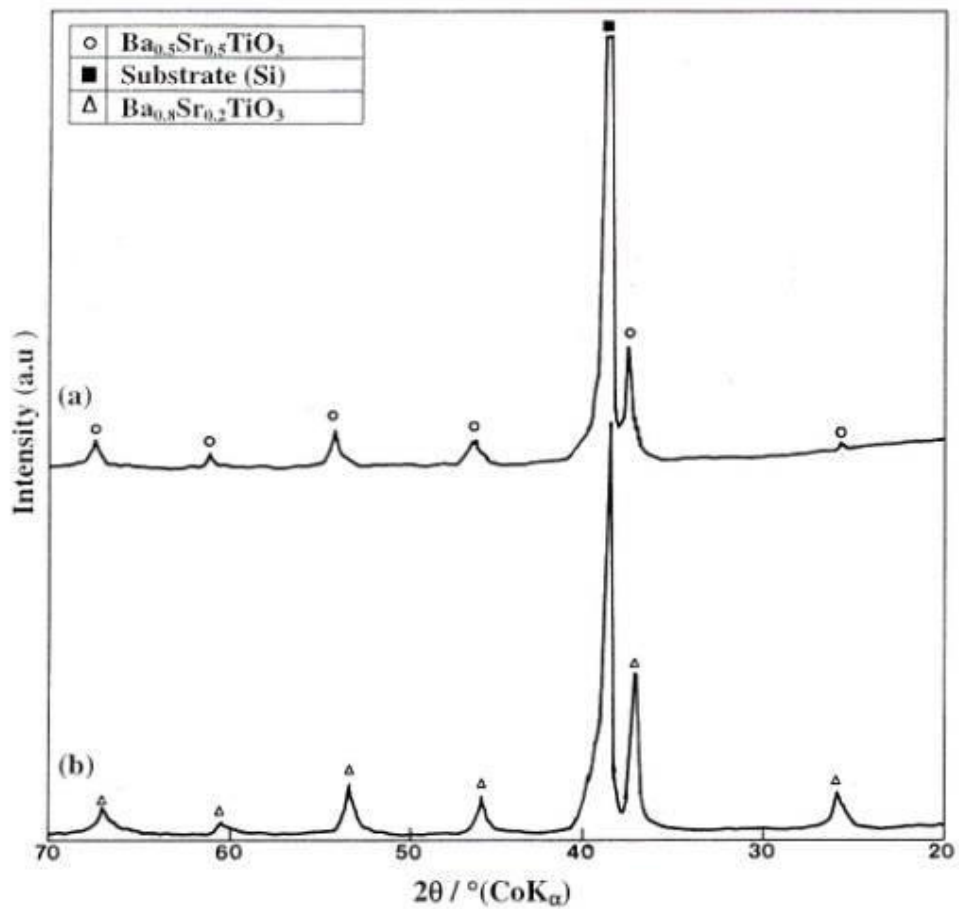


Figure 4.3. XRD spectra of (a) 5 layers, 1 μm thick $\text{Ba}_{0.5}\text{Sr}_{0.5}\text{TiO}_3$ film on Si, sintered at 800°C (b) 5 layers, 1 μm thick $\text{Ba}_{0.8}\text{Sr}_{0.2}\text{TiO}_3$ film on Si, sintered at 800°C .

There was no intermediate phase observed in the diffractograms. The peaks in the $20^\circ - 80^\circ$ range matched completely in intensity and angle with JCPDS files for both $\text{Ba}_{0.5}\text{Sr}_{0.5}\text{TiO}_3$ and $\text{Ba}_{0.8}\text{Sr}_{0.2}\text{TiO}_3$ films. Some researchers have detected an intermediate complex carbonate phase for BT and ST, and they claim that same phase should be seen for BST, which is a solid solution of BT and ST. This carbonate phase was reported only for the films derived from acetate-based precursors (in general, long-chain carboxylate precursors) and below the crystallization temperature of BST phase around 600°C ; up to 750°C , independent of Ti precursor used [30, 31, 37]. The exact stoichiometry of the intermediate phase is not known, but Gopalakrishnamurthy suggested a composition $\text{Ba}_2\text{Ti}_2\text{O}_5\text{CO}_3$ for BT, and a similar composition was suggested for BST: $(\text{Ba},\text{Sr})_2\text{Ti}_2\text{O}_5\text{CO}_3$; a different suggestion was $(\text{Ba},\text{Sr})\text{TiO}_2\text{CO}_3$ [23]. Although there is no intermediate phase detected for BST films coated on Si substrates at different sintering temperatures, it is possible that films contain an intermediate phase. The intensity of intermediate phase peaks were reported as low so the films might not be thick enough so that reflections from the intermediate layer are less than required to differentiate the small intermediate phase peaks in the diffractograms. As the thickness of the film decreases, the number of counts taken from the film decreases relative to the counts from the substrate so intensity of BST peaks decreases with decreasing thickness.

The effect of the intermediate phase on the crystallization behaviour was studied by some researchers. Hasenkox et al. studied the effect of different precursors on the crystallization behaviour [31]. They claim that amorphous BST film first crystallizes into an intermediate phase before crystallizing into the perovskite structure. According to them, this intermediate phase favors grain growth in the BST films derived from acetate precursors compared to films prepared by using other precursors than acetates. Because, the formation of some intermediate phase in the films from acetate precursors means that the crystallization process still proceeds at high temperatures where it has already terminated for thin films prepared by using different precursors. Such a delayed crystallization favoring the growth of grains combined with high mobility of the ions due to the high temperatures may also support the densification of the film. These two factors can lead to the observed

increase in the permittivity of thin films prepared from the acetate precursor. They also claim that this delayed crystallization can also be the origin of columnar grain growth of ST films on platinized silicon substrates derived from acetate precursors. This can be a point that justifies our choice of acetate precursors in this study.

For measuring the electrical properties, BST films of three different compositions were coated on Pt/Ti/SiO₂/Si instead of bare Si substrates. Since the adhesion and growth of films on different substrates might be different, crystallization studies were repeated for the films coated on Pt/Ti/SiO₂/Si. Again, Ba_{0.5}Sr_{0.5}TiO₃ composition was used for this study. Figure 4.4 shows the x-ray diffractograms for Ba_{0.5}Sr_{0.5}TiO₃ thin films coated on Pt/Ti/SiO₂/Si substrates and sintered at 600°C, 700°C and 800°C. This time, BST film sintered at 600°C showed peaks other than BST and substrate (Pt) peaks. These peaks are suspected to be intermediate phase peaks, the one at 50.7° is determined to be a BaCO₃ (JCPDS: 74-1628) peak, the other one at 28.8° is Ba₂Ti₅O₁₂ (JCPDS: 17-661). At 700°C, these unfamiliar peaks of possible intermediate phase disappeared but the intensity of the other peaks did not significantly change. At 800°C, intensity of BST peaks increased remarkably, showing better crystallization of the films.

The above study was done for the films coated by using first BST route. Upon addition of ethylene glycol, solution precursor chemistry thus thermal decomposition and crystallization behaviour of the films changed, so this crystallization study was repeated for the films coated by the second solution route on INOSTEK Pt/Ti/SiO₂/Si substrates. Figure 4.5 shows the x-ray diffractograms for Ba_{0.5}Sr_{0.5}TiO₃ thin films coated on these Pt/Ti/SiO₂/Si substrates and sintered at 700°C, 750°C and 800°C using second solution. The film sintered at 750°C had similar peak intensities to film sintered at 800°C, but intensity of peaks of BST film sintered at 700°C was lower than the other two.

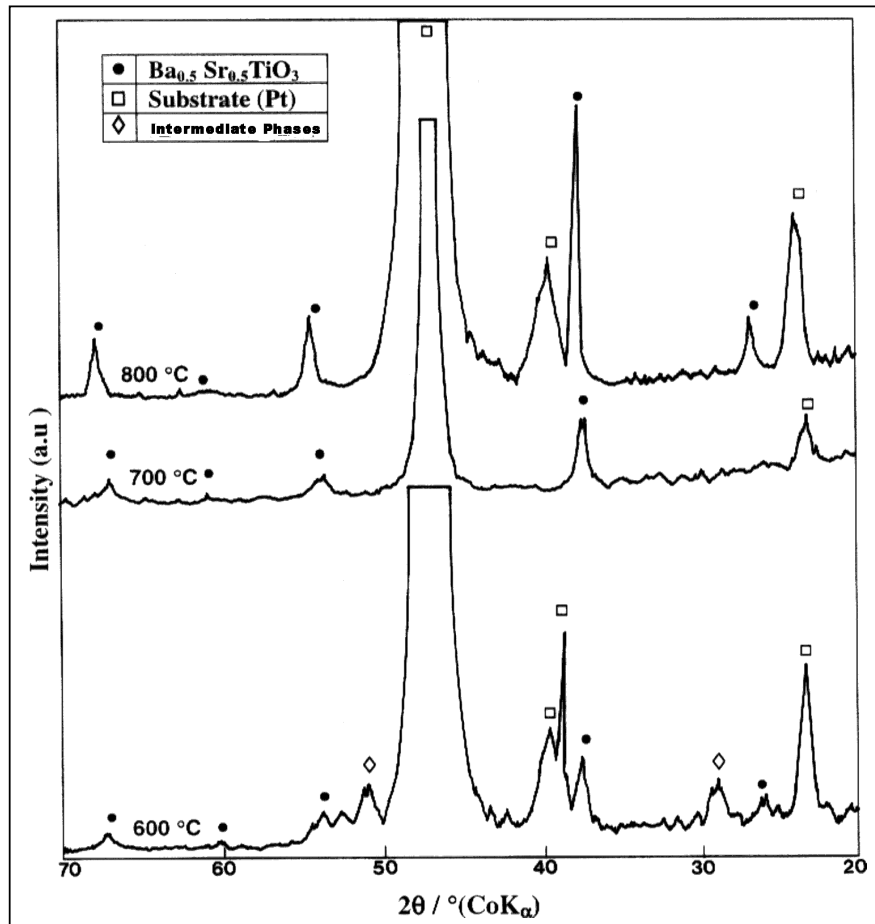


Figure 4.4. X-ray diffractograms for $\text{Ba}_{0.5}\text{Sr}_{0.5}\text{TiO}_3$ thin films coated on Pt/Ti/SiO₂/Si substrates and sintered at 600°C, 700°C and 800°C using first solution route.

The phase formation behaviour of $\text{Ba}_{0.7}\text{Sr}_{0.3}\text{TiO}_3$ and $\text{Ba}_{0.9}\text{Sr}_{0.1}\text{TiO}_3$ films was also checked by x-ray diffraction. Figure 4.6 shows the x-ray diffractograms of $\text{Ba}_{0.9}\text{Sr}_{0.1}\text{TiO}_3$ (JCPDS card of BaTiO_3 was used: 5-626), $\text{Ba}_{0.7}\text{Sr}_{0.3}\text{TiO}_3$ (JCPDS card of $\text{Ba}_{0.67}\text{Sr}_{0.33}\text{TiO}_3$ was used: 89-0274) and $\text{Ba}_{0.5}\text{Sr}_{0.5}\text{TiO}_3$ (JCPDS: 39-1395) films all sintered at 800°C for 3 hours. All films showed well crystallization with intense peaks. In order to differentiate between the different films better, the (110) peaks of the films are given in figure 4.7. The shift in the diffraction angle of the peaks to lower degrees with the increase in Sr content of the films is obvious. This shift was in accordance with JCPDS cards of the films, suggesting that the composition of the films were correct.

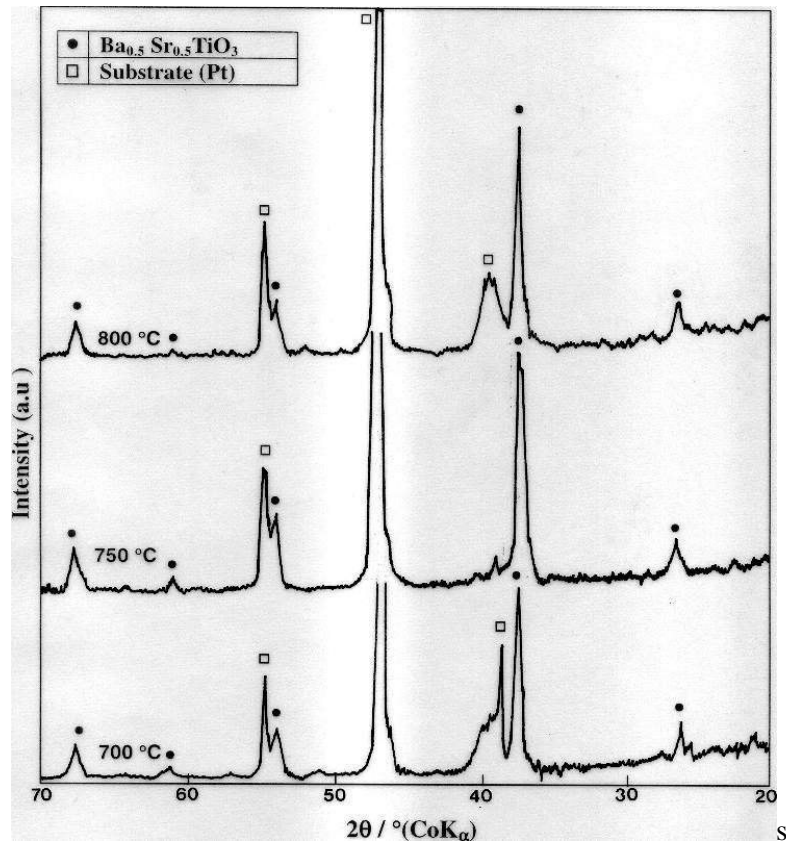


Figure 4.5. X-ray diffractograms for $\text{Ba}_{0.5}\text{Sr}_{0.5}\text{TiO}_3$ thin films coated on different Pt/Ti/SiO₂/Si substrates and sintered at 700°C , 750°C and 800°C using second solution route (using ethylene glycol).

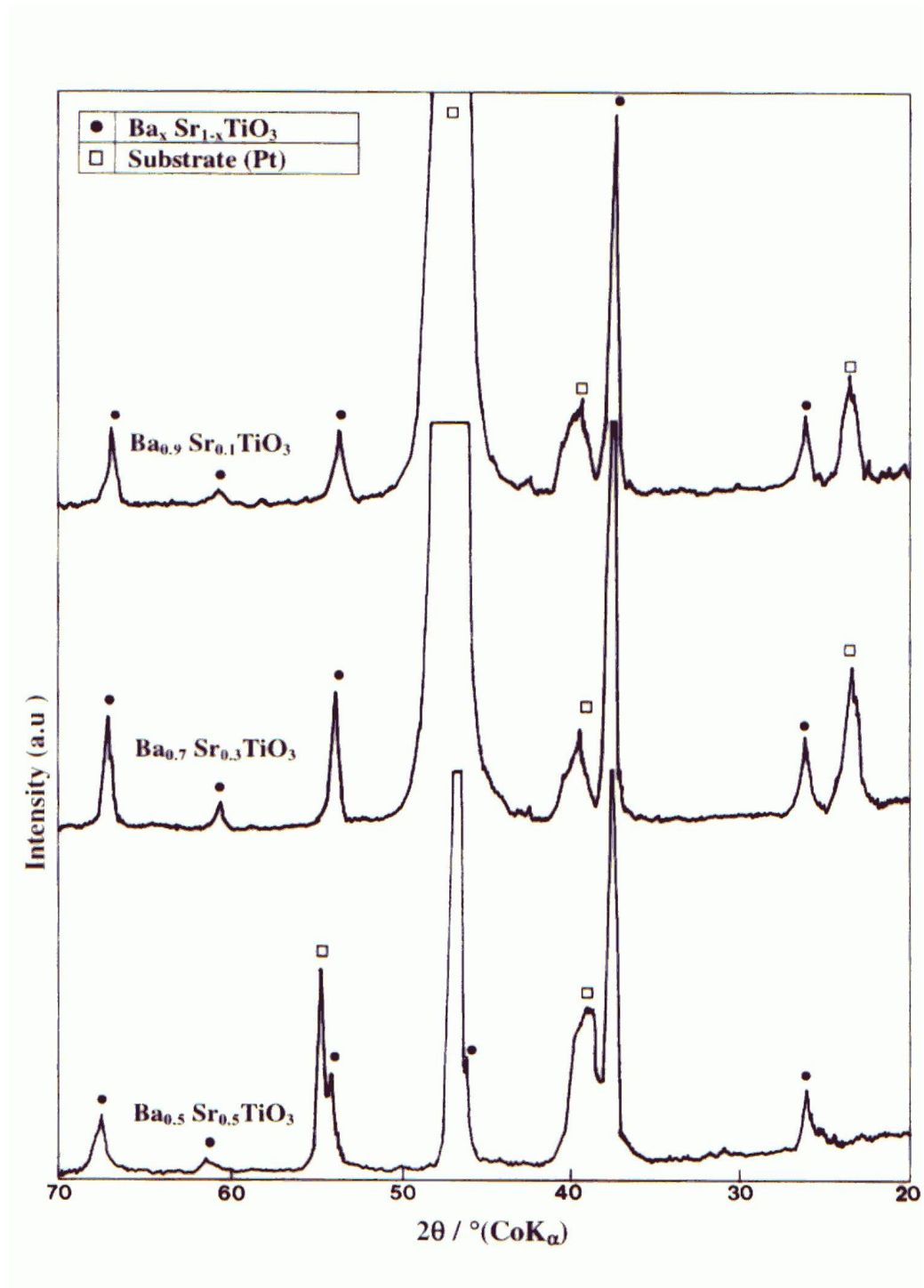


Figure 4.6. X-ray diffractograms of Ba_{0.5}Sr_{0.5}TiO₃, Ba_{0.7}Sr_{0.3}TiO₃ and Ba_{0.9}Sr_{0.1}TiO₃ films (from bottom to top) sintered at 800°C for 3 hours.

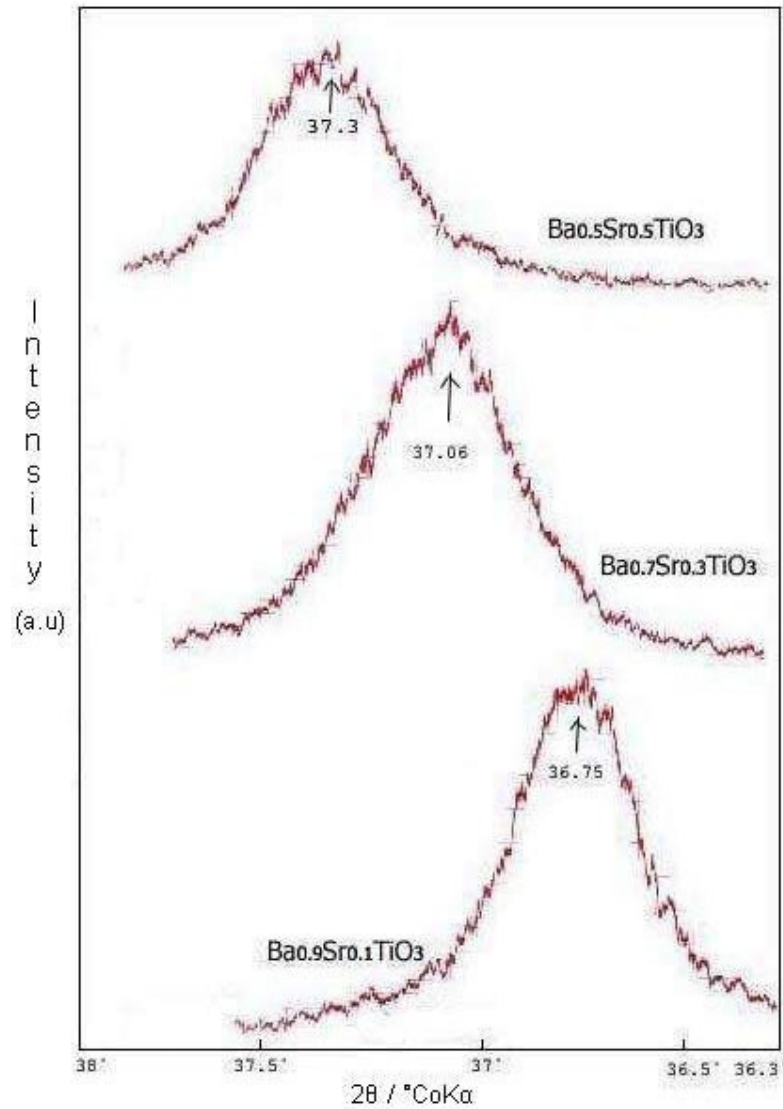


Figure 4.7. X-ray diffractograms of (110) peaks of Ba_{0.5}Sr_{0.5}TiO₃, Ba_{0.7}Sr_{0.3}TiO₃ and Ba_{0.9}Sr_{0.1}TiO₃ films (from bottom to top) sintered at 800°C for 3 hours.

4.4. Morphology of the BST Films

Surface of the films was examined by optical microscopy and SEM for possible cracks and inhomogeneities. The films prepared from 0.4M solution (second solution containing ethylene glycol) had crack-free and homogeneous surface up to 600 nm thickness (Figure 4.1(b)). Since the grains of BST thin films synthesized by sol-gel processing are typically in the order of 20-70 nm. [13, 29, 38] excluding epitaxially grown films [14, 31], magnification of SEM is not enough to see individual grains and grain morphology. In this study, average grain size and grain size distribution couldn't be determined by using SEM for this reason. But, average grain sizes were estimated by using Scherrer's Formula, which is a technique based on measuring the full width of x-ray diffraction peaks at the half maximum height of the peak.

The formula is as follows [39]:

$$t = \frac{0.94 \times \lambda}{B \times \cos \theta} \quad \text{Eq. [4.1].}$$

where, t is the average grain size, λ is the wavelength of radiation of the x-ray beam used, B is the width of the peak at the half of the maximum intensity (in radians) and θ is the half of the diffraction angle 2θ . The contribution to the peak broadening from instrumental broadening must be subtracted by the help of a reference sample, however, since instrumental contribution is only significant for large particle sizes ($t > 30$ nm), it was neglected. For BST grain size determination, the most intense diffraction peak, (110) was used. Among the three $\text{Ba}_{0.5}\text{Sr}_{0.5}\text{TiO}_3$ films in Table 4.3, the one sintered at 600°C for 3 hours had an average grain size of 16.9 nm. The average grain size didn't change much for the one sintered at 700°C but increased to 25.4 nm for the film sintered at 800°C for 3 hours (Table 4.3). To increase the accuracy in the width measurements, (110) peak was studied separately by making diffraction studies using $1/8^\circ$ per second speed and three different other diffractograms corresponding to $\text{Ba}_{0.9}\text{Sr}_{0.1}\text{TiO}_3$, $\text{Ba}_{0.7}\text{Sr}_{0.3}\text{TiO}_3$, and $\text{Ba}_{0.5}\text{Sr}_{0.5}\text{TiO}_3$ were obtained (Figure 4.7). The grain size did not change much with Sr content, it was 30 nm approximately.

Table 4.3 Grain sizes of 1 μm thick BST films sintered at different temperatures.

Composition	Sintering Temperature	Grain Size (nm)
$\text{Ba}_{0.5}\text{Sr}_{0.5}\text{TiO}_3$	600°C	16.9
$\text{Ba}_{0.5}\text{Sr}_{0.5}\text{TiO}_3$	700°C	17.2
$\text{Ba}_{0.5}\text{Sr}_{0.5}\text{TiO}_3$	800°C	25.4
$\text{Ba}_{0.5}\text{Sr}_{0.5}\text{TiO}_3$	800°C	33.9
$\text{Ba}_{0.7}\text{Sr}_{0.3}\text{TiO}_3$	800°C	27.5
$\text{Ba}_{0.9}\text{Sr}_{0.1}\text{TiO}_3$	800°C	29.6

The cross-section of BST films was examined by SEM for determining film thickness and checking the quality of Pt / BST interface. The thickness of the films changed from 400 nm to 1 μm accordingly with the number of layers coated. For example, 0.4M solution derived film spun at 4000 rpm for 30 seconds, and coated by 2 coating-pyrolysis cycles was 400 nm, whereas another film coated by 3 cycles was 600 nm thick. SEM micrographs of these films are shown in Figure 4.8 and 4.9, respectively. The interfaces between the BST and Pt were distinct and homogeneous.

As mentioned in Chapter 3, the composition of BST thin films cannot be checked by energy dispersive analysis of SEM, due to overlapping of x-ray peaks of elements constituting the film. Therefore, we made use of EDS in order to understand whether any impurities exist in the film. Analysis indicated that the elements of BST: Ba, Sr, Ti, and O are found in the films without any residuals, e.g. carbon. The cross-section of a $\text{Ba}_{0.5}\text{Sr}_{0.5}\text{TiO}_3$ film obtained from the first route coated on Si substrate is shown in the Figure 4.10. The EDS figures of BST film and the substrate are included in Figure 4.11 and 4.12 respectively. The overlapping of energies of elements Ba, Ti and Si, Sr can be seen in the EDS Spectra. Nickel (Ni) came from conductive coating for preparing the sample to SEM analysis.

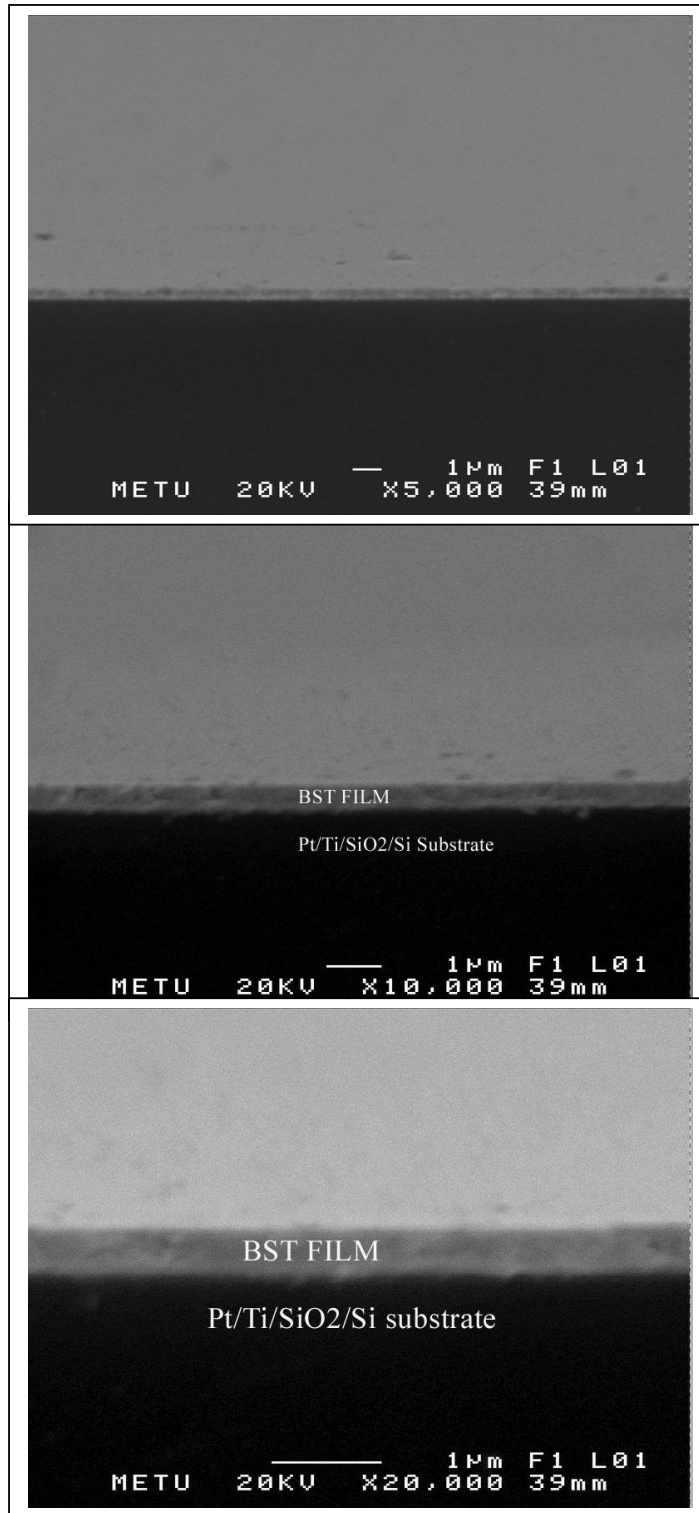


Figure 4.8. Cross-section SEM micrograph of 2 layers Ba_{0.5}Sr_{0.5}TiO₃ film on Pt/Ti/SiO₂/Si substrate, (top ×5000, middle ×10000, bottom ×20000).

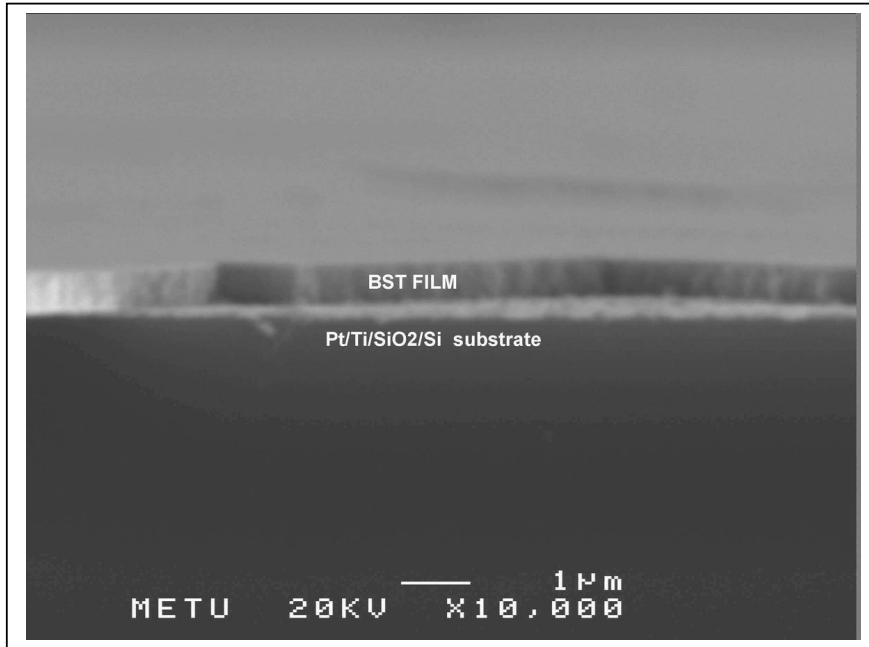


Figure 4.9. Cross-section SEM micrograph of 3 layers $\text{Ba}_{0.5}\text{Sr}_{0.5}\text{TiO}_3$ film on Pt/Ti/SiO₂/Si substrate, sintered at 800°C for 3 hours.

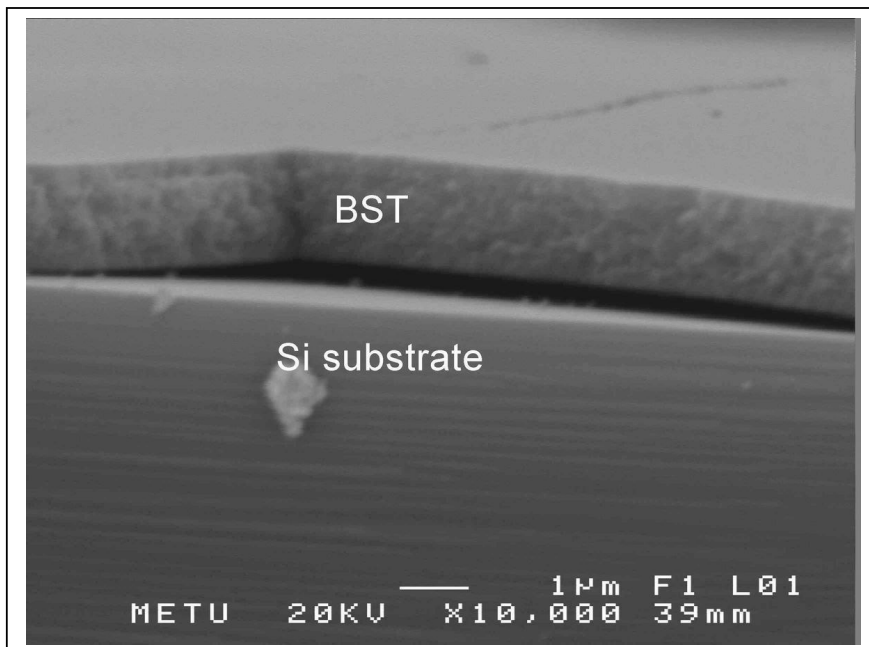


Figure 4.10. SEM micrograph of $\text{Ba}_{0.5}\text{Sr}_{0.5}\text{TiO}_3$ film on Si substrate.

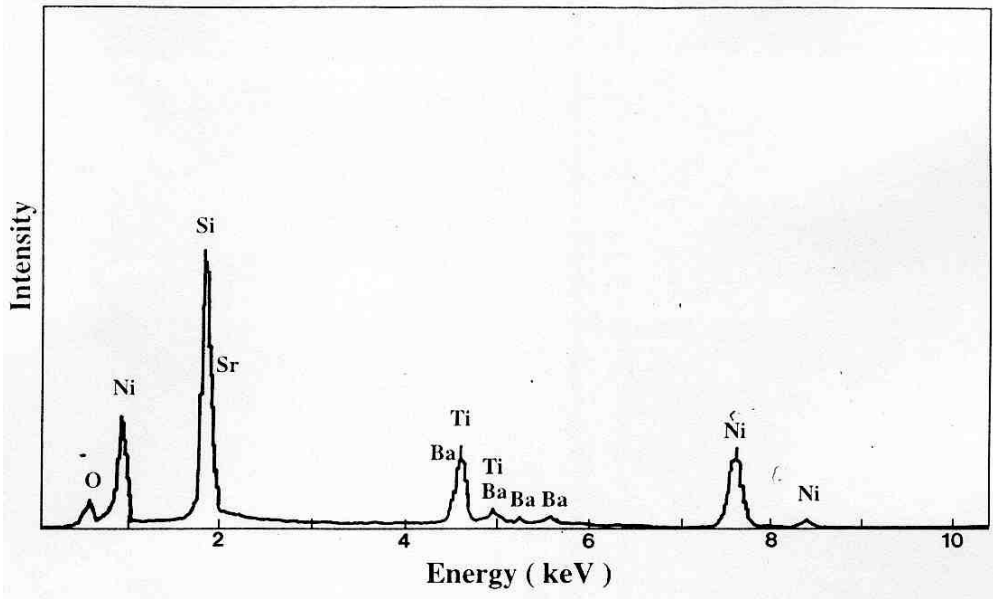


Figure 4.11. EDS spectra of $\text{Ba}_{0.5}\text{Sr}_{0.5}\text{TiO}_3$ film on Si substrate, sintered at 800°C for 3 hours.

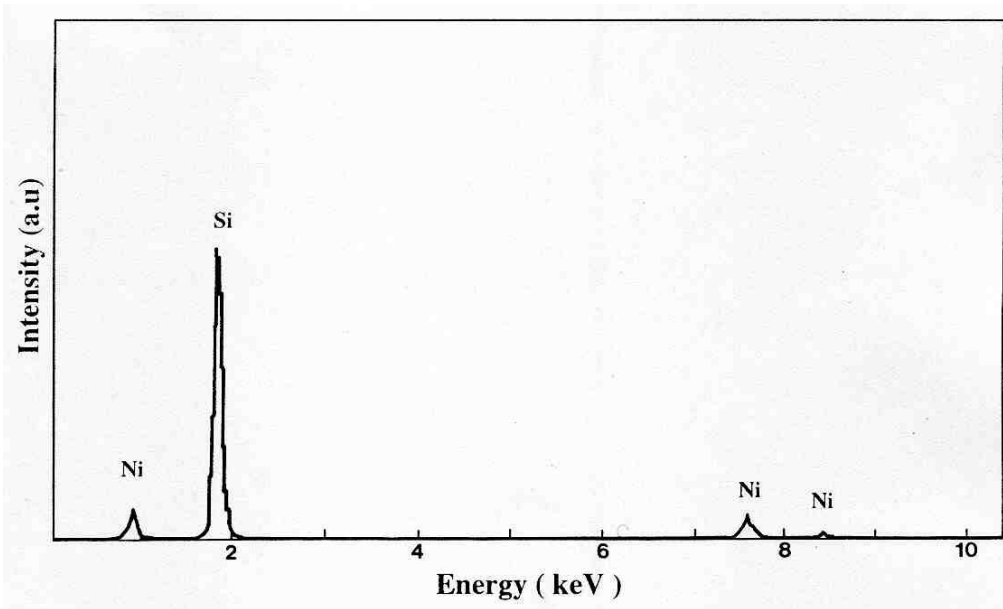


Figure 4.12. EDS spectra of Si substrate.

Same elemental analysis was repeated for BST films coated on Pt/Ti/SiO₂/Si substrates. EDS spectra of the 6 layers $\text{Ba}_{0.5}\text{Sr}_{0.5}\text{TiO}_3$ film and underlying Pt/Ti/SiO₂/Si substrate is shown in Figure 4.13 and 4.14, respectively. Presence of

Au in the EDS spectras is due to conductive coating layer for preventing discharge during SEM analysis.

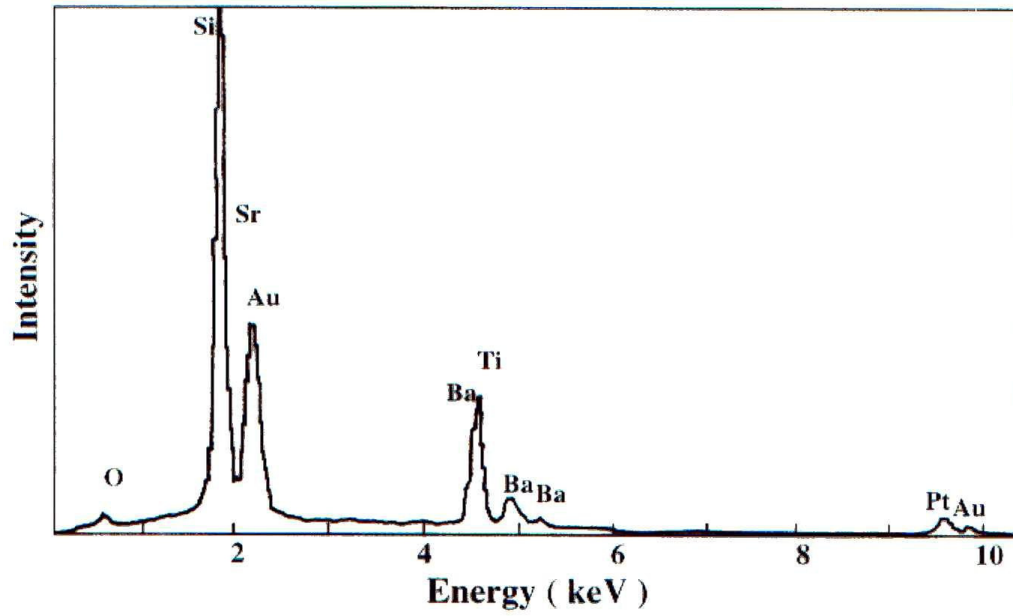


Figure 4.13. EDS spectra of 6 layers $\text{Ba}_{0.5}\text{Sr}_{0.5}\text{TiO}_3$ film on Pt/Ti/SiO₂/Si substrate.

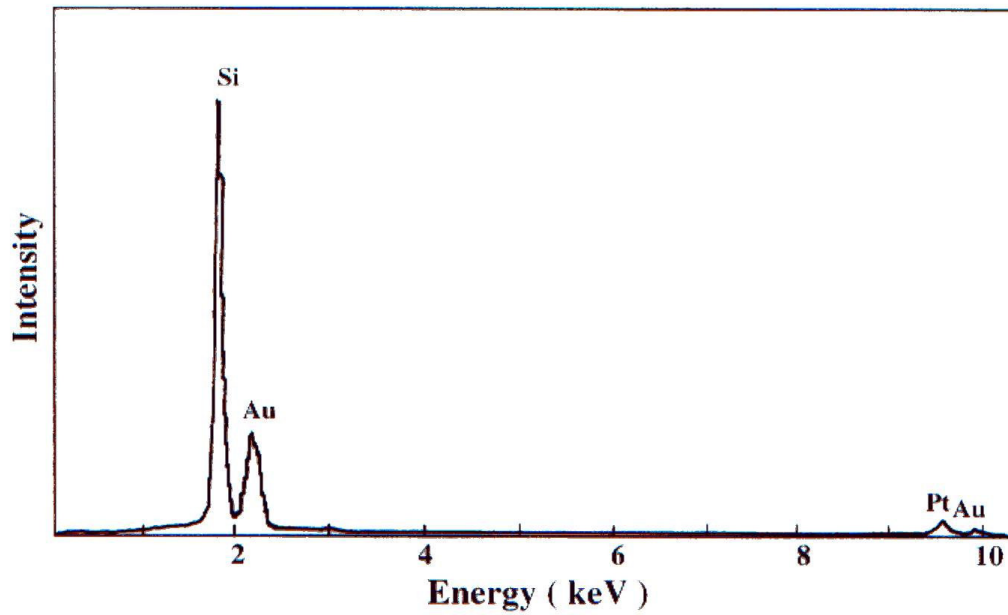


Figure 4.14. EDS spectra of Pt/Ti/SiO₂/Si substrate.

4.5. Dielectric Properties of BST Films

Dielectric properties of films like dielectric constant and loss depends on microstructural features of the films like grain size, crystallinity, porosity and hence give valuable information about the film's quality. In this study, dielectric constant and loss of the films that differ in composition, thickness and heat treatment schedule were measured.

Capacitance and dielectric loss of the BST films were measured by HP 4194A Impedance-Gain Phase Analyzer. These properties were measured in the frequency range 100 Hz - 1 MHz, with an oscillating AC voltage of 0.5 V. There was some dispersion in the capacitance of films with frequency. The change of capacitance and dielectric constant calculated from those capacitance values of 600 nm $\text{Ba}_{0.7}\text{Sr}_{0.3}\text{TiO}_3$ film with frequency are given in Figures 4.15 and Figure 4.16, respectively.

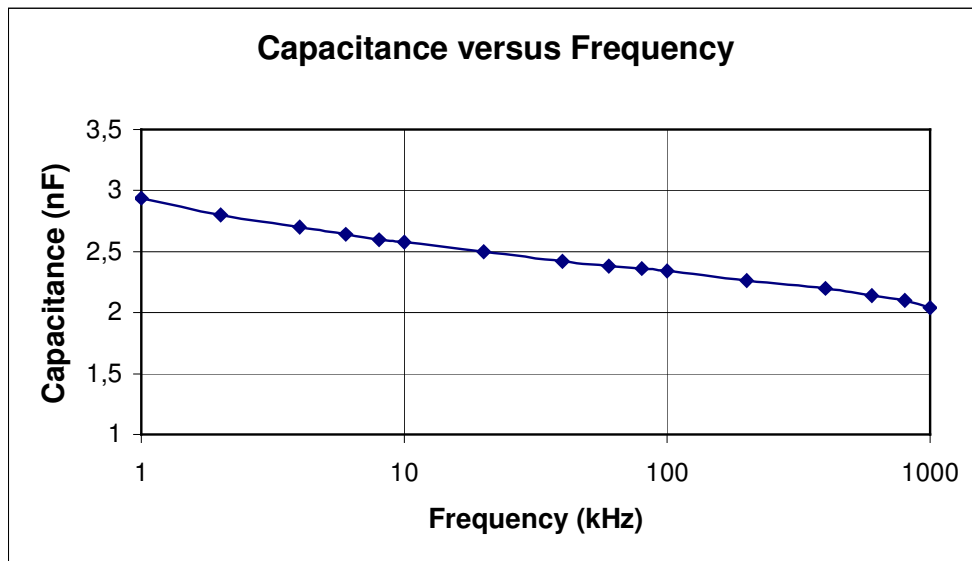


Figure 4.15. The change of dielectric constant with frequency for 3 layers $\text{Ba}_{0.7}\text{Sr}_{0.3}\text{TiO}_3$ film ($t = 600$ nm).

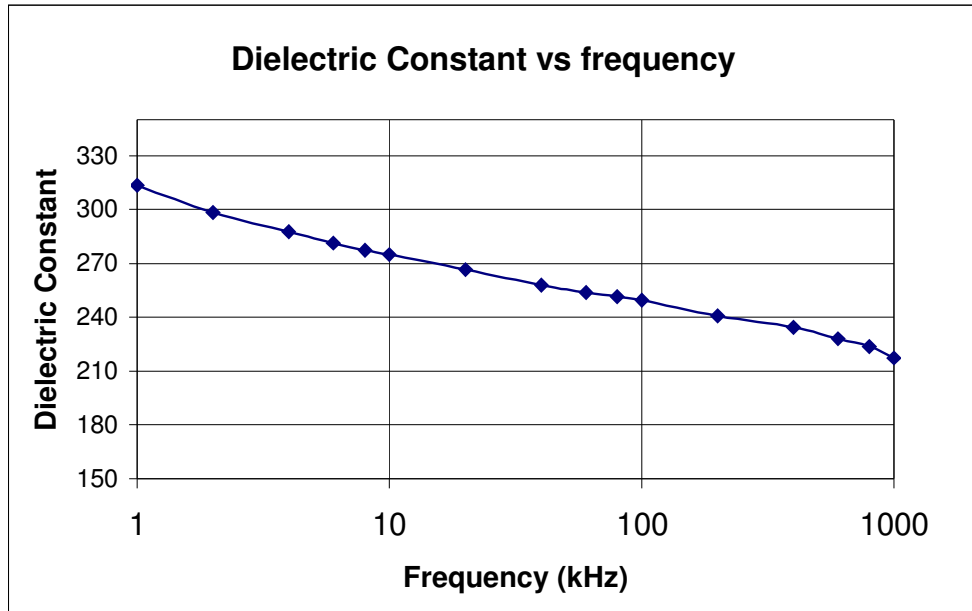


Figure 4.16. The change of dielectric constant with frequency for 3 layers $\text{Ba}_{0.7}\text{Sr}_{0.3}\text{TiO}_3$ film ($t = 600 \text{ nm}$).

In order to see the effect of degree of crystallization on dielectric properties, dielectric constant of films having the same thickness, sintered at different sintering temperatures was measured. Three $\text{Ba}_{0.5}\text{Sr}_{0.5}\text{TiO}_3$ films, 3 layers in thickness, 600 nm, were sintered at 600°C , 700°C and 800°C . There was an increase in dielectric constant (measured at 1 kHz) with increasing sintering temperature (Figure 4.16). This increase is due to better crystallinity of the films and increase in grain size at higher sintering temperatures. Also, film porosity is reduced at high sintering temperatures. As previously given x-ray diffraction results also showed, at 600°C and 700°C , the films were poorly crystallized compared to the films sintered at 800°C . This was confirmed by lower dielectric constant of these films with respect to the film sintered at 800°C .

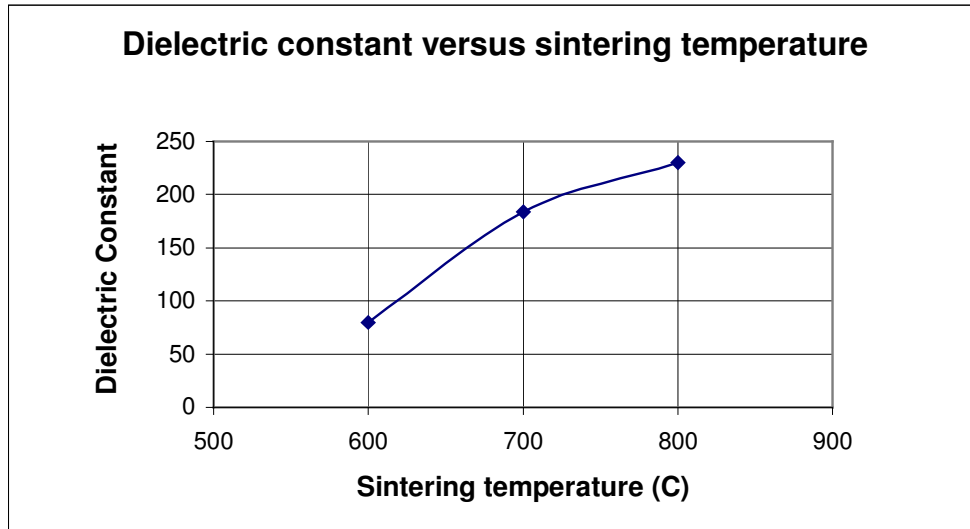


Figure 4.17. Change in dielectric constant (at 1 kHz) with different sintering temperatures, for 3 layers $\text{Ba}_{0.5}\text{Sr}_{0.5}\text{TiO}_3$ films.

The dielectric properties of $\text{Ba}_x\text{Sr}_{1-x}\text{TiO}_3$ films depend on Ba/Sr ratio and these composition tunable properties were investigated by monitoring the change in dielectric properties with composition. For this study, Ba rich portion of continuous solid solution scale was chosen. 2 layers and 3 layers $\text{Ba}_{0.5}\text{Sr}_{0.5}\text{TiO}_3$, $\text{Ba}_{0.7}\text{Sr}_{0.3}\text{TiO}_3$ and $\text{Ba}_{0.9}\text{Sr}_{0.1}\text{TiO}_3$ films were produced and their dielectric properties were compared. The dielectric constant of 3 layers BST films with different compositions as a function of frequency are shown in Figure 4.18. The highest dielectric constant was measured for 3 layers $\text{Ba}_{0.7}\text{Sr}_{0.3}\text{TiO}_3$ film (approximately 600 nm in thickness) and it was 313 at 1 kHz. The other two films that were 3 layers thick had lower dielectric constants, $\text{Ba}_{0.5}\text{Sr}_{0.5}\text{TiO}_3$ film had a dielectric constant of 230 and $\text{Ba}_{0.9}\text{Sr}_{0.1}\text{TiO}_3$ film had 228. Other researchers also observed similar trend in the change of dielectric constant of BST films with composition. For example, Tahan et al. also obtained highest dielectric constant for $\text{Ba}_{0.75}\text{Sr}_{0.25}\text{TiO}_3$ films at room temperature; for 400 nm film, they measured 440 at 1 kHz [13]. Also, Pontes et al. reported higher dielectric constant for $\text{Ba}_{0.8}\text{Sr}_{0.2}\text{TiO}_3$ film than $\text{Ba}_{0.4}\text{Sr}_{0.6}\text{TiO}_3$ film, 749 and 680 respectively at 1 kHz [40]. It is known that Curie temperature of bulk

BST decreases with increasing strontium content according to the approximation: $T_c = 371x - 241$, where x is the fraction of barium [11]. So, addition of 0.3 mole percent Sr would bring the Curie temperature of the BaTiO_3 to room temperature, where the dielectric constant is maximum (Figure 4.19). So, this explains why $\text{Ba}_{0.7}\text{Sr}_{0.3}\text{TiO}_3$ film displays the highest dielectric constant and why $\text{Ba}_{0.5}\text{Sr}_{0.5}\text{TiO}_3$ and $\text{Ba}_{0.9}\text{Sr}_{0.1}\text{TiO}_3$ films have similar dielectric constants. The latter two compositions are equally distant from the transition temperature where the dielectric constant peaks at room temperature.

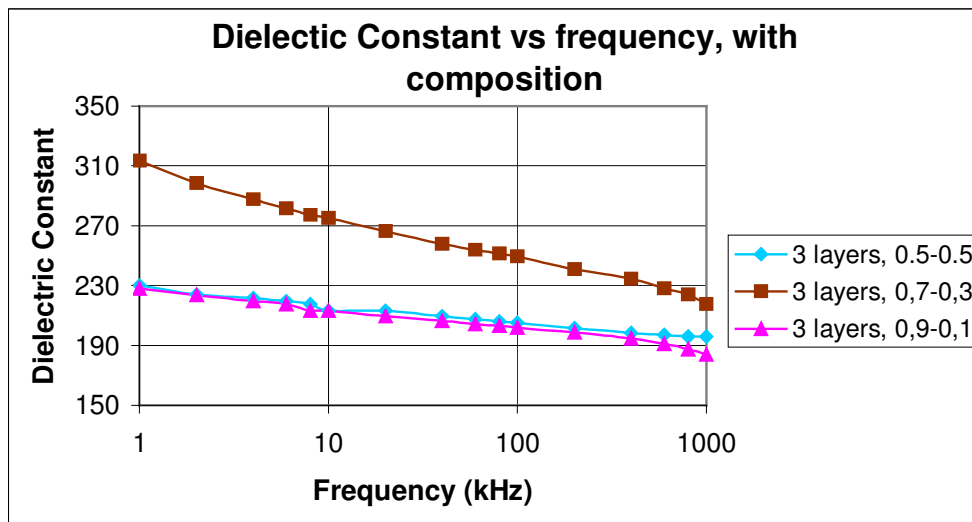


Figure 4.18. Dielectric constant of BST films with different compositions as a function of frequency for 600 nm films.

Similar composition dependence behaviour was also observed for 2 layers (approximately 400 nm) BST films. Again $\text{Ba}_{0.7}\text{Sr}_{0.3}\text{TiO}_3$ film has shown the highest dielectric constant, 176 at 1 kHz measuring frequency, but this time dielectric constant of $\text{Ba}_{0.9}\text{Sr}_{0.1}\text{TiO}_3$ film was close to that of $\text{Ba}_{0.7}\text{Sr}_{0.3}\text{TiO}_3$, it was 175. $\text{Ba}_{0.5}\text{Sr}_{0.5}\text{TiO}_3$ had the lowest of three, 119 at 1 kHz. The dielectric constant of 2

layers BST films with different compositions as a function of frequency are shown in Figure 4.20.

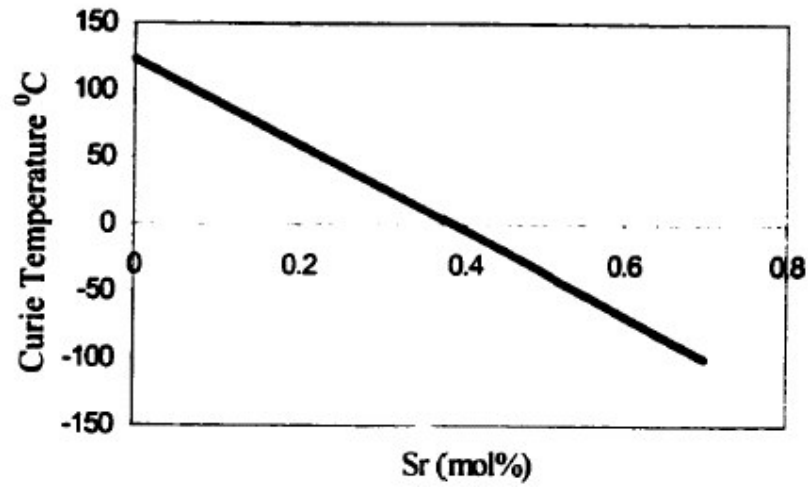


Figure 4.19. The decrease in the Curie temperature of BaTiO₃ with Sr addition [11].

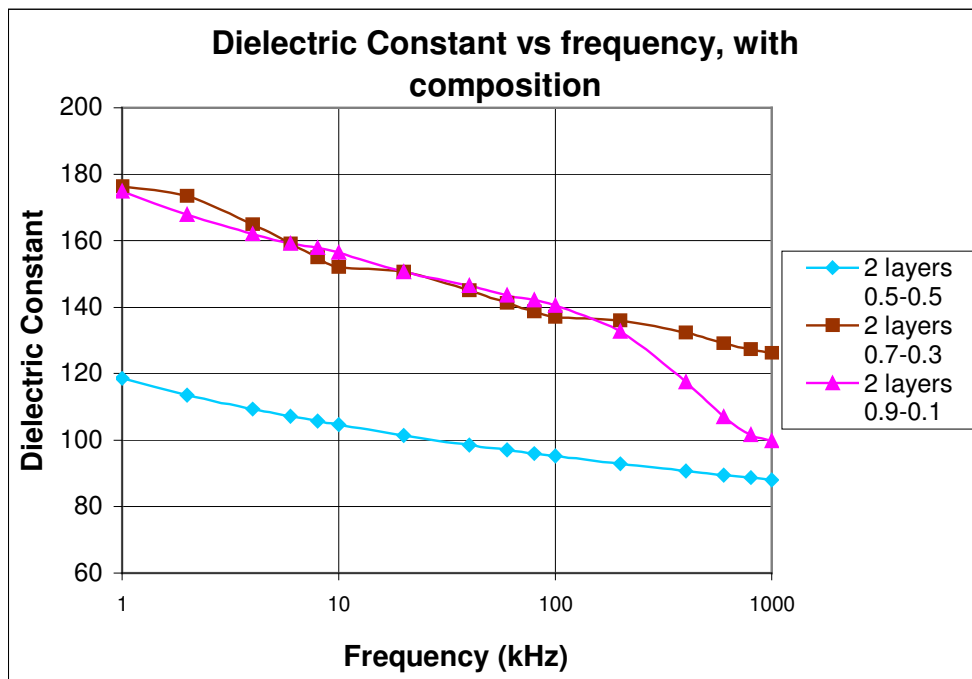


Figure 4.20. Dielectric constant of BST films with different compositions as a function of frequency for 400 nm films.

Dielectric properties of some sol-gel derived BST films from literature varying in composition, thickness, precursors and heat treatment temperatures are given in Table 4.4 for comparison. It can be seen that dielectric constant of BST films obtained in this study are comparable with other sol-gel deposited films but lower than that of epitaxial films. This may be due to the variation in the microstructure. In the epitaxial films crystallization is highly oriented, normally vertical to the surface of the films, and this provides a stronger polarization direction. This highly oriented structure tends to form a concentrated polarization which results in higher dielectric constant. But in the present case the films were polycrystalline with random orientation, which implies an almost equal polarization in all directions [41].

Film stoichiometry should also have a pronounced effect on dielectric constant. Several groups have pointed out that the permittivity at room temperature is maximum when the (Ba+Sr)/Ti is 1:1, and decreases when the films are either titanium rich or titanium poor [42, 43]. Similar results have been obtained for SrTiO₃. The dependence on (Ba+Sr)/Ti ratio becomes much less marked when the film thickness is decreased [42]. Since, EDS analysis couldn't be used for BST films due to overlapping of x-ray energy peaks of Si-Sr and Ba-Ti, the exact stoichiometry of the films couldn't be checked. Therefore lower dielectric properties compared to other sol-gel derived films, encountered in the present case may be due to possible non-stoichiometry in the films.

Dielectric loss of the films was also measured. For all BST films, independent of composition, thickness and sintering temperature, dielectric loss showed the same dispersion characteristics, it was nearly constant with frequency in the 1 kHz-100 kHz range, then it increased in 100 kHz-1 MHz range. Same dispersion characteristics were also observed for other BST films [38, 40]. In figure 4.21, the dielectric loss with respect to frequency for 3 layers of BST films with different compositions is shown. Dielectric loss of the films was between 4 and 7 % for Ba_{0.5}Sr_{0.5}TiO₃ and Ba_{0.9}Sr_{0.1}TiO₃ films up to 1 MHz, whereas it changed from 7 to 10 % for Ba_{0.7}Sr_{0.3}TiO₃. There is a tendency for the dielectric loss to increase remarkably above 1 MHz for all films. Several possible sources exist for such

Table 4.4. Dielectric properties of some sol-gel derived films with different processing parameters. Properties of films that were deposited using other common BST deposition techniques are also provided to give an idea.

Reference	Thickness	Heat treatment	Composition	Dielectric Loss (%)	Dielectric constant
[13].	400 nm	700°C, 1h	Ba _{0.75} Sr _{0.25} TiO ₃	4	440 (@ 1kHz)
[40]	400 nm	700°C, 2h	Ba _{0.4} Sr _{0.6} TiO ₃ Ba _{0.8} Sr _{0.2} TiO ₃	1 4	680 (@ 100 kHz) 749 (@ 100 kHz)
[14]	300 nm	750°C, 10 min (RTA)	Ba _{0.8} Sr _{0.2} TiO ₃	Not reported	680 (@ 100 kHz)
[41]	400 nm	700°C, 2h	Ba _{0.7} Sr _{0.3} TiO ₃	2,36	120 (@ 100kHz)
[28]	600 nm	800°C, 30 min	Ba _{0.67} Sr _{0.33} TiO ₃	Not reported	350 (@ 1kHz)
[38]	160 nm	800°C 1 min (RTA)	Ba _{0.5} Sr _{0.5} TiO ₃	2	230 (@ 100kHz)
[44] (PLD)	40 nm	700°C, 1h	Ba _{0.5} Sr _{0.5} TiO ₃	3,5	150 (@ 1 MHz)
[45] (MOCVD)	30 nm	625°C	Ba _{0.7} Sr _{0.3} TiO ₃	Not reported	208 (@ 1 kHz)
[46] (RF-Sputtering)	80 nm	650°C	Ba _{0.5} Sr _{0.5} TiO ₃	2	530 (@ 10 kHz)

dispersion, including the finite resistance of the electrodes, the presence of a barrier layer between the insulating film and the electrode surface, or leaky grain boundaries [40].

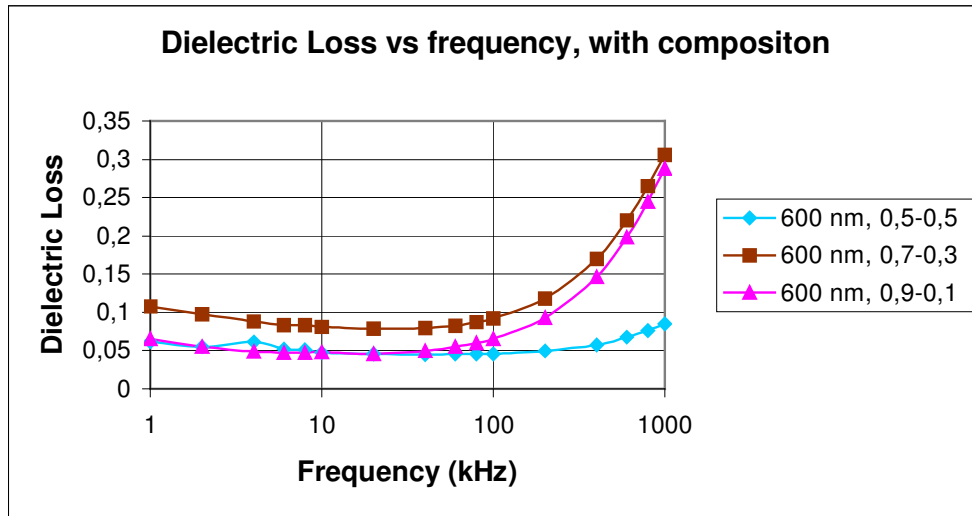


Figure 4.21. Dielectric loss as a function of frequency for 600 nm (3 layers) $Ba_xSr_{1-x}TiO_3$ films.

Dielectric loss originates from two mechanisms: resistive loss and relaxation loss. Resistive loss mechanism involves energy consumption by the mobile charges in the film; whereas, in the case of relaxation loss mechanism, it is the relaxation of dipole which dissipates the energy. If there are very few charges in the film then the latter mechanism is dominating. The resistive loss mechanism is directly connected to the leakage current of the film: if the leakage current is higher the loss is also higher. Alternatively, if the dielectric constant of the film is large, then an increase in dielectric loss is obvious due to the contribution from the relaxation mechanism. Enhanced polarization increases the dissipation during the relaxation [19]. In our films, dielectric loss at 800°C is lower than the value at 600 and 700°C (Figure 4.22). This may be due to achievement of lowest resistive loss due to complete crystallization into pure BST phase. Although relaxation component of dielectric loss is higher at 800°C, resistive loss is lower so overall dielectric loss is lower than that

of 600 and 700°C. However, this can only be a possible explanation. In order to verify this suggestion, leakage current measurements should be made. Since, resistive loss component of dielectric loss is directly proportional to leakage current, it may be possible to estimate the magnitude of resistive loss of the films sintered at different temperatures.

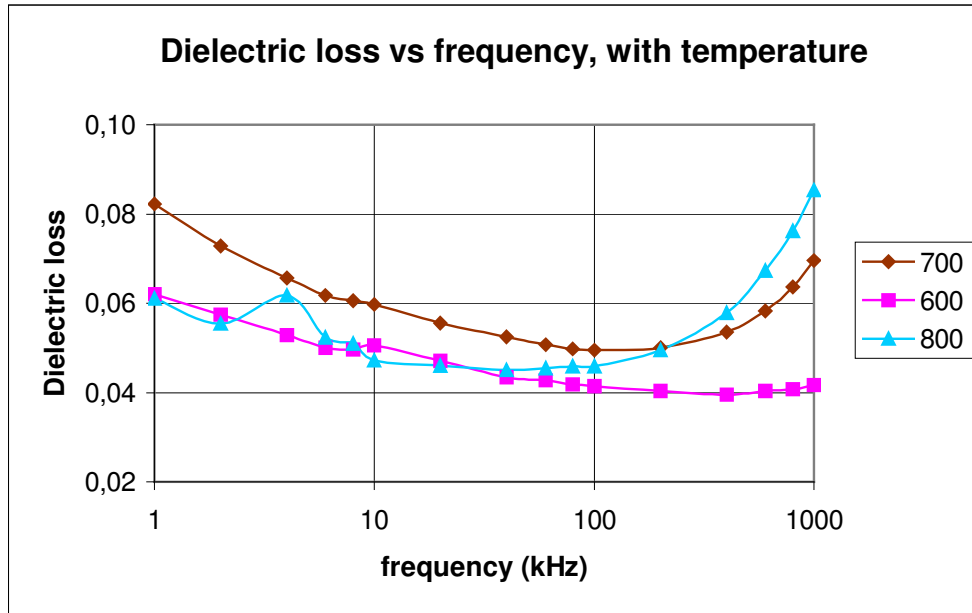


Figure 4.22. Dielectric loss of $\text{Ba}_{0.5}\text{Sr}_{0.5}\text{TiO}_3$ films as a function of frequency sintered at different temperatures for 600 nm films.

The above paragraph explains the causes of the high dielectric loss for $\text{Ba}_{0.7}\text{Sr}_{0.3}\text{TiO}_3$ film evident from Figure 4.20. Since, dielectric constant for this composition is the highest amongst the others, dipole moment density is also highest, resulting in an increase in dipole relaxation loss. As the dielectric constants thus dipole moments densities of $\text{Ba}_{0.5}\text{Sr}_{0.5}\text{TiO}_3$ and $\text{Ba}_{0.9}\text{Sr}_{0.1}\text{TiO}_3$ films are comparable, their dielectric loss values are also comparable.

The dependence of dielectric constant and loss on thickness was also studied. Table 4.5 shows the comparison of dielectric constant and loss for films of different thickness both measured at 10 kHz.

Table 4.5. Change in dielectric properties with increasing film thickness, for different compositions.

Composition	K (2 layers, 400 nm)	K (3 layers, 600 nm)	tan δ (2 layers, 400 nm)	tan δ (3 layers, 600 nm)
Ba _{0,5} Sr _{0,5} TiO ₃	105	213	0,07	0,05
Ba _{0,7} Sr _{0,3} TiO ₃	152	275	0,08	0,08
Ba _{0,9} Sr _{0,1} TiO ₃	156	213	0,08	0,05

The increase of dielectric constant with film thickness was obvious. This increase in the dielectric constant with increasing thickness was expected because of three main reasons: First, dielectric constant depends on grain size [7], and the grain size of the films increases with increasing film thickness. Secondly, as the film thickness increases, the density of dipoles increases, which in turn increases the polarization density and dielectric constant. Third and most important reason is the presence of a low dielectric constant interfacial layer between Pt bottom electrode and BST film [43, 47]. In a thinner film near either electrode-film interface, the ionic contribution to dielectric constant is suppressed; that is, a region of few lattice constant acts as a low permittivity or a “dead” layer. An applied voltage is dropped across the interfacial layers and bulk of the film in series. This effect of interfacial layer is more pronounced for thinner films [17]. This low dielectric constant interfacial layer acts as a series capacitor with the BST film and decreases the overall capacitance of BST stack. Since the overall capacitance of these capacitors connected in series is equal to

$1/C_{eq} = 1/C_i + 1/C_b$, where C_{eq} is the overall capacitance, C_i is the capacitance of the interfacial layer, and C_b is the bulk capacitance corresponding to the actual capacitance of the BST film, interface layer with the low capacitance significantly decreases the overall capacitance. This explains why bulk permittivities of BST, which are in the order of thousands, could not be realized in thin films together with grain size and thickness dependencies of thin films which are called together as size effects in thin films. There are many suggestions explaining the possible reasons for the formation of this interfacial layer [42], existence of which was also verified by TEM recently [47].

Apart from grain size, dielectric constant of the films also depend on grain morphology. Columnar-grained films are reported to exhibit larger dielectric constants [37]. The change in magnitude can be dramatic: from 500 to 900. A granular microstructure with random orientation of the grains typically occurs from homogeneous nucleation in an amorphous matrix as obtained after the pyrolysis step during chemical solution deposition (CSD). Often, there is a competition between heterogeneous nucleation at the bottom interface which may lead to formation of oriented or epitaxial films and random homogeneous nucleation. The nucleation type is controlled by first, the film material, second, the type of substrate interface, and third, the processing parameters. Columnar grain growth in thin films can only be achieved if the possibility for a single nucleation event is favored over the other nucleation events. Regarding to the theory of glass crystallization, heterogeneous nucleation can be favored over homogeneous nucleation by a lowering of the driving force for crystallization which can be achieved by increasing the crystallization temperature or by the influence of an intermediate phase. In BST thin films columnar grains were reported to be obtained only for precursor solutions which transform to the perovskite phase via intermediate alkaline earth-titanium-oxo-carbonate phase. Due to delayed crystallization, the driving force is lowered which results in a favoring of heterogeneous nucleation events. In contrast to the intensively investigated PZT thin films which crystallize via the intermediate fluorite phase and easily form columnar grains, the BST films only exhibit a columnar grain growth for a small thickness (approximately 10 nm) of the individual crystallized layers [37].

Dielectric properties also depend on the substrate – film interface. RTA (Rapid Thermal Annealing) is a new method that is said to improve this interface [48, 49]. The great advantages of this method are a short annealing time and its relative process simplicity as compared with the conventional furnace annealing. The objective of the short processing time is to basically reduce the time and temperature product such that the desired physical or chemical processes are completed while the unwanted processes such as dopant diffusion, interface reactions, decomposition, or evaporation, etc., are suppressed or minimized. The short rise time to the desired annealing temperature minimizes the interface reactions and results in a dense microstructure [48].

Ren et al. [38] synthesized BST films with the same procedure as in our study, only difference being the usage of RTA instead of conventional annealing. They measured a dielectric constant of 230 and dielectric loss of 0.02 for a 160 nm film, which is better than the results in this study. They claim that RTA minimizes the formation of low-dielectric layer between BST and substrate. A summary of the dielectric properties of all samples produced in our study is given at Table 4.6.

As stated in Chapter 2, hillocks are formed in Pt/Ti electrodes to relieve the compressive stress of Pt film [22]. Therefore hillock formation during BST film formation was also investigated. For this purpose, surfaces of three substrates with different thermal histories were inspected using SEM without coating the BST film on top, in order to see if any metal protrudes from the surface. One of the substrates was inspected in as-received condition without any thermal treatment, another was annealed at 800°C for 1 hours and last one annealed under the same conditions with BST films, at 800°C for 3 hours. SEM micrographs of three samples are given respectively in Figure 4.23.

Table 4.4. Dielectric Properties of Ba_xSr_{1-x}TiO₃ films.

Film Composition	Film Thickness	Heat Treatment Applied	1 kHz		100 kHz		1 MHz	
			Dielectric Constant	Dielectric Loss (%)	Dielectric Constant	Dielectric Loss (%)	Dielectric Constant	Dielectric Loss (%)
Ba _{0.5} Sr _{0.5} TiO ₃	600 nm	800°C, 3 hrs	230	6.1	205	4.6	196	8.53
Ba _{0.5} Sr _{0.5} TiO ₃	600 nm	700°C, 3 hrs	184	8,2	155	4,9	150	6,9
Ba _{0.5} Sr _{0.5} TiO ₃	600 nm	600°C, 3 hrs	80	6.2	70	4.1	66	4.2
Ba _{0.5} Sr _{0.5} TiO ₃	400 nm	800°C, 3 hrs	135	8.3	114	5.7	107	13.5
Ba _{0.9} Sr _{0.1} TiO ₃	600 nm	800°C, 3 hrs	228	6.5	202	6.5	184	28.8
Ba _{0.9} Sr _{0.1} TiO ₃	400 nm	800°C, 3 hrs	175	9.9	141	17	100	42.3
Ba _{0.7} Sr _{0.3} TiO ₃	600 nm	800°C, 3 hrs	313	10.8	249	9.2	217	30.6
Ba _{0.7} Sr _{0.3} TiO ₃	400 nm	800°C, 3 hrs	176	11,7	137	7,3	126	14,2
Ba _{0.5} Sr _{0.5} TiO ₃ (Old Solution)	500 nm	800°C, 3 hrs	188	7,83	160	4,8	152	6,9

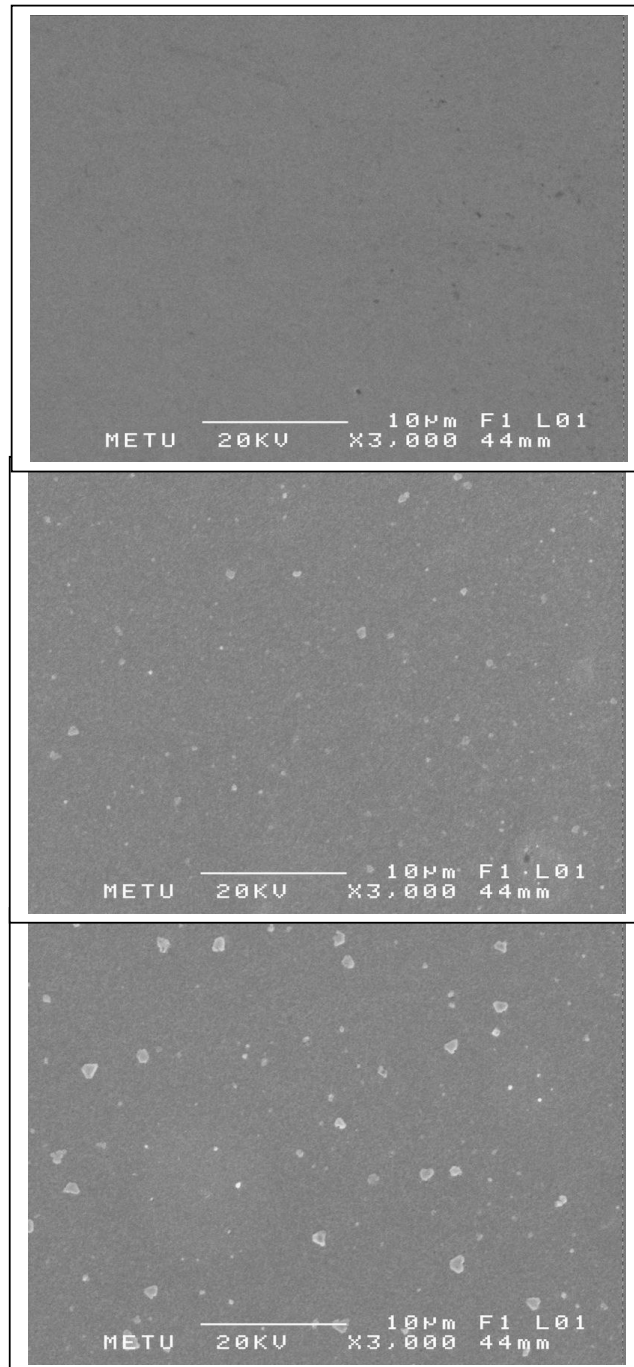


Figure 4.23. SEM micrograph of the surfaces of Pt/Ti/SiO₂/Si substrate: (top) prior to any thermal treatment, (middle) after annealing at 800°C for 1 hour. White dots are hillocks of Pt, (bottom) after annealing at 800°C for 3 hours. White dots have grown in size.

Surface of as received Pt substrate was homogeneous and free of any different contrast features. However, the substrate annealed at 800°C for 1 hour contained some light color dot-shaped features. For the substrate annealed at 800°C for 3 hours, these features grew in size. Same kind of dot-like features protruding from the surface were also observed by Park et al. for a different Pt/Ti/SiO₂/Si substrate [50]. These features were suspected to be hillocks, but first EDS analysis should have been made to assure that they are not second phase particles formed as a result of diffusion process.

The EDS analysis showed that these features are rich in Pt, which makes sense since bottom layers of Ti and Si contributes less to the hillock regions compared to normal regions.

Hillocks are known to form capacitor shorts or result in degradation of electrical properties. In this study, the formation of hillocks was proved by SEM studies on uncoated substrates. But in the actual case, the substrates went into thermal treatment together with the BST layer coated on top of them. So, the formation of hillocks may be enhanced or prevented by the presence of BST layer. Al-Shareef et al. [51] studied the effect of PZT film on the formation of hillocks and found that the presence of PZT film suppresses hillock formation. This suppression was explained by (a) limited surface mobility of Pt atoms due to the presence of top layer, (b) reduced oxygen diffusion to the Pt – Ti interface, (c) reduced stress in the Pt/Ti layer due to the presence of PZT overlayer prior to annealing. On the other hand, Al-Shareef et al. [51] and Nam et al. [22] experimentally verified that hillocks could result in capacitor shorts. They observed that the increase in size of hillocks rather than their density influences the shorting. In our study, some of BST capacitors shorted, but it is hard to prove that shorts arise due to hillocks in Pt/Ti/SiO₂/Si substrates.

4.6. Ferroelectric Properties of BST Films

Change of capacitance with voltage, C-V behaviour in short, gives an idea about ferroelectricity. Therefore, C-V measurements are mentioned within the ferroelectric properties section. The polarization and capacitance vary non-linearly with an applied field due to domain structure. The C-V profile is actually a measure of dP/dE , so the peak in the C-V characteristic corresponds to a large polarization change, or the switching of ferroelectric domains from one orientation to another.

The dc bias was increased from 0 V to 4.5 V in 0.5 V intervals, and then decreased again to 0 V and increased in the reverse polarity down to -4.5 V. The C-V curve for $Ba_{0.7}Sr_{0.3}TiO_3$ is shown in Figure 4.24. The C-V curve was symmetric and nearly no hysteresis was observed due to paraelectric nature and fine grain size of the film, as expected for this composition which is above its Curie temperature at room temperature. C-V curve for $Ba_{0.9}Sr_{0.1}TiO_3$ is shown in Figure 4.25, which is in ferroelectric state at room temperature. This time in contrast to the $Ba_{0.7}Sr_{0.3}TiO_3$ film, there was a butterfly shape in the curve, suggesting a possible ferroelectricity in the film, since BST of this composition is in ferroelectric phase at room temperature.

Ferroelectricity in BST thin films is suppressed. Generally for ferroelectric films below certain grain size called as critical grain size, despite the material is in its ferroelectric state (below its Curie temperature at the ambient temperature), hysteresis loop and dielectric anomaly around the Curie temperature cannot be observed. For barium titanate thin films, this critical grain size for the existence of the ferroelectricity is around 120 nm [36]. The reason for disappearance of ferroelectricity below this critical grain size is unknown [7]. Also, for BST thin films Sr addition to $BaTiO_3$ decreases the tetragonality (c/a ratio) in the perovskite structure and a small value of c/a ratio may not be sufficient to create charge separation and spontaneous polarization in the films, so the fabrication of BST ferroelectric film is even more difficult than that of $BaTiO_3$ [36].

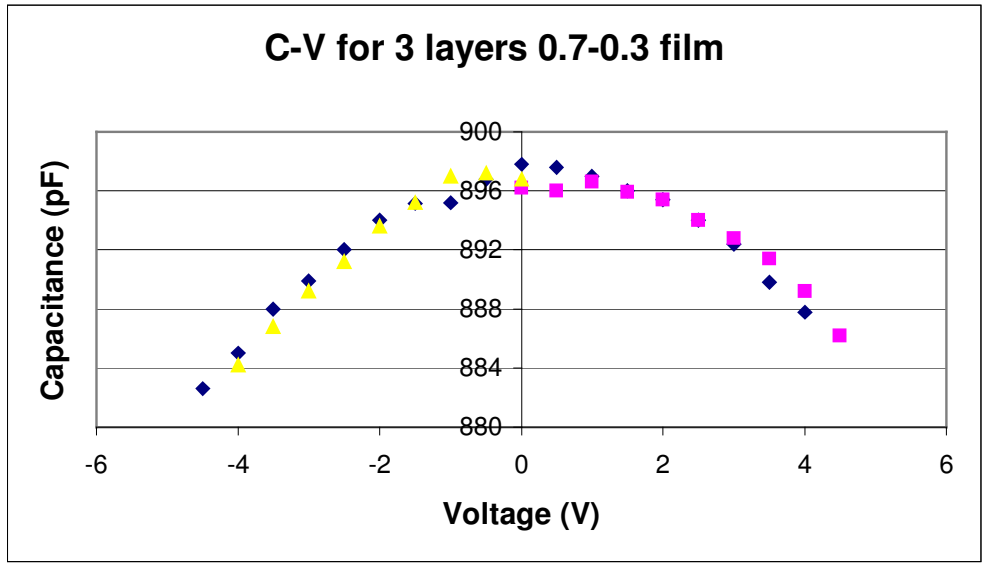


Figure 4.24. C-V curve for a 3 layers $\text{Ba}_{0.7}\text{Sr}_{0.3}\text{TiO}_3$ film.

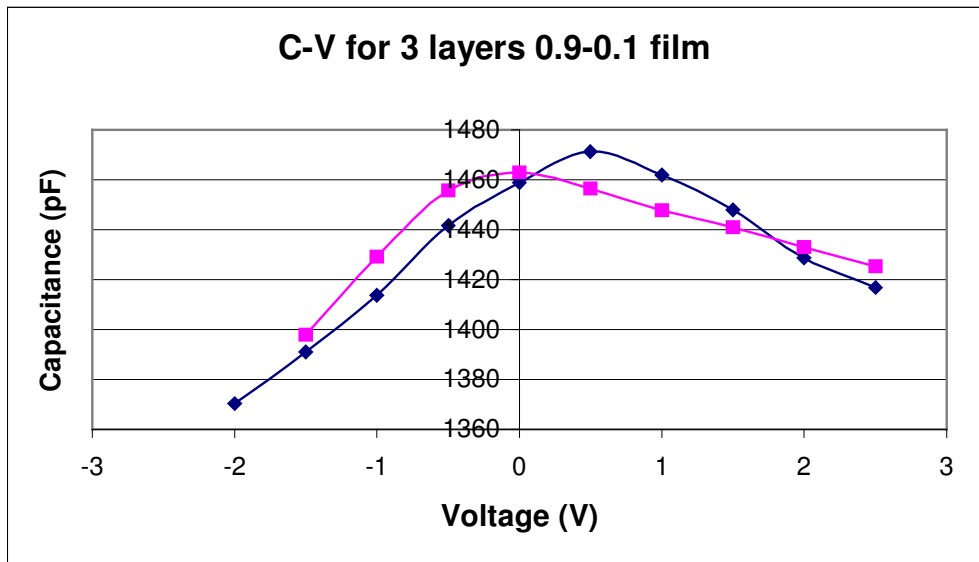


Figure 4.25. C-V curve for a 3 layers $\text{Ba}_{0.9}\text{Sr}_{0.1}\text{TiO}_3$ film.

In this study, conventional sol-gel technique was used. Grain sizes of the films were small, obtained from very rough approximation of Scherrer's formula as 25 nm. This grain size is very small with respect to the critical grain size reported for BT films, which is 120 nm [36]. However, slim hysteresis loops were obtained by the ferroelectric measurements made by constructing modified Sawyer-Tower circuit. Among all BST films produced, only for 3 layers film (600 nm thickness) of composition $\text{Ba}_{0,9}\text{Sr}_{0,1}\text{TiO}_3$, hysteresis loops could be obtained. In figure 4.26, hysteresis of this film obtained at 3 V peak to peak voltage is shown. For other compositions, $\text{Ba}_{0,7}\text{Sr}_{0,3}\text{TiO}_3$ and $\text{Ba}_{0,5}\text{Sr}_{0,5}\text{TiO}_3$, polarization was linear with applied electric field. This was expected because for bulk BST, 0.3 % Sr addition brings the Curie temperature to room temperature, so for $\text{Ba}_{0,7}\text{Sr}_{0,3}\text{TiO}_3$ and $\text{Ba}_{0,5}\text{Sr}_{0,5}\text{TiO}_3$ the material is in paraelectric state at room temperature, likewise C-V curve of $\text{Ba}_{0,7}\text{Sr}_{0,3}\text{TiO}_3$ did not display butterfly shape unlike $\text{Ba}_{0,9}\text{Sr}_{0,1}\text{TiO}_3$. Hysteresis loop parameters for the $\text{Ba}_{0,9}\text{Sr}_{0,1}\text{TiO}_3$ film are given in Table 4.7. It can be seen that both remnant polarization and coercive field values increase with increasing electric field. This is due to alignment of domains with the field. Actual hysteresis loops captured directly from the oscilloscope screen are given in appendix.

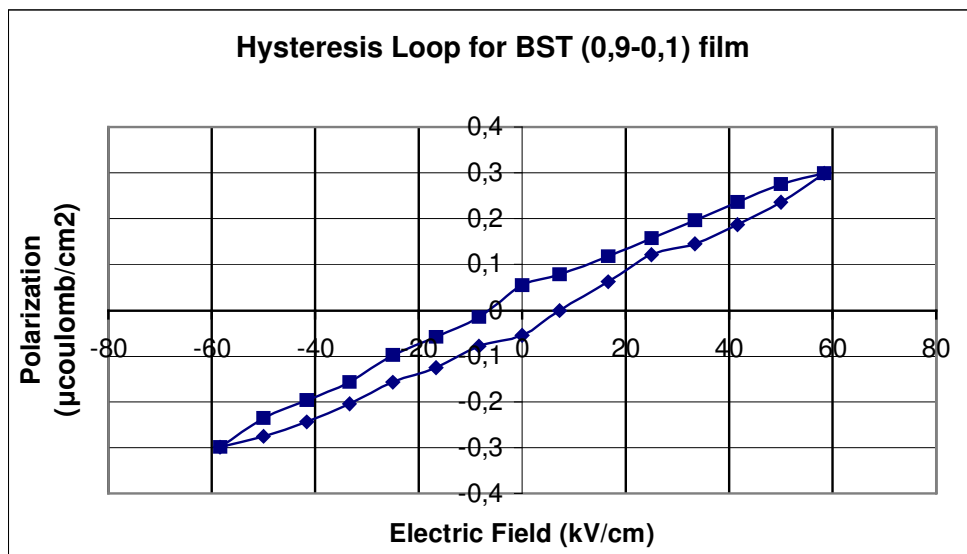


Figure 4.26. Polarization vs electric field behaviour for 600 nm $\text{Ba}_{0,9}\text{Sr}_{0,1}\text{TiO}_3$ film.

Table 4.7. Ferroelectric properties of $\text{Ba}_{0,9}\text{Sr}_{0,1}\text{TiO}_3$ films on Pt/Ti/SiO₂/Si substrates.

Film Thickness	Film Composition	Coercive Field, E_c , (kV/cm)	Remanent Polarization, P_r ($\mu\text{C}/\text{cm}^2$)	Applied E-Field (E_{max}) (kV/cm)	Applied Voltage (V_{max})
0,6 μm	$\text{Ba}_{0,9}\text{Sr}_{0,1}\text{TiO}_3$	4,5	0.0235	41,6	2,5
		4,6	0,0313	50	3
		7,23	0,047	58,3	3,5 V

Remnant polarization and coercive field values of the films are very low for a ferroelectric thin film. This is due to fine grain size of the films. The sol-gel deposition of BaTiO_3 films commonly results in polycrystalline, granular films with grain diameters of lower than 70 nm due to random nucleation in the pyrolyzed gel films [36]. Recently, some researchers [36, 52] managed to fabricate ferroelectric BST films with grain sizes greater than 100 nm by coating highly diluted solutions on lattice and structure matched substrates and sintering each coated layer by rapid thermal annealing in order to promote epitaxial, oriented growth by heterogeneous nucleation from the substrate. For example, Wang et al. [52] succeeded at fabricating columnar grained, 250 nm thick $\text{Ba}_{0,9}\text{Sr}_{0,1}\text{TiO}_3$ films having grain sizes in 80-200 nm range by coating 0.05M solutions on Pt/Ti/SiO₂/Si substrates. They reported remnant field of $7.8 \mu\text{C}/\text{cm}^2$ and coercive field of 56 kV/cm at an electric field of 320 kV/cm.

CHAPTER 5

CONCLUSIONS AND FURTHER SUGGESTIONS

In this study, stable (Ba,Sr)TiO₃ solutions were synthesized by chemical solution deposition, and coated on Pt/Ti/SiO₂/Si and Si substrates with different processing parameters like solution concentration, precursor materials, spinning speed, heat treatment temperatures, and number of layers coated. The microstructure change upon change of these parameters was related to the measured dielectric properties.

It was found that addition of ethylene glycol stabilizes the solution and helps the dissolution of acetates.

Crack-free, homogeneous and dense Ba_xSr_{1-x}TiO₃ films were obtained. Optimum spinning speed and time was determined as 4000 rpm, 30 seconds, whereas x-ray diffraction and dielectric constant measurements suggested optimum sintering parameters as 800°C for 3 hours for the complete crystallization of the films.

Dielectric constant of the films increased with increasing temperature, in agreement with the crystallization studies. It increased from 80 to 230 for a 600 nm Ba_{0.5}Sr_{0.5}TiO₃ film at 1 kHz, when the sintering temperature increased from 600°C to 800°C.

Dielectric constant of the films was slightly decreased with frequency in the range 1 kHz – 1 MHz.

Dielectric constant of the films also changed with Ba/Sr ratio, but this change was not linear with the increase in Sr content. Dielectric constant of $\text{Ba}_{0.5}\text{Sr}_{0.5}\text{TiO}_3$ and $\text{Ba}_{0.9}\text{Sr}_{0.1}\text{TiO}_3$ was close to each other. For 600 nm film thickness, the former was 230 and the latter was 228 at 1 kHz. Dielectric constant of $\text{Ba}_{0.7}\text{Sr}_{0.3}\text{TiO}_3$ was the highest; it was 313 for the same thickness with others, It is known that 0.3 mole percent Sr brings Curie temperature of pure BaTiO_3 to room temperature and dielectric constant displays a peak near phase transition temperature.

Dielectric loss of the films was changed between 4 – 9 % in the measurement frequency range 1kHz – 100 kHz, but increased sharply above 100 kHz up to 30 % similar to what has been reported in the literature.

Dielectric constant increased but the dielectric loss decreased with increasing film thickness for all compositions. The increase in the dielectric constant was due to the minimization of the effect of low dielectric constant interfacial layer in series with the film with increasing film thickness, the reduction in the fraction of pores due to increased number of coating cycles and the increase in the dipole moment density with thickness. The decrease in dielectric loss might be due to reduction of resistive loss component of the total dielectric loss although the dipole relaxation component should increase with film thickness due to increase in the density of dipoles.

The BST films showed typical C-V curves, capacitance decreased with increasing bias voltage. For the $\text{Ba}_{0.5}\text{Sr}_{0.5}\text{TiO}_3$ film, which is above Curie temperature at room temperature, there was no change in C-V curve for negative and positive polarity, suggesting that the film is paraelectric. On the contrary, $\text{Ba}_{0.9}\text{Sr}_{0.1}\text{TiO}_3$ films had a slightly butterfly shaped C-V curve, suggesting a possible ferroelectricity in the film. But, although films with that composition are ferroelectric in bulk form, polycrystalline BST thin films with small equiaxed grains fails to show ferroelectricity.

Only, BST films with the composition $\text{Ba}_{0.9}\text{Sr}_{0.1}\text{TiO}_3$ displayed hysteresis. Remnant polarization of the film was $0.047 \mu\text{C}/\text{cm}^2$ and coercive field was $7.23 \text{ kV}/\text{cm}$ at an applied field of $58 \text{ kV}/\text{cm}$.

For the improvement of the dielectric properties, clean room environment for the preparation of the substrate is a must. Also, RTA (rapid thermal annealing) might be useful in reducing the interfacial layer formed between the film and the substrate.

Oriented or epitaxial films can be synthesized by coating thinner layers using highly diluted solutions on structure and lattice matched oxide substrates like LaAlO_3 or MgO and applying RTA. The usage of oxide electrodes limits the dielectric losses.

Measurement of leakage current of the films may be helpful to characterize the electrical properties. Leakage current is a crucial parameter for DRAM applications.

Increasing sintering temperature improves the densification by decreasing the pore density. This increase in densification can be monitored by measuring refractive index of the films using spectroscopic ellipsometry or visible-UV spectroscopy.

The dielectric properties strongly depend on grain size and morphology of the films. Since, small equiaxed grains of BST films synthesized by sol-gel processing can not be differentiated by SEM, higher magnification electron microscopes like TEM or FESEM may be used to measure grain size.

REFERENCES

- [1] N. Setter, R.Waser, “Electroceramic Materials”, Acta Materialia, Vol. 48, pp. 151-178, (2000).
- [2] A.I. Kingon, S.K. Streiffer, “Ferroelectric Films and Devices”, Current Opinion in Solid State & Materials Science, Vol. 4, (1999).
- [3] International Technology Roadmap for Semiconductors (ITRS) Report (2001), <http://public.itrs.net>.
- [4] Principles of Electronic Ceramics, L.L. Hench and J.K. West, John Wiley & Sons, (1989).
- [5] Ceramic Materials for Electronics, Edited by R. C. Buchanan, Marcel Dekker Inc., (1991).
- [6] Cem Başçeri, “Electrical and Dielectric Properties of (Ba,Sr)TiO₃ Capacitors for Ultra-High Density Dynamic Random-Access Memories”, PhD Dissertation, North Carolina State University, (1997).
- [7] Dragan Damjanovic, “Ferroelectric, Dielectric and Piezoelectric Properties of Ferroelectric Thin Films and Ceramics”, Rep. Prog. Phys. 61, pp 1267-1324, (1998).
- [8] G.H. Haertling, “Ferroelectric Ceramics: History and Technology”, JACS, Vol. 82 [4], pp. 797-818, (1999).

- [9] B.A. Baumert, L.H. Chang, A.T. Matsuda, C.J. Tracy, N.G. Cave, R.B. Gregory, P.L. Fejes, "A Study of Barium Strontium Titanate Thin Films for Use in Bypass Capacitors", Journal of Materials Research, Vol. 13 [1], pp. 197-204, (1998).
- [10] S. Ezhilvalavan, T.Y. Tseng, "Progress in the Developments of (Ba,Sr)TiO₃ (BST) Thin Films for Gigabit Era DRAMs", Materials Chemistry and Physics, Vol.65, pp. 227-248, (2000).
- [11] Piezoelectric Ceramics, Bernard Jaffe, Academic Press, (1971).
- [12] A. I. Kingon, J.P. Maria, S.K.Streiffer, "Alternative Dielectrics to Silicon Dioxide for Memory and Logic Devices", Nature, Vol. 406, pp. 1032-1038, (2000).
- [13] D.M. Tahan, A. Safari, L.C. Klein, "Sol-Gel Preparation of Barium Strontium Titanate Thin Films", JACS, Vol. 79, pp. 1593, (1996).
- [14] J.G. Cheng, X.J. Meng, J. Tang, S.L. Guo, J.H. Chu, "Fabrication and Electrical Properties of Sol-Gel Derived Ba_{0.8}Sr_{0.2}TiO₃ Ferroelectric Films from a 0.05-M Spin-On Solution", Applied Physics A, Vol. 70, pp. 411-414, (2000).
- [15] S. Liu, M. Liu, Y. Zeng, Y. Huang, "Preparation, Phase Transition Diffuseness and Ferroelectric Fatigue Behaviour of Ba_{0.85}Sr_{0.15}TiO₃ Thin Film for Uncooled Infrared Focal Plane Arrays", Materials Science and Engineering B, Vol. 90, pp. 149-153, (2002).
- [16] S.B. Majumder, M. Jain, A. Martinez, R.S. Katiyar, F.W. Van Keuls, F.A. Miranda, "Sol-Gel Derived Grain Oriented Barium Strontium Titanate Thin Films for Phase Shifter Applications", Journal of Applied Physics, Vol.90 [2], pp. 896-903, (2001).

- [17] T.M. Shaw, Z. Suo, M. Huang, E. Liniger, R.B. Laibowitz, J.D. Baniecki, "The Effect of Stress on the Dielectric Properties of Barium Strontium Titanate Thin Films", Applied Physics Letters, Vol. 75 [14], pp. 2129-2131, (1999).
- [18] R.W. Schwartz, P.G. Clem, J.A. Voight, E.R. Byhoff, M.V. Stry, T.J. Headley, N.A. Missert, "Control of Microstructure and Orientation in Solution-Deposited BaTiO₃ And SrTiO₃ Thin Films", JACS, Vol. 82 [9], pp. 2359-2367, (1999).
- [19] M. Nayak, S.Y.Lee, Tseung-Yuen Tseng, "Electrical and Dielectric Properties Of (Ba_{0.5}Sr_{0.5})TiO₃ Thin Films Prepared by a Hydroxide-Alkoxide Precursor-Based Sol-Gel Method", Materials Chemistry and Physics, Vol. 77, pp. 34-42, (2002).
- [20] J.M. Bell, P.C. Knight, G.R. Johnston, "Electrode Materials for Ferroelectric Film Capacitors and Their Effect on The Electrical Properties", Ferroelectric Thin Films: Synthesis and Basic Properties, edited by C.A. Paz de Araujo, J.F. Scott, G.W. Taylor, Gordon and Breach Publications, (1996).
- [21] H.N.Al-Shareef, A.I. Kingon, "Electrode Materials for Ferroelectric Film Capacitors and Their Effect on the Electrical Properties", Ferroelectric Thin Films: Synthesis and Basic Properties, edited by C.A. Paz de Araujo, J.F. Scott, G.W. Taylor, pp. 193-230, Gordon and Breach Publications, (1996).
- [22] H.J. Nam, D.K. Choi, W.J. Lee, "Formation of Hillocks in Pt/Ti Electrodes and Their Effects on Short Phenomena of PZT Films Deposited by Reactive Sputtering", Thin Solid Films, Vol. 371, pp. 264-271, (2001).
- [23] M. C. Gust, L.A. Momoda, N.D. Evans, M.L. Mecartney, "Crystallization of Sol-Gel Derived Barium Strontium Titanate Films", JACS, Vol.84 [5], pp. 1087-92, (2001)

- [24] Brian D. Fabes, Brian J. J. Zelinski, Ronald R. Uhlmann, "Sol-Gel Derived Ceramic Coatings", in Ceramic Films and Coatings, Edited by John B. Wachtman, Richard A. Haber, Noyes Publications, Park Ridge, NJ, USA, (1993)
- [25] D. E. Bornside, C. W. Macosko, L. E. Scriven, Journal of Imaging Technology, Vol. 13, pp. 122-129, (1987).
- [26] Sol-Gel Science, C.J. Brinker, G.W. Scherer, Academic Press, (1990).
- [27] G. Yi, M. Sayer, "Sol-Gel Processing of Complex Oxide Films", Ceramic Bulletin, Vol. 70, No. 7, pp. 1173-1179, (1991).
- [28] E. Dien, R. Verveur, M. Lejeune, A. Smith, "Preparation and Properties of Ba_{1-x}Sr_xTiO₃ Thin Films Deposited by the Sol-Gel Technique", Journal of Physics IV France, Vol. 8, pp. 9-73-9.77, (1998).
- [29] F.M. Pontes, E.R. Leite, D.S.L. Pontes, E. Longo, E.M.S. Santos, S. Mergulhao, P.S. Pizani, F. Lanciotti, T.M. Boschi, "Ferroelectric and Optical Properties of Ba_{0.8}Sr_{0.2}TiO₃ Thin Film", Journal of Applied Physics, Vol. 91 [9], pp. 5972-5978, (2002).
- [30] H.Y. Tian, W.G. Luo, X.H. Pu, A.L. Ding, "Synthesis and Microstructure of the Acetate-Based Sr-Doped Barium Titanate Thin Films Using a Modified Sol-Gel Technique", Journal of Materials Science Letters, Vol. 19, pp.1211-1213, (2000).
- [31] U. Hasenkox, S. Hoffmann, R. Waser, "Influence of Precursor Chemistry on the Formation of MTiO₃ (M = Ba, Sr) Ceramic Thin Films", Journal of Sol-Gel Science and Technology, Vol.12, pp. 67-79, (1998).

- [32] D.M. Tahan, "Microstructure and Property Characterization of Barium Strontium Titanate Thin Films Prepared by a Sol-Gel Technique For DRAM Applications", Ph.D. Dissertation, Rutgers University, (1997).
- [33] D.P. Birnie II, "Esterification Kinetics in Titanium Isopropoxide-Acetic Acid Solutions" Journal of Materials Science, Vol. 35, pp. 367-374, (2000).
- [34] L.L. Lopez, J. Portelles, J.M. Siqueiros, G.A. Hirata, J. McKittrick, "Ba_{0.5}Sr_{0.5}TiO₃ Deposited by PLD on SiO₂/Si, RuO₂/Si and Pt/Si Electrodes, Thin Solid Films, Vol. 373, pp. 49-52, (2000).
- [35] S. Kim, T.S. Kang, J.H. Je, "Structural Characterization of Laser Ablated Epitaxial (Ba_{0.5}Sr_{0.5})TiO₃ Thin Films on MgO (001) by Synchrotron X-ray Scattering", Journal of Materials Research, Vol.14[7], pp.2905, 1999.
- [36] J.G. Cheng, X.J. Meng, J. Tang, S.L. Guo, J.H. Chu, "Fabrication and Electrical Properties of Sol-Gel-Derived Ba_{0.8}Sr_{0.2}TiO₃ Ferroelectric Thin Films from a 0.05-M Spin-On Solution", Applied Physics A, Vol. 70, pp. 411-414, (2000).
- [37] S. Hoffmann, R. Waser, "Control of the Morphology of CSD-Prepared (Ba,Sr)TiO₃ Thin Films", Journal of the European Ceramic Society, Vol.19, pp. 1339-1343, (1999).
- [38] T.L. Ren, X.N. Wang, J.S. Liu, H.J. Zhao, T.Q. Shao, L.T. Liu, Z.J. Li, "Characteristics of Silicon-Based Ba_xSr_{1-x}TiO₃ Thin Films Prepared by a Sol-Gel Method, Journal of Physics D: Applied Physics, Vol. 35, pp. 923-926, (2002).
- [39] Elements of X-ray Diffraction, B.D. Cullity, Addison-Wesley Publishing Company, Inc., (1978).

- [40] F.M. Pontes, E. Longo, E.R. Leite, J.A. Varela, "Study of the Dielectric and Ferroelectric Properties of Chemically Processed $\text{Ba}_x\text{Sr}_{1-x}\text{TiO}_3$ Thin Films", Thin Solid Films, Vol. 386, pp. 91-98, (2001).
- [41] N.V. Giridharan, R. Jayavel, P. Ramasamy, "Structural, Morphological and Electrical Studies on Barium Strontium Titanate Thin Films Prepared by Sol-Gel Technique", Crystal Research Technology, Vol. 36 [1], pp. 65-72, (2001).
- [42] S.K. Streiffer, C. Başçeri, C.B. Parker, S.E. Lash, A.I. Kingon, "Ferroelectricity in Thin Films: The Dielectric Response of Fiber-Textured $(\text{Ba}_x\text{Sr}_{1-x})\text{Ti}_{1+y}\text{O}_{3+z}$ Thin Films Grown by Chemical Vapor Deposition", Journal of Applied Physics, Vol.86 [8], (1999).
- [43] S.Stemmer, S.K. Streiffer, N.D. Browning, C.Başçeri, A.I. Kingon, "Grain Boundaries in Barium Strontium Titanate Thin Films: Structure, Chemistry and Influence on Electronic Properties, Interface Science, Vol. 8, pp. 209-221, (2000).
- [44] Yang G, Gu H, Zhu J, Wang Y, "The Fabrication and Characteristics of $(\text{Ba}_{0.5}\text{Sr}_{0.5})\text{TiO}_3$ Thin Films Prepared by Pulsed Laser Deposition", Journal of Crystal Growth, Vol. 242, pp. 172-176, (2002).
- [45] Fitsilis F, Regnery S, Ehrhart P, Waser R, Schienle F, Schumacher M, Dauelsberg M, Strzyzewski P, Juergensen H, "BST Thin Films Grown in a Multiwafer MOCVD Reactor", Journal of the European Ceramic Society, Vol. 21, pp. 1547-1551, (2001).
- [46] Im J, Auciello O.P.K., Baumann P.K., Streiffer S.K., Kaufman D.Y., Krauss A.R., "Composition Control of Magnetron Sputter Deposited $(\text{Ba}_x\text{Sr}_{1-x})\text{Ti}_{1+y}\text{O}_{3+z}$ Thin Films for Voltage Tunable Devices", Applied Physics Letters, Vol.76 [5], pp. 625-627, (2000).

- [47] H.Z. Jin, J. Zhu, P.Ehrhart, F. Fitsilis, C.L. Jia, S. Regnery, K. Urban, R. Waser, “An Interfacial Defect Layer Observed at (Ba,Sr)TiO₃/Pt Interface”, Thin Solid Films, Vol. 429, pp. 282-285, (2003).
- [48] P.J. Joshi, S. Ramanathan, S.B. Desu, S. Stowell, “Microstructural and Electrical Characteristics of Rapid Thermally Processed (Ba_{1-x}Sr_xTiO₃) Prepared by Metalorganic Solution Deposition Technique”, Physica Status Solidi (a), Vol. 161, pp. 361-370, (1997).
- [49] D. Wu, A. Li, H. Ling, X. Yin, C. Ge, M. Wang, N. Ming, “Preparation of (Ba_{0.5}Sr_{0.5})TiO₃ Thin Films by Sol-Gel Method with Rapid Thermal Annealing, Applied Surface Science, Vol.165, pp. 309-314, (2000).
- [50] K.H.Park, C.Y.Kim, Y.W.Jeong, H.J.Kwon, K.Y.Kim, J.S.Lee, S.T.Kim “Microstructures and Interdiffusions of Pt/Ti Electrodes with respect to Annealing in the Oxygen Ambient“, Journal of Materials Research, Vol.10 [7], pp. 1790-1794 (1995).
- [51] H.N. Al-Shareef, D. Dimos, B.A. Tuttle, M.V. Raymond, “Metallization Schemes for Dielectric Thin Film Capacitors”, Journal of Material Research, Vol. 12 [2], pp. 347-354, (1997).
- [52] G.S. Wang, J. Yu, Q. Wang, Q. Zhao, J.L. Sun, X.J. Meng, S.L. Guo, J.H. Chu, “Structure and Optical Properties of Ba_{0.9}Sr_{0.1}TiO₃ Ferroelectric Thin Films Prepared by Chemical Solution Routes”, Physica Status Solidi (a), Vol. 194 [1], pp. 56-63, (2002).
- [53] “Powder Diffraction File, Alphabetical Index: Inorganic Phases”, (JCPDS), Swarthmore, PA, (1986).

APPENDIX

Actual Hysteresis Loops

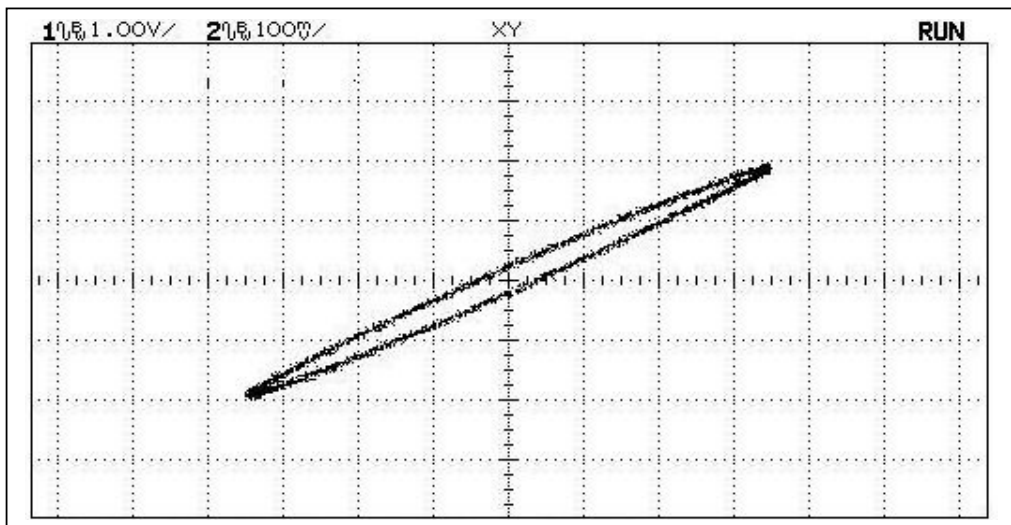


Figure A.1. Polarization versus electric field behaviour for 600 nm $\text{Ba}_{0.9}\text{Sr}_{0.1}\text{TiO}_3$ film at $V_x = 3.5$ V.

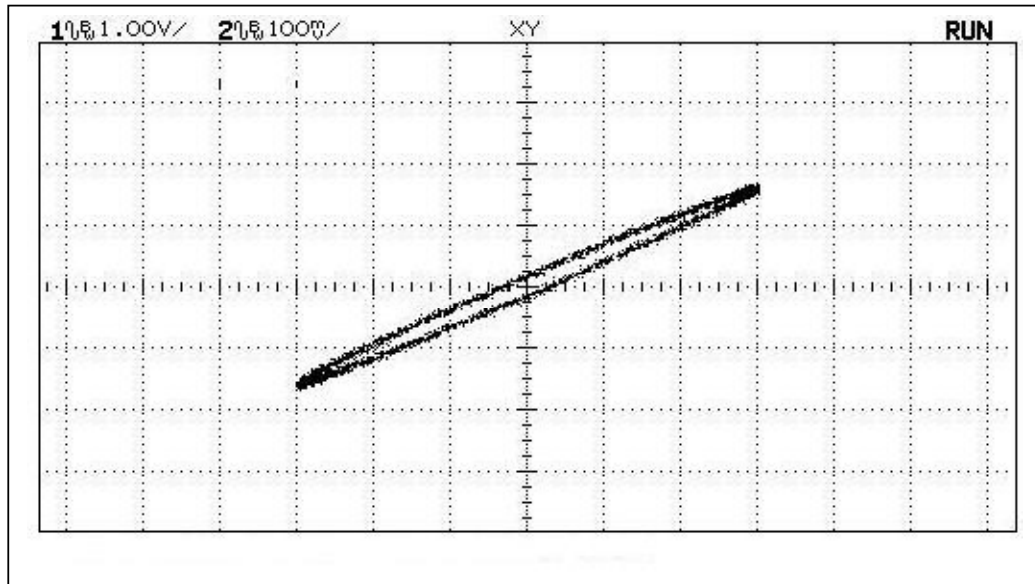


Figure A.2. Polarization versus electric field behaviour for 600 nm Ba_{0.9}Sr_{0.1}TiO₃ film at V_x = 3 V.

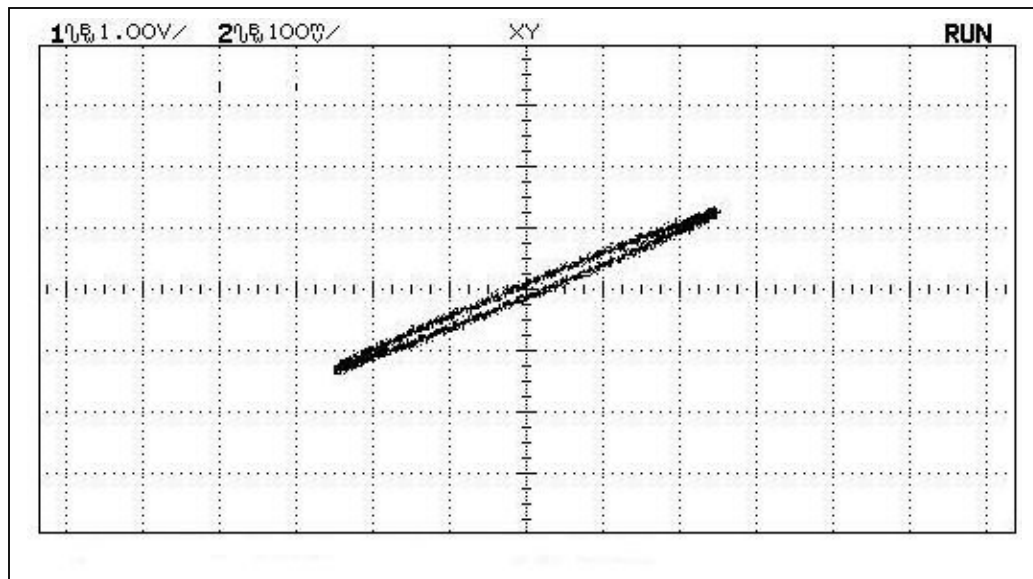


Figure A.3. Polarization versus electric field behaviour for 600 nm Ba_{0.9}Sr_{0.1}TiO₃ film at V_x = 2.5 V.